UNIVERSITAT DE BARCELONA

Hippocampal theta-gamma phase-amplitude coupling in memory encoding and retrieval

Ludovico Saint Amour di Chanaz

UNIVERSITAT DE BARCELONA

Hippocampal theta-gamma phase-amplitude coupling in memory encoding and retrieval

Ludovico Saint Amour di Chanaz

Submitted for the degree of Doctor in Psychology

Doctoral Program in Brain, Cognition and Behaviour

Cognition and Brain Plasticity Unit

Department of Cognition, Development and Educational Psychology

University of Barcelona

PhD Supervisors: Dr. Lluis Fuentemilla Garriga and Dr. Alexis Perez-Bellido

Barcelona 2023

Acknowledgments

I have always found it strange how people could have one single passion and stick to it for all of their lives. It was only when I was 28 years old that I discovered that the reason why I never seemed to fit in anywhere, and why my vision of the world was always different from people around me was a condition called ADHD (Attention-Deficit Hyperactivity Disorder). As much as this is considered a disorder and impacted negatively my life in several ways it is also the reason why I always saw the world with eyes that were curious and full of wonder.

It is that curiosity that I carried with myself during my whole life and this pursuit of truth and of understanding that led me in 2018 to move to Barcelona to pursue my PhD. Along the way, I was seen and have been helped by many people, who despite my many shortcomings due to my unique brain structure, have believed in me and kept me going, even at times when I, myself, did not see the light at the end of the tunnel.

First, I would like to thank my supervisor, Lluis Fuentemilla, the man who made my PhD possible. Thank you for being a great mentor and a brilliant scientist, for correcting my drafts and teaching me the patience needed to make figures. Thank you for trusting my judgment and skills, even at times when your own opinion was not to let me pursue them, you still encouraged me and allowed me to explore the data and my project in ways that I could never have with someone more rigid or less trusting. So first and foremost, thank you for not doubting me, even when I was doubting myself.

Thank you to Alexis Perez-Bellido for his help during most of my PhD. You gave me structure and discipline where my scattered brain had difficulties. You helped me with more technical sides of my projects where at times I did not believe I could not do it on my own. You were there when I took my first steps into the vast world of EEG analysis until I was able to fly on my own, and then you watched me soar and encouraged me along the way.

Thank you to Antoni Valero-Cabré, whom I met in Paris, and whose trust in me and my abilities was the reason I met Lluis in the first place. Thank you, because without you I would not have been able to be in this project at all and would not be where I am today.

Thank you to Diego Lonzano-Sevilla for teaching me to go further and deeper into complex analyses that I did not think I was capable of understanding or performing. Thank you for the patience you exhibited during the explanations you gave me about various techniques, analyses, and reasoning. Nothing is ever set in stone, and you taught me to look at everything with an even more critical eye.

Thank you to the people in the DMF research group, Xiongbo, Joan, Marta, Marc, Alexandrosd, with whom I have dear memories despite the fact that I was not the most present person in the lab.

Thank you to David Cucurell and Joan Rodriguez for helping me and always being present for technical and administrative issues, always with a kind word and a smile. You make Bellvitge a better place.

Thank you to my few long-time friends who have been supportive and understanding through this journey. Theo, Felix, Jonathan, Cecile, Antoine, Alexandra, Nik, Sasha, Laura, Sara. You all come from different places and I have met you at different times of my life, but you all have been present in your own way during this journey.

Thank you to Jonas Koblin, and to the whole team of Sprouts Schools for welcoming me so warmly into a world I knew nothing about. For giving me a glimpse of the afterlife – life after the PhD – and what it could be like. Thank you for giving me the occasion to nurture and educate people on a platform with a wide audience, and making me see that life is not a straight line, but rather a network of paths that are all intertwined and interconnected with one another. That it is always possible to walk on a different one once in a while.

Thank you to Jessica and her channel How to ADHD, to Beth, Chris, and Hayley Honeyman on TikTok for making me feel less alone and making me understand a bit more why my brain worked the way it did. Thank you to Mara Ambrosie for her writing group on Sundays that allowed me to rekindle my love for creative writing and to help my imagination run wild.

Thank you to my parents. Thank you for always making me feel loved and supported, and for allowing me to pursue my interests, no matter how strange or diverse they were. For giving me a childhood that was happy and full of wonder and adventures. For the dolphins I saw in the Mediterranean, the monuments of Rome, the culture, and the education you gave me. The trust you exhibited each step of the way during my studies. Thank you for allowing me to be who I am without making me feel like I ever was too much.

Finally, thank you to my beloved girlfriend and future wife Marie Masson Jeandroz. I have never felt as much seen and understood as when I am with you. You are a very special person whose brain is similar to mine, whose brain goes as fast as mine and goes to the same strange and wonderful places. Thank you for supporting me and helping me to see the light at times when I did not see it myself. Thank you for having been a constant support for the past eight years, never giving up on me or on us. For staying by my side no matter how difficult the situation was, no matter how much we disagreed, for always showing me love and friendship. For being my best friend and partner, and the main reason I did not give up on this project even when the burnout was real. I cannot enough put into words how much you have helped me and how much, thanks to you have I felt loved and supported and seen in ways I never had before. I hope to be able to show you, hopefully with more energy and time from now on.

Table of Contents

List of abbreviations

ANOVA	Analysis of Variance
CA	Cornu Ammonis
CFC	Cross Frequency Coupling
DG	Dentate Gyrus
DKL	Kullback-Leibler Divergence
EEG	Electroencephalography
ERP	Event-Related Potential
F	F statistic
Hz	Hertz
iEEG	intracranial electroencephalography
fMRI	Functional Magnetic Imaging Resonance
ITC	Inter Trial Coherence
JSD	Jensen Shannon Divergence
MEG	Magneto Encephalogrpahy
MI	Modulation Index
mPFC	Medial Prefrontal Cortex
ms	milliseconds
MTL	Medial Temporal Lobe
MI	Modulation Index
MOVI	Mean Opposition Vector Index
MVL	Mean Vector Length
NC	Neocortex
LMEM	Linear Mixed Effects Model
LFP	Local Field Potential
LTD	Long-Term Depression
LTP	Long-Term Potentiation
P	p-value
PAC	Phase Amplitude Coupling
PACOI	Phase Amplitude Coupling Opposition Index
PFC	Prefrontal Cortex

PLV	Phase Locking Value
PPC	Pairwise Phase Consistency
S	seconds
STD	Standard Deviation
SWS	Slow Wave Sleep
TFA	Time-Frequency Analysis
Z	z-score
mV	millivolts

List of Figures

Abstract

Deciphering the mechanism of human memory formation and retrieval is one of the still unsolved mysteries of neurosciences. Theoretical models of underlying mechanisms of memory formation and retrieval have led the memory field for the past decade (Hasselmo, Bodelon, & Wyble, 2002). However, with methodological and technological limitations these models have yet to been shown in humans, especially deep brain areas such as the hippocampus, traditionally not easily recorded with non-invasive techniques.

It has been reported in rodent studies, that theta-gamma interactions modulate memory processes and that phase-states and interactions between oscillations may be of importance for the successful formation and recall of episodic memories (Manns, Zilli, Ong, Hasselmo, & Eichenbaum, 2007). It is well accepted that memory formation relies on the coupling and interaction of theta-gamma oscillations (Tort, Komorowski, Manns, Kopell, & Eichenbaum, 2009) in humans, but phase-preference mechanisms similar to those observed in rodents have yet to be found in humans. According to the latest evidence in human studies, memory formation of humans may rely on differential communication between brain areas (Griffiths et al., 2019) and to different phase states in the hippocampus (Kerren, Linde-Domingo, Hanslmayr, & Wimber, 2018).

Here, we are aiming to advance the understanding of how theta-gamma interactions in the human hippocampus may be reflective of underlying mechanisms that could differ between encoding and recall states, and how they could predict the success of memory formation and retrieval. We conducted an iEEG study on intracranially implanted epileptic patients, in order to analyse direct recordings from the hippocampus and relate them to an episodic sequential memory task. We believe that the analysis of theta-gamma interactions in the hippocampus are key to differentiating mnemonic processes and predicting successful memory retention.

In Study 1, we describe the Mean Opposition Vector Length (MOVI) a new method to analyze phase-preference differences between neurophysiological datasets. This method was developed during this thesis. We have tested it on simulated synthetic data in order to really understand its potential and limitations, and have compared it with the Jensen Shannon

Divergence, a more established method of analysis of phase-preference opposition between distributions. To assess the validity of our new index, we compared MOVI and JSD using Matthew's Correlation Coefficient (MCC) that aids in determining the accuracy of a test when the outcome is known. We found that our new index is more sensitive than the established techniques, more resistant to noise, and detects specific variations in the data that other methods ignore. In this way we proposed a novel technique of analysis for assessing distribution opposition between datasets that can be used in future studies on phase-preference.

In Study 2, we explored neural signatures of epileptic patients implanted with deep brain electrodes. During the recording of their brain activity, they performed a task of encoding and recall of series of congruent images to emulate life-like episodic memories. We first explored the specific neural signatures found during encoding and recall in our sequential task by analyzing increases and decreases in power via a time-frequency analysis. Then we explored relationships between frequencies by analyzing theta-gamma phase-amplitude coupling. Finally we explored theta-gamma phase preference during encoding and recall. We have shown that theta-gamma interactions in the hippocampus are predictive of memory processes and can differentiate between encoding and recall. More importantly, we found that this phase-coupling preference was predictive of the successful retention of sequential mnemonic traces.

Our results from these two main studies suggest that the study of phase amplitude coupling (PAC) and phase opposition is essential to research that focuses on the mechanistic processes underlying memory formation and retrieval. Additionally, we bridge the gap with rodent studies and show a mechanism underlying mnemonic processes so far never observed in humans, but consistent with previous findings on the communication between different brain areas. Altogether these findings shed a light on the neural mechanisms that support memory formation, early recall, and delayed recall, and on the different analytical methods that can be used to assess phase-amplitude interactions. This advances the understanding of human memory, of the neurophysiological mechanisms underlying different processes, and on the analytical methods used to understand them.

Resumen

Descifrar el mecanismo de formación y recuperación de la memoria humana es uno de los misterios aún sin resolver de las neurociencias. Los modelos teóricos de los mecanismos subyacentes de formación y recuperación de la memoria han liderado el campo de la memoria durante la última década (Hasselmo, Bodelon y Wyble, 2002). Sin embargo, debido a limitaciones metodológicas y tecnológicas, estos modelos aún no se han demostrado en humanos, especialmente en áreas profundas del cerebro como el hipocampo, que tradicionalmente no se registran fácilmente con técnicas no invasivas.

Se ha informado en estudios con roedores que las interacciones theta-gamma modulan los procesos de la memoria y que los estados de fase y las interacciones entre las oscilaciones pueden ser importantes para la formación exitosa y la recuperación de los recuerdos episódicos (Manns, Zilli, Ong, Hasselmo y Eichenbaum, 2007). Es ampliamente aceptado que la formación de la memoria depende del acoplamiento y la intera
cción de las oscilaciones theta-gamma (Tort, Komorowski, Manns, Kopell y Eichenbaum, 2009) en humanos, pero aún no se han encontrado mecanismos de preferencia de fase similares a los observados en roedores. Según la evidencia más reciente en estudios con humanos, la formación de la memoria en humanos puede depender de la comunicación diferencial entre áreas cerebrales (Griffiths et al., 2019) y de diferentes estados de fase en el hipocampo (Kerren, Linde-Domingo, Hanslmayr y Wimber, 2018).

Aquí, nuestro objetivo es avanzar en la comprensión de cómo las interacciones theta-gamma en el hipocampo humano pueden reflejar mecanismos subyacentes que podrían diferir entre los estados de codificación y recuperación, y cómo podrían predecir el éxito en la formación y recuperación de la memoria. Realizamos un estudio de EEG intracraneal en pacientes epilépticos con implantes, con el fin de analizar registros directos del hipocampo y relacionarlos con una tarea de memoria secuencial episódica. Creemos que el análisis de las interacciones theta-gamma en el hipocampo es clave para diferenciar los procesos mnemónicos y predecir la retención exitosa de la memoria.

En el Estudio 1, describimos la Longitud del Vector de Oposición Media (MOVI) un nuevo método para analizar diferencias de preferencia de fase entre conjuntos de datos neurofisiológicos. Este método fue desarrollado durante esta tesis. Lo hemos probado en datos sintéticos simulados para comprender realmente su potencial y limitaciones, y lo hemos comparado con la Divergencia de Jensen Shannon, un método de análisis más establecido de la oposición de preferencia de fase entre distribuciones. Para evaluar la validez de nuestro nuevo índice, comparamos MOVI y JSD utilizando el Coeficiente de Correlación de Matthew (MCC) que ayuda a determinar la precisión de una prueba cuando el resultado es conocido. Encontramos que nuestro nuevo índice es más sensible que las técnicas establecidas, más resistente al ruido y detecta variaciones específicas en los datos que otros métodos ignoran. De esta manera, propusimos una nueva técnica de análisis para evaluar la oposición de distribución entre conjuntos de datos que se puede utilizar en futuros estudios sobre preferencia de fase.

En el Estudio 2, exploramos las firmas neuronales de pacientes epilépticos implantados con electrodos cerebrales profundos. Durante la grabación de su actividad cerebral, realizaron una tarea de codificación y recuerdo de series de imágenes congruentes para emular recuerdos episódicos similares a la vida. Primero exploramos las firmas neuronales específicas encontradas durante la codificación y el recuerdo en nuestra tarea secuencial analizando aumentos y disminuciones de potencia a través de un análisis de tiempo-frecuencia. Luego exploramos las relaciones entre frecuencias analizando el acoplamiento de fase-amplitud theta-gamma. Finalmente exploramos la preferencia de fase theta-gamma durante la codificación y el recuerdo. Hemos demostrado que las interacciones theta-gamma en el hipocampo son predictivas de los procesos de memoria y pueden diferenciar entre codificación y recuerdo. Más importante aún, encontramos que esta preferencia de acoplamiento de fase era predictiva de la retención exitosa de trazas mnemónicas secuenciales.

Nuestros resultados de estos dos estudios principales sugieren que el estudio del acoplamiento de fase y la oposición de fase es esencial para la investigación que se centra en los procesos mecanísticos subyacentes a la formación y recuperación de la memoria. Además,

cerramos la brecha con los estudios en roedores y mostramos un mecanismo subyacente a los procesos mnemónicos que hasta ahora no se había demostrado en humanos, pero que es coherente con hallazgos previos sobre la comunicación entre áreas cerebrales.

En conjunto, estos hallazgos arrojan luz sobre los mecanismos neurales que respaldan la formación de la memoria, el recuerdo temprano y el recuerdo tardío, y sobre los diferentes métodos analíticos que se pueden utilizar para evaluar las interacciones entre fase y amplitud. Esto avanza en la comprensión de la memoria humana, de los mecanismos neurofisiológicos subyacentes a los diferentes procesos y de los métodos analíticos utilizados para comprenderlos.

1. Chapter 1: Introduction

1.1. From neurons to LFP

The nervous system is the main information processing system in our body. The unit of that system is the neuron that exchanges information with other neurons through electrical potentials. When networks of neurons continuously exchange information, electrical rhythmic patterns arise, what we call brain waves, or neural oscillations. These patterns are generated by the collective activity of large groups of neurons firing together in a synchronized manner (Varela, Lachaux, Rodriguez, & Martinerie, 2001).

When a single neuron fires an action potential, it generates a brief electrical pulse that propagates along its axon, as this potential travels. This electrical potential is then passed to other neurons through synapses. When the electrical potential attains the axon, it stimulates the release of neurotransmitters in the extracellular space, that activating receptors on the dendrite of the next neuron, will induce an electrical potential in the post-synaptic cell. Excitatory neurons release neurotransmitters that depolarize the post-synaptic neuron, and increase its chances of firing an action potential. Inhibitory neurons on the other hand, release neurotransmitters that induce the hyperpolarization of the post-synaptic neuron, and reduce its chances of firing an action potential. When an action potential propagates through the neuron, it induces a current in the intracellular space, and due to ionic movements within and outside the membrane, it also causes a temporary change in the electrical potential of its immediate vicinity. This extends into the extracellular space that contains ions such as sodium, potassium, chloride and calcium, which can conduct electrical signals. When the action potential passes through extracellular space, it induces a redistribution and a movement of ions, creating a local and transient electric field. When several neurons fire or are active in a certain setting, this local change in potential can be detected by electrodes that are placed near the neuron, or neurons of interest. When many neurons fire simultaneously or in close succession, the individual electrical fields they generate summate, resulting in a larger and measurable potential change in the local extracellular space (Schaul, 1998).

The synchronized firing of neurons provides valuable insights into the underlying cellular processes, which is crucial in the study of memory formation. Synchronized neural activity – when the post-synaptic neuron fires soon after the pre-synaptic neuron - can enhance synaptic strength, a phenomenon known as Long Term Potentiation (LTP) (Hebb, 1955; Seung, 2000). Similarly, when the activity of neurons is desynchronized, it promotes synaptic depotentiation, also known as Long Term Depression or LTD (Hebb, 1955; Seung, 2000). Those are forms of synaptic plasticity that for a long time were thought to drive neural interactions and core functions such as memory formation. We note that recent alternative views showed that Hebbian plasticity is not the only one that exists, although non-Hebbian plasticity seems to rely on slower homeostatic processes, reliant on different forms of neural activity patterns (Park, Jung, & Eun, 2014).

There are roughly 80 billion neurons in the human brain, and an estimated 60 trillion possible connections, therefore technologically we lack the tools to analyse each neuron individually when studying processes. For this reason, cognitive studies use changes in concentration of oxygen in the blood with functional magnetic resonance imaging (fMRI) (Ogawa, Lee, Kay, & Tank, 1990; Ogawa et al., 1992) or the study of Local Field Potential (LFP) changes with electroencephalography (EEG) (Proekt, 2018), magnetoencephalography (MEG) (Hamalainen, 1991) or intracortical EEG (iEEG) (Jobst et al., 2020). LFP has several frequencies and additive properties that can be decomposed and analysed (Contreras & Steriade, 1995). Changes in the LFP have therefore a power, a frequency and other characteristics that representative of the underlying neural activity (Figure 1).

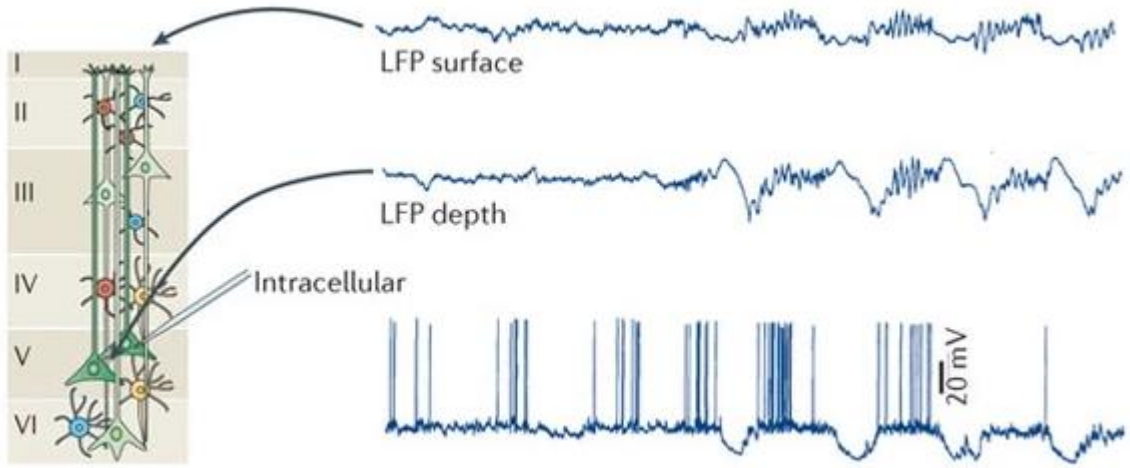

Figure 1-1: LFP detection and its relationship to neural activity, adapted from (Buzsaki, Anastassiou, & Koch, 2012)

LFP surface represents the observed LFP from a scalp EEG recording. LFP depth represents the activity measured with depth electrodes. Intracellular trace measures the spiking activity of a single neuron. Changes in the LFP of both intracortical and scalp recordings can be linked to changes in spiking activity (Buzsaki, Anastassiou, & Koch, 2012).

The study of LFP is therefore useful to infer on neural mechanisms underlying complex brain functions such as memory, and to better understand processes such as memory formation, consolidation, and retrieval. Other neuroimaging methods such as functional magnetic resonance imaging (fMRI) also allow to study brain activity. However it is an indirect measure of brain activity, as it relies on the oxygenation of blood vessels near networks of neurons that have an increased activity (Ogawa et al., 1990). Thus, it provides less temporal precision than the study of LFPs, and does not allow for the direct study of electrical activity in the brain, where frequencies of activity cannot be studied individually. The study of LFPs can be done non-invasively with scalp EEG, and invasively with intracortical EEG. The advantage of scalp EEG is that it is more accessible data. The helmets for EEG have multiple channels that have a pre-determined position, which makes it easier to generalize result found with scalp EEG. However scalp EEG relies on the recording of cortical activity mainly, whilst deep brain areas are less easily analyzed, except with techniques such as beamforming and source reconstruction that still have somewhat elusive characteristics and do not have a unified mathematical approach (Westner et al., 2022). This is where invasive methods such as

intracortical EEG (iEEG) shine. Implantation of electrodes in hospitalized patients allows access to the recordings of deep brain areas, where electrical variations can be studied with a better temporal precision and decomposition of the signal than with fMRI, and with a purer signal compared to source reconstruction in sEEG. In this thesis, we focused on the study of intracortical LFPs and how they impact memory formation within key areas of the memory system.

1.2.The episodic memory system

Memory is a system essential to survival. We gather information about things and events we have seen or experienced and use this information to make predictions about the future (Schacter, Addis, & Buckner, 2007). In evolutive terms, that means that individuals who have a better way of remembering and interpreting information about the past better survive new conditions. On one hand, individuals need to remember information about their surroundings which can be behaviors or shapes, sounds, or places, that indicate either danger, reward, or safety. On the other individuals also need to remember how to do things, like walking, running, hunting, reading, communicating, or simply grabbing a glass of water. Although seeming very different, these declarative and non-declarative memory systems respectively, both rely on mnemonic functions (Squire & Zola, 1996) and the brain structures that support them.

In this thesis, we are going to focus mainly on the declarative aspect of memories, and how the events that we see or experience can be translated into a memory trace that we can recollect in a meaningful way, and not as a disjointed succession of sensory information.

In fact, memory on its own, as a gathering of seemingly incongruent information about the past serves little purpose, but it is the way we link this information together, and the way we interpret the past, discerning events, patterns and creating internal models that we can truly understand the past, navigate the present and infer about the future. Seemingly, it is this interpretation of the world that we end up remembering as memory traces, which might also be the reason for the appearance of false memories (Muschalla & Schonborn, 2021). This

being said, there is clear evidence that memories and memory traces also contain some vivid recollection of sensory events (Kensinger & Schacter, 2007).

All of this speaks to the complex and interconnected nature of memories that need inputs – either internal as emotions and states, or external as sensory stimuli – an interpretation that can be based on past knowledge – or semantic memories – or links to other memories. For example, if I said, "I remember during the pandemic seeing a lot of PhD students that like me were burnt-out, which is not surprising as 74% of PhD students experience at least a major depressive or anxiety episode during their years of study (Forrester, 2021; Woolston, 2021)." The pandemic is the context, students being burnt out is what I remember from the tweets and articles I was reading at the time. The exact words in the articles I could not recall, however, I remember the message and the main point, and the emotions felt at that moment. I remember the interpretation I had of the sensory inputs that I have received. And finally, I linked this to my overall state, and to another memory, and fact, that made me interpret that singular event slightly differently. In a single sentence, I recollected external sensory inputs, their interpretations, internal inputs, and another seemingly disconnected memory that helped me understand the first one better. Furthermore, this specific recollection fits the criteria for what we call an episodic memory, which is the focus of our study and of my thesis.

Episodic memories are defined as the ability to remember specific events in a highly detailed manner. It is a type of long-term memory that allows people to remember detailed information about the past including places, people, faces, sensory details and contextual information associated with them in a temporal order. It involves a conscious mental "time-travel" that enables an individual to re-experience events from the past. It is a type of declarative memory that is different from semantic information – that can include the recollection of facts and repeated events – but can rest on it. (Fossati, 2013; Martinelli, Sperduti, & Piolino, 2013; Morris, 2001; Paller & Wagner, 2002; Tulving, 2002; Tulving & Markowitsch, 1998). Lesion studies showed that the medial temporal lobe is highly involved in the encoding and recall of episodic memories (Gabrieli, Cohen, & Corkin, 1988), but also other areas such as the thalamus (Aggleton & Brown, 1999) seem to participate to the formation of memories and their recollection.

With this framework, and thanks to rodents and human studies, we have reached an important understanding of the brain regions involved in memory formation and recall. Studies on rodents showed that what seems to happen during memory formation is that the layers 2 and 3 of the entorhinal cortex seem to receive processed sensory inputs and send them to the hippocampus (Ito & Schuman, 2008; Madronal et al., 2016; Rosen, Cheung, & Siegelbaum, 2015; Stone et al., 2011) through the perforant path (PP) to the dentate gyrus (DG) and through the temporoamminic pathway (TA) to the *Cornu ammonis* (CA1). An accepted view is that the DG is responsible for pattern regularity (J. E. Lisman & Grace, 2005), the CA3 for pattern similarity, and the CA1 for pattern differentiation (Hainmueller & Bartos, 2018). The DG then has projections to CA3 that itself has projections back to the CA1 through the Schaffer Collateral Pathway (SC) (Nakamura, Flasbeck, Maingret, Kitsukawa, & Sauvage, 2013), where seemingly contextual and detailed information are gathered as separated entities (Ito & Schuman, 2008). This phenomenon seems to be happening because of the different neurons involved in the pathways. The TA pathway has direct projections to CA1 pyramidal cells, while the PP is a disynaptic inhibitory path passing through interneurons toward the dentate gyrus (Mori, Abegg, Gahwiler, & Gerber, 2004). Interestingly, the CA1 also receives projections from other brain areas, like the ventral tegmental area (VTA) that informs on a reward obtained during the memory (J. E. Lisman & Grace, 2005), with dopamine impacting the TA-CA1 pathway by disinhibiting it (Ito & Schuman, 2007). It also receives information from the amygdala (Kitamura et al., 2017; Kitamura et al., 2015) about the salience of a memory, especially important for fear conditioning. The CA1 then has projections towards the subiculum for a feedback loop of novelty, salience, and reward (J. E. Lisman & Grace, 2005) and the CA3 has projections towards layer 5 of the entorhinal cortex that seemingly acts as a switchboard between the hippocampus and other brain areas such as the prefrontal cortex, the amygdala, the anterior cingulate cortex (ACC) and the retrosplenial cortex (RSC) (Figure 1-2) (Eichenbaum, Sauvage, Fortin, Komorowski, & Lipton, 2012; Nakashiba, Buhl, McHugh, & Tonegawa, 2009; Susumu Tonegawa, Morrissey, & Kitamura, 2018). From the prefrontal cortex and the amygdala, there are also communications towards the hippocampal CA1 through the pedicubpontine nucleus (J. E. Lisman & Grace, 2005).

Neuroimaging studies in humans contributed to further our understanding that memories are not set in a specific brain area, but they change, evolve, and are over time integrated in different brain regions than when they were first encoded. In fact, there is evidence in both rodents (Kitamura et al., 2017; Susumu Tonegawa et al., 2018) and humans (Takashima, Jensen, et al., 2006; Takashima, Petersson, et al., 2006) that, over time, memories are transferred from the hippocampus towards neocortical areas. This process also seems to be heavily mediated by sleep (Cirelli & Tononi, 2017; Genzel, Kroes, Dresler, & Battaglia, 2014; Genzel, Spoormaker, Konrad, & Dresler, 2015; Tononi & Cirelli, 2006).

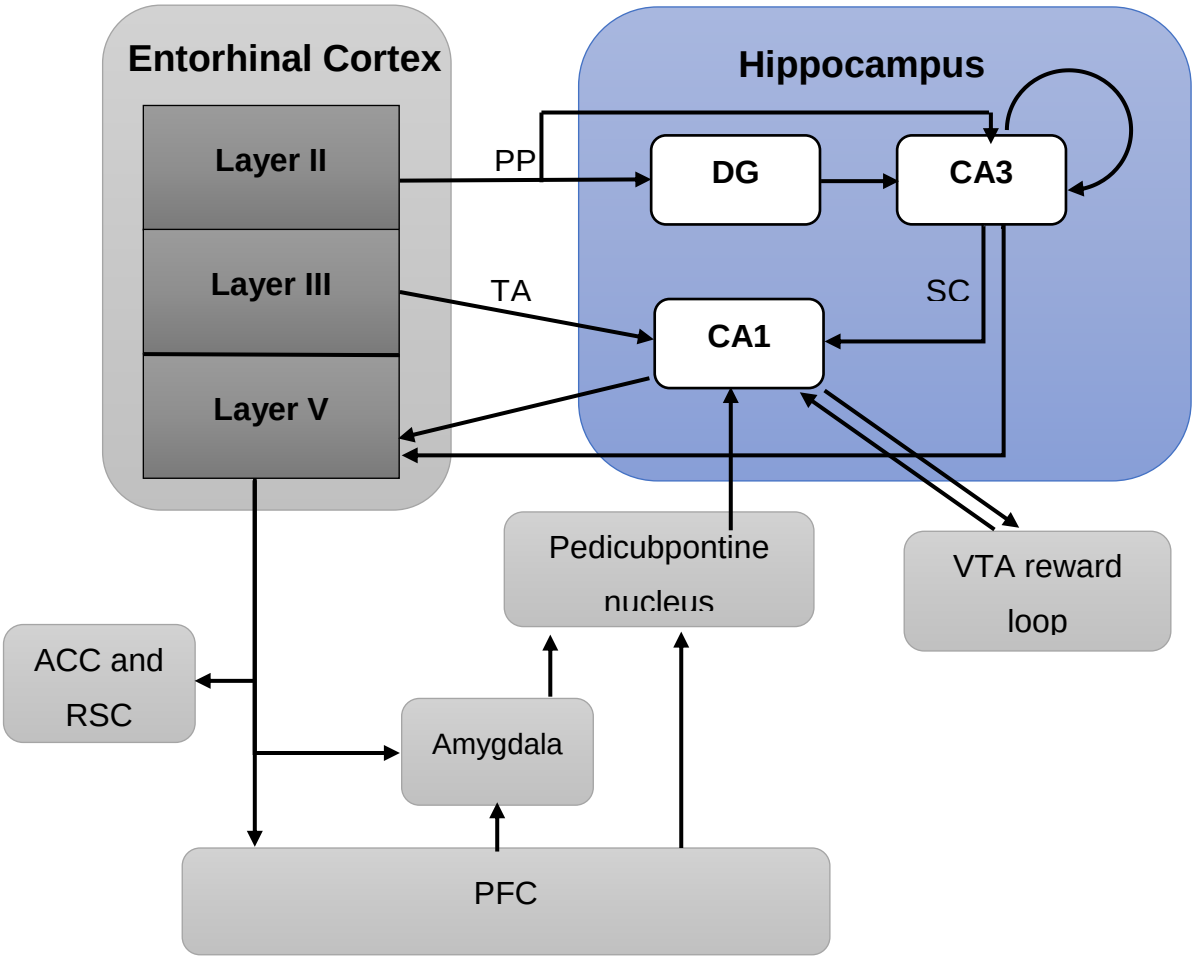

Figure 1-2: Simplified summary of the memory system

Representation of the connections between brain areas contributing to memory. In blue the Hippocampus is central to encoding and recall processes that in this figure are not separated. The entorhinal cortex sends sensory inputs from layers 2 and 3 towards the hippocampus

subfields DG, CA1, and CA3, and receives in its layer 5 processed mnemonic information that is then reprocessed or transferred to cortical areas. These cortical areas also exert a control and modulate how memories are created and at a later time recalled.

1.3.The hippocampus

The hippocampus (HPC) sits at the apex of the memory system. The importance of the HPC in memory formation and retrieval has been especially highlighted by lesion studies (Aggleton & Brown, 1999; Eichenbaum, 1992; Mumby, Astur, Weisend, & Sutherland, 1999; Rosenbaum et al., 2000; Scoville & Milner, 1957, 2000; Sinnamon, Freniere, & Kootz, 1978) and at a later time by optogenetics (Kitamura et al., 2017; Nakashiba et al., 2009; Roy et al., 2016; Susumu Tonegawa et al., 2018; S. Tonegawa, Pignatelli, Roy, & Ryan, 2015).

Nevertheless, the HPC does not seem to be strictly necessary for all memory processes, in particular those involving the recollection of very remote memories (Bontempi, Laurent-Demir, Destrade, & Jaffard, 1999; Rosenbaum et al., 2000). The history of patient H.M. (Scoville & Milner, 1957) shows us that the removal of most of the medial temporal lobe resulted in a severe anterograde amnesia. Although procedural and working memory were intact, patient H.M. could not commit new events to his explicit memory. He was also impaired in the formation of new semantic knowledge. He was able to remember events up to 2 years before his surgery, but after that, he had a complete memory loss. Similarly, patient K.C. who had, following a motorcycle accident a lesion to the brain that implicated an almost complete bilateral loss of hippocampal function had anterograde amnesia and could not remember episodic events of his life. However, his semantic memories and his noetic consciousness were preserved (Tulving, Schacter, McLachlan, & Moscovitch, 1988). The history of these two patients helped confirm the necessary role of the hippocampus and of the temporal lobe in the encoding and recall of especially autobiographical memories. Other studies in humans showed that the bilateral resection of the hippocampus prevents or makes more difficult the encoding of new memories, and suppresses recent memories (Milner & Klein, 2016; Scoville & Milner, 2000) further confirming the idea that the hippocampus is necessary for encoding processes, and suggesting that its role in recall may be dependent on

the age of the memory. In fact, an fMRI study done over the course of 3 months showed that early memories activate preferentially the hippocampus, but that over time the same memories activate cortical areas (Takashima, Petersson, et al., 2006). This shows that the hippocampus is necessary for at least initial memory processes, but that over time memories become less and less hippocampus dependent.

This being said, the multiple-trace theory (Moscovitch et al., 2005) argues that the hippocampus is essential to the initial storage of memories but also is recruited in the recollection of a detailed episodic event independently of how distant it is from the present. Inversely, it may not be essential to retrieve memories that do not contain detailed sensory information, like general knowledge (for example what is the capital of a certain country) or repeated actions that no longer have detailed information (the path one takes every day to go somewhere) (Moscovitch, Nadel, Winocur, Gilboa, & Rosenbaum, 2006). This research taken together underlies the importance of the hippocampus in the encoding and early storage of memories. It also plays an essential part in the early or detailed retrieval of memories, making it a central and essential part of the whole mnemonic system. Because of this, it is the focal point of this thesis on the encoding and recall of episodic memories.

1.4.From Rodents to Humans

1.4.1. Theta oscillations and memory

Theta oscillations represent the “online” state of the hippocampus (Buzsaki, 2002) and is the activity that most dominates this area. Consequentially, it has been studied, especially in rodents, originally in the context of movement and locomotion (O'Keefe & Dostrovsky, 1971). These low-frequency oscillations (4-9Hz) have been found first in rodents and seem to be correlated to several memory processes (Landfield, McGaugh, & Tusa, 1972). In the case of the study of Landfield and colleagues, they showed that the theta oscillations in the EEG of rats during a fear conditioning task were correlated to the degree of subsequent retention. The theta rhythm was also central in the research that led to the discovery of place cells (O'Keefe & Conway, 1978) showing that theta oscillations also impacted navigation. The decrease in theta activity in navigation tasks in rodents also predicted a decrease in memory

performance (Winson, 1978). The causal effect of theta on memory performance was found in a stimulation study (Staubli & Lynch, 1987) where bursts of pulses were administered in a theta pattern and increased memory performance of rodents. The influence of the theta rhythm on memory functions seems to happen through the mediation of cellular types within hippocampal subfields. The hippocampus contains two main types of cellular types: inhibitory granule cells and excitatory pyramidal cells. Granule cells seem to reach their highest discharge rates during active exploration in rodents, and during theta-concurrent activities. On the other hand, pyramidal cells appear to be active in the form of sharp waves when immobility is reached. The two-stage model (Buzsaki, 1989) suggests that during exploratory behavior, theta transfers cortical sensory information to the CA3 of the hippocampus causing weak and transient potentiation in pyramidal cells. Once the exploratory activity terminates, the subgroup of pyramidal cells then initiates a sharp-wave that transmits the information to CA1 neurons. Navigational studies in rodents (O'Keefe, 1993) show that the theta rhythm also may serve as a clock-like rhythm to organize cortical sensory information within hippocampal networks and modulate the associated mnemonic processes.

Memory research using a rodent model has yielded remarkable findings, shedding light on the complex and interconnected processes involved in episodic memory formation and retrieval. However, all these results provide only inferential evidence on how human memory formation works.

Human research has also highlighted the significance of the theta rhythm in memory formation. For instance, (A. P. Burgess & Gruzelier, 1997) demonstrated an increase in theta synchronization and activity during recognition memory tasks. (Tesche & Karhu, 2000) revealed that theta activity was correlated with working memory performance. Additionally, the duration of the stimulus-locked theta increased with working memory load.

These findings taken together with findings on fear-conditioning tasks and recognition tasks in humans suggest that the theta rhythm is necessary to the sensory processing of cortical information sent to the hippocampus, and perhaps to its organization. Although several theoretical models arose from literature on rodents, it is important to test these models on

humans too to generalize the results found in mice, which is what we tried to achieve in this thesis.

1.4.2. Gamma activity and memory

Gamma activity (30-120Hz) indicates the fast activity of neuronal assemblies firing together. It is another particularly important rhythm in the study of memory formation. One of the reasons gamma power appears to be so important is because of its link with plasticity mechanisms. Gamma oscillations appear to drive spike-timing dependent plasticity (Bliss & Collingridge, 1993; Sjostrom, Turrigiano, & Nelson, 2001) by being beneficial to synaptic potentiation among stimulated neurons (Li, Liang, & Zhou, 2021). This may explain why successful memory formation occurs when neuronal firing is coupled with ongoing gamma oscillation (Roux et al., 2022). In fact studies in rodents (Bragin et al., 1995; Buzsaki & Wang, 2012; Headley & Weinberger, 2011) and humans (Griffiths et al., 2019; Lam, Schoffelen, Udden, Hulten, & Hagoort, 2016; Lin, Umbach, Rugg, & Lega, 2019; Staresina et al., 2016) indicate that increases in gamma power predict successful memory formation, or retrieval.

In addition to plasticity mechanisms, successful encoding and retrieval of memories is also based on the effective communication between brain areas. Incoming information in sensory cortices needs to activate the relevant cell assemblies in the hippocampus to ensure associative binding. Similarly, during retrieval neural communication between areas ensures that the reactivation of hippocampal networks induces neocortical activity to allow reinstatement of an episode (Staresina et al., 2016). A prominent theory that binds gamma activity to information transfer is the “communication through coherence” theory (Fries, 2005). It proposes that information is relayed from one brain region to another when gamma oscillations in the two regions synchronize and input from the “sender” arrives at the “receiver” when is at its most excitable phase, and therefore most likely to induce plastic changes. This theory is supported by experimental evidence in non-human primates (Csorba, Krause, Zanos, & Pack, 2022) and humans (Fell et al., 2006). Additionally, when humans successfully recall a memory, gamma-band coherence between areas predicts the degree of reinstatement of the reactivated memory (Pacheco Estefan et al., 2021). However, if gamma band connectivity is involved in relaying both new and old information, interference may arise during this communication. One suggestion based on empirical observations is that distinct

gamma bands support these two mechanisms. It was proposed that a fast gamma oscillation (60-100Hz) facilitates encoding of information, while a slower gamma oscillation (30-50Hz) facilitates retrieval, by allowing traces to propagate from CA3 to CA1 (Colgin, 2015a). This model is supported by experimental evidence in both rodents (Bieri, Bobbitt, & Colgin, 2014; Zheng, Bieri, Hsiao, & Colgin, 2016) and humans (Griffiths et al., 2019; Vivekananda et al., 2021). That said, in both humans and rodents, measurements of "slow" gamma may be disrupted by theta harmonics (Zhou et al., 2019). Given the importance of the theta rhythm in memory formation as discussed in the above section, it is difficult to disentangle what effects exactly can be attributed to theta or its harmonics and what can be attributed to "slow" gamma.

It comes to question, however, how gamma-band coherence can support communication over distances of >1cm, given mechanical factors such as axonal conduction delay (Ray & Maunsell, 2015). This long-range communication seems to be better supported by slower (e.g. theta) oscillations (Solomon et al., 2017). These concerns can be addressed by considering cross-frequency coupling phenomena, in which fast gamma oscillations are nested within a slower oscillating rhythm (Bonnefond, Kastner, & Jensen, 2017). When the low-frequency oscillations of two distant regions become coherent, and local gamma activity locks to a specific phase of the ongoing lower rhythm, gamma coupling becomes more precise than what would happen based on long-range gamma communication. In sum, it is suggested that theta and gamma oscillations interact to facilitate communication between areas and to facilitate plasticity processes that underlie memory formation and retrieval.

1.5.Theta-gamma interactions and memory

Memory processes rely partly on the interaction of neurophysiological oscillations of different frequencies interacting with one another (Hyafil, Giraud, Fontolan, & Gutkin, 2015; Jensen & Colgin, 2007; Tort, Komorowski, Eichenbaum, & Kopell, 2010). Among the various forms of coordination, Phase-Amplitude Coupling (PAC) seems to stand out the most as the interaction between the phase of the low-frequency oscillation and the power of the high-frequency one. It can be detected in animal studies (Jensen & Lisman, 1996; Pavlides, Greenstein, Grudman,

& Winson, 1988; Tort et al., 2009; Tort et al., 2008) and human brain recording using magnetoencephalography (MEG) (Fuentemilla, Penny, Cashdollar, Bunzeck, & Duzel, 2010), intracortical LFP recordings (iEEG) (Axmacher et al., 2010; Canolty et al., 2006; Saint Amour di Chanaz et al., 2023; Tort et al., 2009) and recordings of single units (Rutishauser, 2019; Rutishauser, Ross, Mamelak, & Schuman, 2010).

Studies on memory show that an increase in PAC also reflects an increased success of memory processes (Canolty et al., 2006; Lega, Burke, Jacobs, & Kahana, 2016; Tort et al., 2010), which could be a reflection of the increased communication between areas. During encoding sensory inputs are more clearly communicated to the hippocampus, and during recall, mnemonic traces are sent to neocortical areas (Griffiths et al., 2019). This directionality could rely on PAC mechanisms where gamma activity nested within lower frequencies increases communication between areas (Bonnefond et al., 2017). However, this explanation still does not elucidate how a continuous stream of sensory information is processed and stored coherently so that when we recall a memory we also recall the order of the events that happened.

One possible explanation is phase-precession which also relies on theta-gamma interactions. Studies on rodents have shown that during navigation, cell assemblies that code for a particular place or position are locked to distinct phases of theta as a function of how the rat moves in two dimensions (Jensen & Lisman, 1996; O'Keefe & Burgess, 2005). These findings suggest that gamma activity codes for the temporal order or spatial position of a particular memory by locking itself to a distinct phase of theta. Subsequent studies on rodents (Huxter, Senior, Allen, & Csicsvari, 2008; Oliva, Fernandez-Ruiz, Buzsaki, & Berenyi, 2016) showed that this neural code in fact predicted the position of the rat in two dimensions and that the interaction of theta with gamma activity within the CA1, CA2 and CA3 differentially coded for sequences of discrete events and position. In humans, phase precession was observed in temporal coding, where distinct items during sequence encoding were locked to slightly different theta phases (Heusser, Poeppel, Ezzyat, & Davachi, 2016) suggesting that theta-gamma interactions also code for the order of discrete events within a sequence, and add the

temporal dimension to episodic memories (Reddy et al., 2021) dependent on cortico-hippocampal communication (Robinson et al., 2017).

Taken together these findings suggest that theta-gamma coupling underlies communication between areas that promotes encoding or recall, and organize continuous sensory inputs into discrete sequential events within an episode. It is still unclear however, how encoding and recall can coexist while they seemingly rest on similar neural mechanisms within the same areas. The theory stating that encoding and recall processes avoid overlapping by relying on two distinct gamma bands, (Colgin, 2015a) can be explored in humans by priming a behavior during observation: Asking participants specifically to either encode an item or a sequence or to recall one. However, in rodent studies, this is more complicated, as encoding and recall often can overlap (Igarashi, Lu, Colgin, Moser, & Moser, 2014) and make the story more complex.

An alternative explanation was proposed by (Hasselmo et al., 2002) suggesting that encoding and recall were primed by theta states. The model suggested that high phases of theta promoted directional communication between the entorhinal cortex and CA1 and CA3 subfields of the hippocampus, while during low phases of theta pyramidal CA3 cells preferentially communicated with CA1 that communicated back to cortical areas. It proposed that theta acted as a switch between encoding and recall states, modulating local activity as a function to projections from other areas (Figure 3).

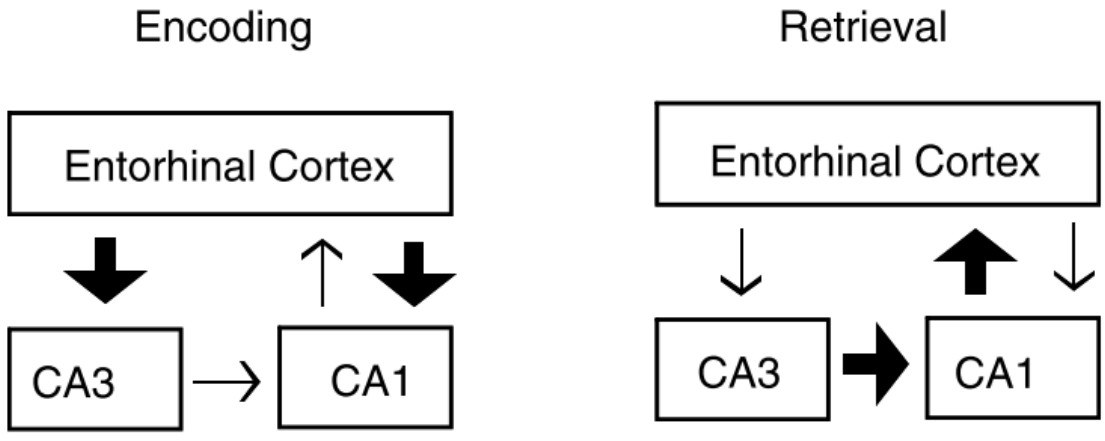

Figure 1-3: Model of hippocampal network during encoding and recall, adapted from (Manns, Zilli, Ong, Hasselmo, & Eichenbaum, 2007)

During Encoding the entorhinal cortex sends information to the hippocampus to the CA1 and CA3, and the communication between CA3 and CA1 is suppressed. During Recall, CA3 sends information to the CA1 that then sends it back to the entorhinal cortex.

Although this model seems to have been observed in rodents during navigational tasks (Manns et al., 2007), it is not yet generalizable to humans, and to episodic memory, hence the question arises of whether this phenomenon can be observed in the human hippocampus during episodic memory processing, and if the methods that we have at our disposal are sufficient to analyze these mechanisms.

1.6. Studying Phase coupling and phase opposition

When talking about the study of phase-amplitude interactions the question we are asking is whether a population of neurons preferentially fires during some phases of an ongoing rhythm. If local populations of neurons fire during certain phases of an ongoing rhythm, it means that those populations of neurons are preferentially selected by this ongoing rhythm that acts as a "switch" between encoding and recall, or at the very least that theta phases induce optimal states for selective populations of neurons, that as a result have a higher probability of firing during those phase-states. An electrophysiological study by Hyman and colleagues (Hyman, Wyble, Goyal, Rossi, & Hasselmo, 2003) showed that the stimulation of CA1 pyramidal cells during up phases of the theta rhythm induced LTP, while the stimulation of the same neurons during the low phase of CA1 induced LTD. This shows that the populations of neurons firing during specific phases of the theta rhythm might induce lasting changes in the local plasticity of the hippocampus. In the model of (Hasselmo et al., 2002) it was proposed that encoding happens preferentially at high phases of the theta rhythm, and these electrophysiological findings, along with the rodent findings by (Manns et al., 2007) seem to support this idea. Given that studies were able to discern phase-amplitude coupling phenomena between theta and HFA activity in the hippocampus in the study of item-context associations (Tort et al., 2009) and of within-context temporal coding (Heusser et al., 2016), we believe that it is possible to find a way to discriminate encoding and recall processes in

the human hippocampus, based on their phase-amplitude interactions. These findings taken together are also coherent with the idea that phase selectivity plays a role in memory processes, and speaks to the need of finding appropriate techniques to discern phase-coupling and phase preference.

PAC analyses the degree of coupling between high-frequency activity and a low oscillation. Within an ongoing time series, PAC determines how consistently HFA is nested within specific angles of low oscillations. This is reflected in neurophysiological data by a power increase of HFA, locked to a consistent phase of a lower oscillation. Several analytical methods allow to observe PAC strength, the two most used being the Mean Vector Length (MVL) (Canolty et al., 2006) and the Modulation Index (MI) (Tort et al., 2010). These methods merely measure the degree of coupling, but not necessarily inform on the angle of preference, or on the consistency of this preference across conditions or trials, should there be any.

The angle of preference can be observed when summarizing the data by binning it. This means separating the phase time-series into equal bins. For example if phase is separated into 18 bins, each bin will represent a 20^{o} area in polar space. If we were to talk in degrees instead of radians, this means that, for example, bin 1 would go from -180^{o} to -160^{o}, bin 2 from 160^{o} to 140^{o}, and so on. To then obtain a binned distribution, we extract the gamma amplitude information that corresponds to each phase bin by relating it to time points within the phase and amplitude time series. For example, if the phase time series exhibits an angle between -180^{o} and -160^{o} for time points 1 to 40 and then 176 to 198, then we extract the average amplitude for those same time points. We obtain a distribution where each bin has a phase information given by the bin order, and an amplitude information given by the mean amplitude per phase bin.

The analytical aspects that allow to determine phase preference and to compare phase preferences across conditions or datasets are discussed in General Methods and Study 1.

2. Chapter 2: Research Aims

The main goal of the current thesis is to advance the understanding of the mechanistic underpinning of the formation and retrieval of human episodic memory, and how the study of phase-amplitude interactions and the methods associated may be associated with memory formation. In what follows, I argue the objectives in more detail:

2.1. Objective 1: To understand and develop methodologies that allow the study of phase-amplitude interactions (Study 1)

Given that phase amplitude coupling and phase preference processes appear to underlie mnemonic processes, adequate techniques of analysis to distinguish these unique features in neurophysiological data are needed. We explore the different methodologies linked to the study of phase-coupling and phase-preference processes, in order to understand on a deeper level what the analyses mean in terms of neurophysiological underpinnings. We will discuss what questions and methods are used to study phase-coupling and phase-preference processes answer, and which one to use as a function of the experiment, model, available data, and hypothesis. We also will focus on the creation and use of synthetic data to better understand how the steps we take in the processing of data for phase-coupling analyses affect the data, and what are the signatures that end up being extracted.

Then, we will present a new method to analyze phase-preference differences between two conditions, explaining what parameters this novel method allows to explore, and in what cases it is preferable to other existing and validated analytical methods. We will test this new method on synthetic data and compare it with an existing one, testing its sensitivity and selectivity, and discussing its possible uses in noisy neurophysiological data.

2.2. Objective 2: To examine how phase-amplitude interactions mediate different memory processes (Study 2)

Much work in rodents and humans provided evidence that theta-gamma interactions play an important role in the formation and retrieval of episodic memory (Griffiths et al., 2019; Heusser et al., 2016; Manns et al., 2007; Tort et al., 2009). Encoding and recall of memories in fact appear to rely on similar coupling mechanisms (Axmacher et al., 2010; Lega et al., 2016), but it is still unclear how these two mechanisms are separated in the hippocampus to avoid interference. One model proposed that encoding and recall rely on two distinct gamma bands (Colgin, 2015a). Another proposed that theta oscillations are instead a switch between encoding and recall, and inform on how different brain areas communicate (Hasselmo et al., 2002). Although evidence in rodents supports this model (Manns et al., 2007), it remains unclear in humans if the phase preference of theta-gamma interactions predict memory processes and their success. Here, we ask whether phase-coupling interactions occur with a preferential theta phase state as a function of different memory processes, i.e., if encoding, or recall rest on different phase-coupling mechanisms. By analyzing iEEG recordings from the human hippocampus, we specifically explore phase-coupling processes during encoding and recall, and as a function of memory retention, to see if they differ in terms of strength, or frequencies, and explore whether phase preference is predictive of memory processes, and of retention.

3. Chapter 3: General Methods

1.1. Epileptic patients as a model

The use of the brain of epileptic patients as a model in the study of neural processes other than the epilepsy itself started in the 1940s by Dr Albert Grass who conducted research with his colleagues to investigate brain activity related to perception. Because of the advances in technology such as electrode construction, surgery techniques, and improved signal amplifiers, intracortical electroencephalography (iEEG) has taken a more important place in neurophysiological research and has lately been used to assess cognitive processes not related to epilepsy.

This allows high temporal resolution research that focuses on brain areas that are normally inaccessible with non-invasive techniques such as EEG, MEG, and the investigation of cognitive processes that involve those brain areas. One of those areas is the hippocampus, and thanks to epilepsy patients and iEEG we can investigate memory processes with data that directly comes from brain areas that we know are involved in memory formation and retrieval.

Because of their epilepsy, patients are implanted with depth electrodes, traditionally with several recording contacts each. Implantation and the contacts, or channels of each electrode are strategically placed around the brain area where neurologists believe the epileptic locus comes from. Patients stay in the hospital for 1 to 3 weeks in function of the hospital's procedures in the hopes that with the recordings from within the brain and epileptic crises, the technical team will be able to identify where the locus – or starting point – of the epilepsy is. During this time, researchers can come and present patients with cognitive tasks while their brain activity is recorded, and the recordings matched to triggers corresponding to different events of the cognitive task allows us to correlate brain activity to processes. This is what we did, presenting a mnemonic cognitive task to epileptic patients, and then focused on their hippocampal recordings.

Data included in this thesis were recorded from patients from two hospitals: the Hôpital Pitié-Salpétrière in Paris (France) and the Hospital Clínic - IDIBAPS in Barcelona (Spain). Electrode placement was exclusively guided by the clinical needs of localizing the seizure onset zone in and consider the indications and feasibility of ulterior surgical resections. Participant selection was based on the following inclusion criteria: 1) normal IQ; 2) electrodes implanted in the hippocampus contralateral to or outside of the epileptogenic region were included for the analysis of neurophysiology signals. The studies were conducted according to the Declaration of Helsinki and approved by the local ethics committee, and all patients provided written informed consent.

The experiment was conducted in the hospital, with participants sitting upright in a comfortable chair or on their bed. The stimuli were presented on a 13-inch portable computer, placed on an over-bed table at approximately 60 cm distance in front of the patients. Patients used the keyboard of the laptop to complete the behavioral task, and their responses were recorded internally. Trial onsets and offsets TTL triggers were sent to the EEG amplifier via a parallel port or an Arduino simulating a parallel port, each trigger corresponding to a different event. In Paris, the recordings were performed using the ATLAS amplifier (Atlas, Neuralynx®, Inc., Bozeman, MO; 160 channels at 4096 Hz; bandpass filter between 0.1 Hz and 1000 Hz). The macro electrodes (AdTech®, Wisconsin) used consisted of 4-12 platinum channel electrodes with a diameter of 1.12 mm and length of 2.41 mm, with nickel-chromium wiring. The distance between the centres of 2 contacts was 5 mm. In Barcelona at the Hospital Clinic, recordings were performed using a clinical EEG system (Natus Quantum LTM Amplifier) with a 1024Hz sampling rate and an online bandpass filter from 0.1Hz to 4000Hz. Intracerebral electrodes (Microdeep, DIXI Medical) were used for recordings. Each multielectrode had 8 to 18 contacts, spaced 5 mm and 1 to 2 mm long with a diameter of 0.8 mm. Verbal recalls were recorded with an external audio recorder placed on the over-bed table next to the laptop computer used for the task. Responses were given in native languages: In French in Paris and Spanish or Catalan in the Hospital Clinic. These verbal responses were then listen to and the behavioral output of memory accuracy was manually introduced in a table used subsequently for Behavioural analyses.

3.1.Structural processing and electrode localization

For the surgical procedure, patients must undergo a T1 MRI scan before electrode implantation, and a CT scan afterward in order to make sure the electrodes (figure 3-2 A) are in the target areas. With these structural scans we can also identify where contacts are and if they are within our regions of interest (ROI). In order to do this we used the fieldtrip (https://www.fieldtriptoolbox.org/) pipeline for analyzing human ECoG and iEEG recordings that involved the following steps.

First we determined the coordinate system we wanted to use for the T1 and decided to use the acpc coordinate system, and realigned the T1 scan interactively using the anterior and posterior commissures, an interhemispheric location at the top of the brain, and an interhemispheric location on the right of the brain. The volume was then realigned to these new axes and coordinate systems.

We extracted cortical and subcortical surfaces running a parcellation and segmentation of the T1 scans using Freesurfer (Fischl, 2012; Fischl, Sereno, & Dale, 1999) (https://surfer.nmr.mgh.harvard.edu/). We controlled the correct automated extraction of cortical and subcortical surfaces using Freeview (Figure 3-2 B) and when necessary applied correction points manually to re-extract structures that might not have been taken into account the first time.

We then imported the CT scan and converted its coordinates to acpc, realigning it manually as we did with the T1. For the CT however, we were using the left and right preauricular points (just in front of the ear canals) and an interhemispheric location at the top of the brain.
We then aligned and fused the CT with the MRI using the spm12 toolbox (Statistical Parametric Mapping, https://www.fil.ion.ucl.ac.uk/spm/software/spm12/). We examined the accuracy of the fusion with a visual inspection making sure the CT and MRI were correctly co-registered.

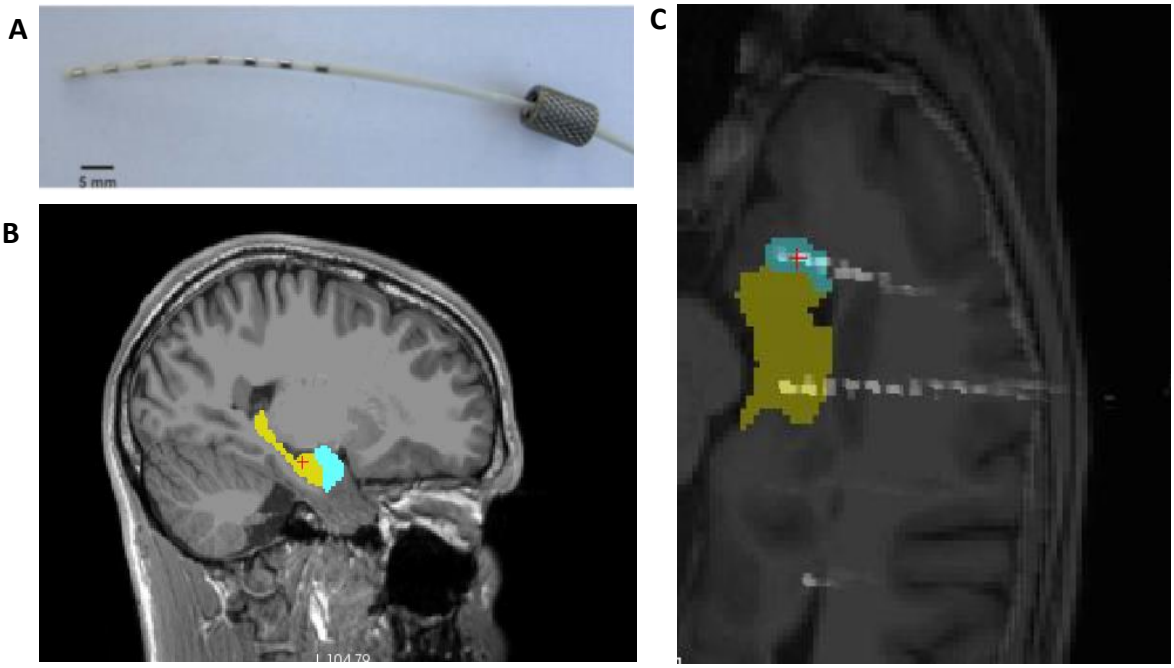

Figure 3-1: Implantation and electrode localization

A: Picture of an intracortical electrode used to implant epileptic patients in the Hospital Pitié-Salpetrière in Paris, adapted from (Amengual, Vernet, Adam, & Valero-Cabre, 2017).

B: Superposition of the pre-operatory T1 MRI of a patient with the localization of the hippocampus and amygdala of the aparc-aseg2009 atlas generated after freesurfer automatic parcellation of cortical and subcortical structures.

C: Example of superposition of the pre-operatory T1 MRI of a patient, a CT scan with hippocampal channels and the aparc-aseg2009 localization of the hippocampus and the amygdala of that patient after automatic parcellation and segmentation of brain structures via Freesurfer. The red cross indicates the mouse that is over the second channel of the electrode within the Amygdala. This is how manual electrode localization was done.

Finally, we imported the labels and names of the electrodes and channels and manually placed the labels of the channels on each channel (Figure 3-2.C) using the notes taken during surgery and the pre-implantation plan in order to carefully and successfully localize the right electrodes. Once this step was done a further verification was done by realigning the post-operatory T1 to the preoperatory T1 and by making sure the visible channels on the CT scans (in white) were aligned to the “holes” seen in the post-operatory T1.

Finally, we extracted the coordinates of the localized channels and assigned each channel to a brain area using the aparc-aseg2009 atlas of each patient in native space to increase accuracy.

For the figures presented in our published manuscript, we realigned each patient's scans and electrode placements to MNI space using the fieldtrip and spm12 toolboxes. This allowed to see all patient's electrodes in the same space, but this step can also create a slight distortion in electrode coordinates in function of each individual's brain structure and differences, which is why the initial localization and electrode selection was done in native space.

3.2.iEEG Processing

After acquisition, iEEG data has to be processed. First of all, we passed all of the datasets to BIDS format and down-sampled the raw data to 1000Hz in order for datasets from both hospitals to have the same sampling rate. We identified contacts of interest after Electrode placement and structural processing of each patient. From those contacts, we then extracted epochs for each stimulus from -2 seconds to 4 seconds and performed artifact detection in the following way:

1. We used Fieldtrip 2020 to visualize each trial and all channels for the visual detection of noise or epileptic activity.
2. With the help of an epileptologist we identified trials that contained epileptic activity or noise from a first observation of raw data. In this case, epileptic spikes were of high amplitude and lasted for no longer than 200ms but were disruptive of ongoing brain activity. Some more sustained epileptic activity was also identified, with high-amplitude repetitive patterns that were disruptive of previously ongoing brain activity.
3. We referenced each contact to the next one starting with the deepest contact in the brain (bipolar referencing) and we then proceeded to a second visual inspection of the data. Here we identified trials high frequency epileptic spikes that were disruptive of ongoing brain activity.

4. A Time-frequency decomposition was performed on each trial to control for missed epileptic spikes that may not have been visible during the first two steps of Artifact Rejection but would impact spectral power.
5. Trials with epileptic activity were removed from subsequent analyses.
6. Patients with too much epileptic activity were discarded.

We kept a single bipolar channel for each patient, ROI, and each event in order to perform analyses of activity related to our cognitive task. In the case of our study, we focused mainly on two brain areas: the Hippocampus, and the Middle Temporal Gyrus.

Temporal cortex was generally used for control analyses in order to assess Hippocampal specificity of effects on memory. Channels in the Temporal cortex were selected based on noise, epileptic activity, and other artifacts. All channels that had the label "middletemporal_cx" on the aseg_aparc2009 atlas of freesurfer were eligible for the control analyses. For each event, ROI, and all patients we could analyze a minimum of 15 trials per condition and patient.

3.3. Electrode Selection

Depth electrodes were implanted stereotaxically targeting sites of the temporal lobe. The presence of electrodes in the hippocampus was assessed with the examination of a computed tomography (CT) and (post-electrode removal) Magnetic Resonance Imaging (MRI) T1 scans. Cerebral atlases of each patient were obtained with the parcellation of the preoperatory T1 using Freesurfer (https://surfer.nmr.mgh.harvard.edu). The CT was then co-registered to the T1 and contact tags and names were placed manually using fieldtrip toolbox for ECoG and sEEG recordings (https://www.fieldtriptoolbox.org/). Confirmation of contact placement was then obtained with a co-registration of the post-operatory and post-electrode removal T1 to the preoperatory T1 and via superposition of the electrode placement matrix to the realigned post-operatory T1, and manual correction of the misplaced contact tags.

The selection of channels was done in native space to prevent errors due to distortions while converting in MNI space. MNI space conversion was then done to have a generalized view of the patient's channels of interest. Since channels were referenced to the adjacent more distal contact along the electrode (bipolar referencing) channels of interest for each ROI were

selected based on three main criteria (in this order of decreasing importance): (1) the channel of interest or the referenced one had to be in the hippocampus; (2) if more than one channel was eligible, hence fulfilled the prior criterion, to avoid using white matter references hence limit noise from other brain areas we privileged the channel that had an adjacent distal referencing contact also in the hippocampus (Michelmann et al., 2018) Finally, (3) if more than one pair of adjacent channels were eligible, we selected those that had the least amount of epileptic activity according to an Artifact Rejection procedure (please see section below for details).

To visualize the selected contacts across our sample, we normalized each participant's post-implantation MRI along with their co-registered pre-implantation MRI to MNI space using SPM12 (http://www.fil.ion.ucl.ac.uk/spm/). To facilitate the visualization of contacts across the group, a 5-mm-radius sphere was created around each contact's center point and overlaid across participants (Figure 3-3 A, B). We used the map Aseg_aparc_2009 to select our areas of interest, included in the Freesurfer toolbox.

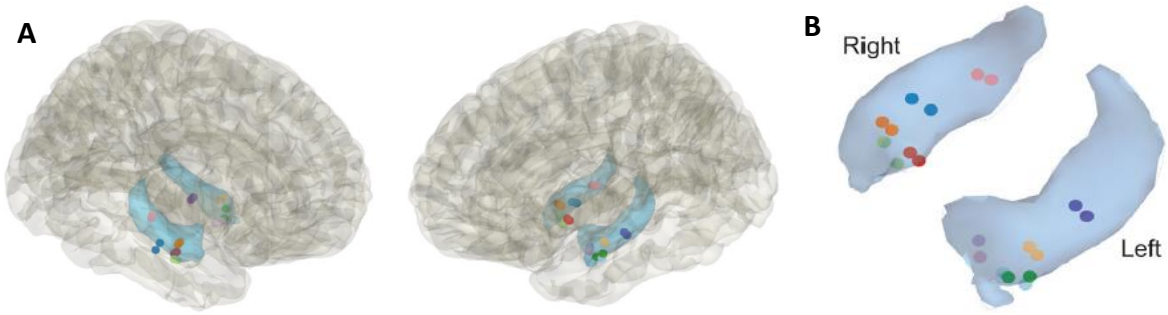

Figure 3-2: MNI representation of the selected Hippocampal channel

A: Representation in MNI space of the selected hippocampal channels for each patient for a whole brain. Each sphere represents a contact, here we show 2 contacts because since we processed our data with bipolar referencing, the resultant signal represents a virtual channel that is channel 1- channel 2.

B: Representation in MNI space of the channels in the hippocampus only.

3.4.Artifact Rejection

Artifact Rejection was done visually using the fieldtrip toolbox. A first round of rejection was done in order to select only the relevant and the selected channels (as specified in the previous section) thanks to the function ft_rejectvisual. In this step, we only selected channels that were within the hippocampus and an additional one to account for the bipolar referencing. After this first step, the selected channels were visually inspected with the function ft_databrowser for each trial, and epileptic activity was manually selected. Epileptic activity classification as overseen by an epileptologist that helped us recognize the signatures of an interictal spike (epileptic spike) or of sustained epileptic activity. The following characteristics were taken into account when performing the visual inspection.

Interictal spikes were detected when they were high in amplitude, lasted less than 200 ms, and were disruptive of an ongoing rhythm. Sustained epileptic activity was detected when it was a sudden change from any ongoing neural activity, disrupted the ongoing rhythm, and had a high amplitude.

After a first visual inspection where trials containing epileptic activity were removed, we performed a bipolar re-referencing of the channels (Channel1-Channel2, Channel2-Channel3, etc…). After referencing we inspected visually the data again, since some epileptic spikes can be undetected when looking at raw data. We inspected the data again and removed the trials where epileptic activity was detected.

Finally, since visual inspection can miss some epileptic activity, we performed a time-frequency decomposition on the data for high frequencies, and inspected each trial to see if there was a significant increase of gamma power in some trials that were not frequency-specific and largely exceeded the increase in power of other trials (twice the standard deviation). In the few cases where missing epileptic spikes were detected, the trials were manually removed. After artifact rejection, a file containing the trial numbers of all compromised trials was saved to avoid repeating these steps. This inspection was carried out for all events that were used during our studies.

3.5.Power Analysis

3.5.1. Event-Related Potential (ERP)

We performed a time-locking analysis on the data to detect Event-Related changes in the Local Field Potential (LFP). To this end, we used the pre-processed, artifact-rejected data and applied the fieldtrip function ft_timelockanalysis on the data of each patient. The function corrected the data by subtracting the mean value of the baseline (-0.5 sec to 0 sec relative to stimulus onset) to the data. With this, we obtained an average change of potential relative to baseline for each patient. Patient data was averaged over trials and the event-related potential was observed across patients. We computed the ERP of all events of interest and separated trials by accuracy. Results are provided in Study 1.

3.5.2. Time Frequency Analysis (TFA)

Time-frequency spectral analysis is used to assess the increase or decreases in power by various frequencies as a function of a task. The analysis of frequency decomposition allows for a better understanding of neurophysiological underpinnings when it comes to brain activity. An increase in power is associated with the synchronized activity of several neurons in the same place, and the frequencies determine the nature of that synchronization.

Data analysis of spectral power was performed using Fieldtrip and standard MATLAB functions. Power analysis was computed for each individual and at the trial level for EEG epochs of -2 to +4 seconds from stimulus onset (trigger). After artifact rejection, frequency decomposition of the data was performed via Fourier analysis based on convolution and with a sliding time window (moving forward with 10 ms increments). We applied for low frequencies (4-29Hz) a hanning taper and the time window decreased relatively to frequency (time window = freq / 7, in seconds). For the analysis of high frequencies (30-140Hz), we applied seven orthogonal Slepian tapers and a fixed time window of 50ms, resulting in a spectral smoothing of ~ $\pm$ 10Hz. The resulting power maps were decibel corrected relative to a baseline (-0.5 secs to 0 secs relative to stimulus onset). Given that we did not have enough time during the baseline to compare baseline activity to post-onset activity, to test for significance we used a time-shuffling procedure where each frequency of each trial was time-

shuffled. This means that we randomly selected a point in the frequency time-series creating two pieces of time series. These two data chunks had their orders inverted (the last one became the first and the first became the last), and this procedure was repeated for all trials before baseline correction. We then averaged the time-frequency maps over trials, thus creating a time-frequency map that had a variance, and a mean around 0. This allowed us to perform a non-parametric cluster-based permutation test (Maris & Oostenveld, 2007) using the function permutest (Gerber, 2023). The p-threshold for cluster detection was set as 5% and the test was a two-way test.

3.6. Phase Amplitude coupling

3.6.1. What is phase-amplitude coupling?

Cross-Frequency coupling informs us on how neurons not only behave reacting to an external environment, but also to each other, and how they modulate or self-regulate their activity. An increase in power informs on the synchronization of neuronal activity, but this synchronization may be modulated not only by external environmental factors, but also by internal physiological factors. For example, it is usually considered that slow waves in the brain are more spread out and that high-frequency waves are more local. In this framework, we consider that high-frequency activity may be modulated by low-frequencies. In a neurophysiological perspective, that can happen because a general increase in power and potential mediated by low frequencies, might give an increased probability of firing to a subset of neurons that are rendered more sensitive by the increased general potential. Or on the contrary, some neurons whose inhibition might be mediated by a general increase in potential might become more sensitive when the local potential is lower.

Since low-modulating frequencies are oscillatory, their power (TFA) can be studied, but also their angle. We can then study the interaction of high-frequency oscillations, supposed to be local, with the angle of low-frequency waves. Like-this, we can try to understand if high-frequency activity is more likely to happen only during certain phases of lower frequency and be therefore modulated, or if instead an increase or decrease in power is independent of lower frequencies. This allows us to assess and understand the interaction of neural activity

with internal physiological changes on top of environmental ones – or the ones relative to the task at hand – and the interaction between these two things.

This involves filtering the signal (Figure 3-4.A) and separating low frequencies (Figure 3-4.B) and high frequencies (Figure 3-4. D). Then we extract the angle (in radians) of the Hilbert transform of the filtered phase (Figure 3-4. C) and the square of the Hilbert transform of the amplitude signal (Figure 3-4. E). For a clearer representation of the coupling between low and high frequencies, we can separate the phase angle into 18 equal bins and calculate the mean amplitude per phase bin (Figure 3-4. F). Coupling strength is calculated based on the binned distribution (Tort et al., 2010; Tort et al., 2009) with the Modulation Index (MI), or with the Mean Vector Length (MVL) (Saint Amour di Chanaz et al., 2023). MVL can also directly be calculated on the angle and the amplitude (Canolty et al., 2006) but this can bias the results and in the case of calculating the MVL directly on the phase and amplitude steps must be taken to ensure that the resulting MVL is unbiased (van Driel, Cox, & Cohen, 2015). In our case, we decided to use the MVL because it detects only unimodal distributions (Tort et al., 2010) and we used it on a normalized binned distribution to avoid biases.

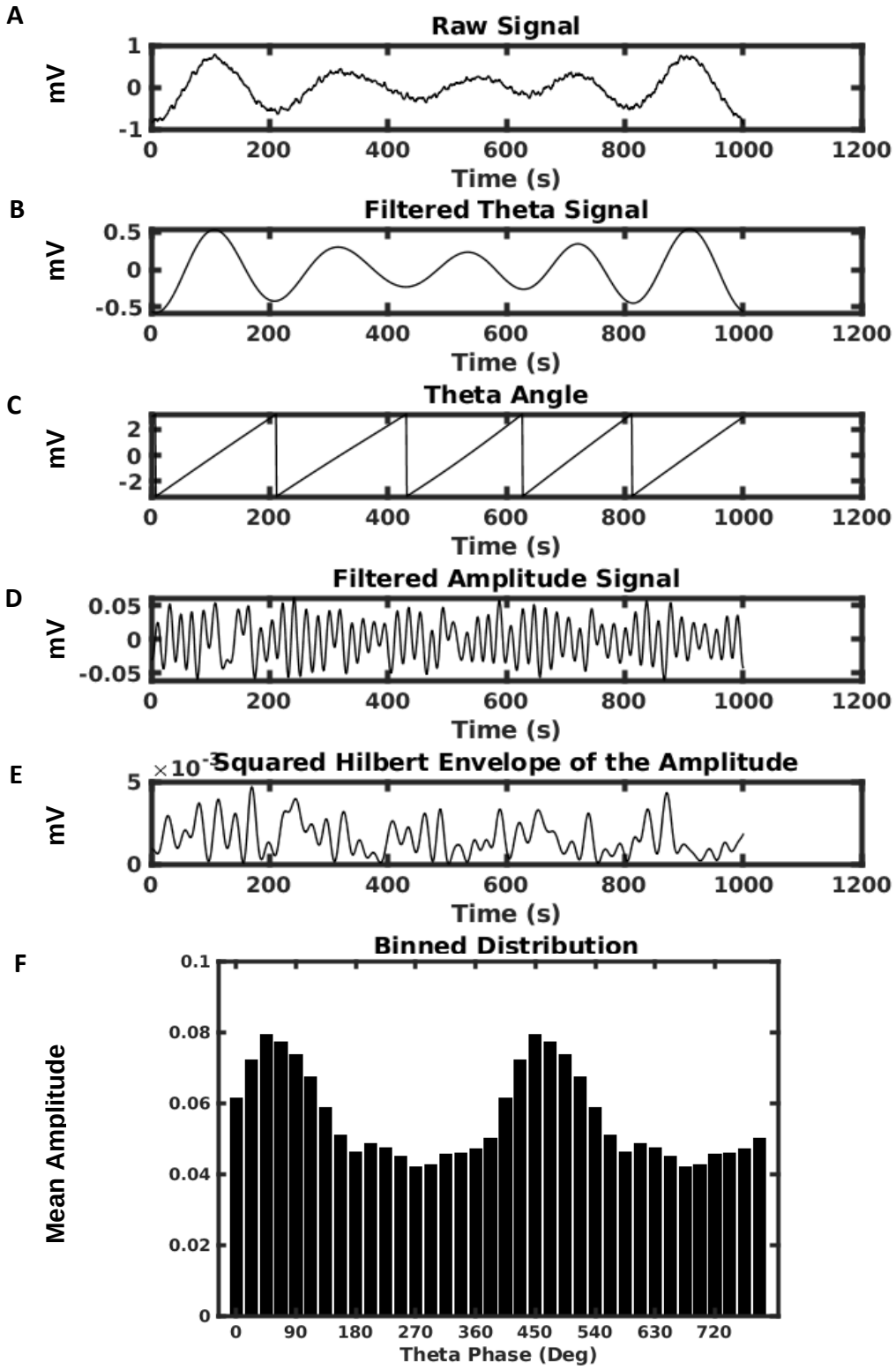

Figure 3-3: Steps in the computation of phase amplitude coupling:

The raw signal (A), here obtained by simulating Cross-Frequency Coupled data (CFC- see study 2) is filtered at the phase (B), and its angle is extracted (C). Then the signal is filtered at the amplitude (D), Hilbert transformed, and the resulting signal is squared (E). The coupling is calculated based on the binned distribution (F).

To perform this analysis we first filtered epochs with the function 'eegfilt' from the EEGLab toolbox of Matlab. Low frequencies (4-12Hz) were filtered with a window of 0.4 times the frequency of interest, centered on each frequency step. For example the filtering window of the frequency of interest 4Hz was between 3.2 Hz and 4.8 Hz, centred on 4Hz. Similarly, high frequencies (30-140Hz) were filtered with a window of 0.7 times the frequency of interest. This allowed for better sensitivity and allowed Δ(hf) to be always bigger than the twice the central low frequency (low frequency *2).

For example if we wanted to assess the coupling between 12 Hz and 40Hz the window of filtering for low frequencies would be from 9.8 Hz to 14.2 Hz, and for high frequencies the delta would be of 28Hz. If we take the delta of high frequencies (Df) as 28Hz (the width of the frequency window for filtering high frequencies), it is bigger than the double of the phase of interest (12 Hz). Because Lf*2 = 24 and Df = 28Hz, hence Df > Lf*2.
This filtering process allows for better precision and avoids biases towards lower modulating frequencies. There are several methods for avoiding such biases. One is to determine the window of interest as a multiplication of the central frequency, like we did, ensuring that the factor of multiplication is lower for low frequencies than for high frequencies. The other is to have a fixed window for low-frequencies and then create the window for high frequencies as a function of the central low frequency, defining it with high_freq-lowfreq to highfreq+lowfreq to always ensure that delta highfreq (Df) is at least the double of the low frequency of interest.

The paper of Aru and colleagues (Aru et al., 2015) underlines the importance of bandwidth, and argues that a fixed bandwidth is not always the best option as it can easily create biases towards lower modulating frequencies. In our case and with the fixed factor of multiplication, we ensured a variable bandwidth of filtering that always respected the delta(hf) > 2*lf rule.

Once we filtered the data, we z-normalized each filtered trial by the mean of all trials in order to avoid having effects driven by spectral increases in power and ERPs. We then extracted the angle of the Hilbert transformation of low frequencies and the square of the absolute value of the Hilbert transform of high-frequency data

Once this was done we binned data: this means that we calculated for each trial the mean amplitude of high frequency for 18 frequency bins of 20 degrees each, thus obtaining a distribution of mean amplitude per phase for each trial. Since we were interested in unidirectional modulations for an event or a task, we averaged the distributions over trials, thus obtaining an average distribution for each patient. We then calculated the Modulation index using the Mean Vector Length method (Canolty et al., 2006) described below.

3.6.2. Choice of Modulation Index

There are many ways to calculate modulation and coupling in a distribution or in a dataset, but there are two main methods that stand out and are more used than the others: The Mean Vector length and the Modulation index by using an adaptation of the Kullback-Leibler Divergence using Shannons's Entropy formula (Tort et al., 2010; Tort et al., 2009). In the case of the MI by Tort in 2009, it is a clever adaptation of the Kullback Leibler Divergence. This formula is usually used to assess the distance between two probabilistic distributions (P and Q whose sum =1

$$DKL\ (P{:}\ Q) = \sum \mathrm{p(x)} * \log \frac{p(x)}{q(x)}$$

But in the case of the Modulation index, it uses Shannon's entropy formula to compare the experimental distribution P to a uniform distribution whose sum =1 and for which each bin has an amplitude equal to 1 over the number of bins. The KL distance formula resembles the definition of Shannon's entropy (H) of a distribution P, defined as such:

$$H(X) = -\sum_{i} P(x_i) * \log P(x_i)$$

DKL is related to Shannon's entropy by the following formula:

$$DKL(P:U) = \log(N) - H(P)$$

Where U is the uniform distribution. Log(N) is the maximal entropy value, which happens precisely for the uniform distribution, or when we have P(j) = 1/N for all bins. Therefore, because H(P) < log(N), the modulation index is the DKL distance of the distribution P from the uniform distribution divided by the log of the number of observations N:

$$MI = \frac{DKL(P:U)}{\log(N)}$$

In the case of the MVL, we transform the distribution of mean amplitude per phase bins into complex polar vectors. Then the sum of these vectors in polar space creates a resultant vector with a unique direction and magnitude. The direction of the polar coordinates of this vector determines the circular angle preference of a distribution. The absolute value of the mean vector is its length, and the mean vector length is predictive of the modulation of a distribution. This is described by the formula below where θ is the angle (in Radians) corresponding to the bin number, n is the bin number, amp is the mean amplitude for the bin n, and N is the number of bins.

$$MVL = \left| \frac{\sum amp_n * e^{(i*\theta_n)}}{N} \right|$$

We decided to use the MVL because the following analysis we performed on most of our data also used vectorization of distributions to assess phase preference (See MOVI section), but

also because during simulation of data for Study 2 we noticed that KLD could give results that were biased for lower modulating frequencies.

A non-uniform distribution can be unimodal (with a single phase preference) or multimodal (with multiple phase preferences). For the way it is computed, the MVL can detect only unimodal phase preferences, as multimodal phase preferences will shift the weight of the mean vectors towards the center and thus reduce its length, and thus the MVL.

On the other hand, DKL is able to pick up on non-uniformity that is multimodal and has various angles of preference. This can be an advantage in some cases, because phase-amplitude coupling can happen at multiple phases for a single event. However, it can also bias results towards lower modulating frequencies. During the simulations done for Study 2, we simulated bimodal distributions by multiplying the frequency of the modulatory sin wave by 2. In this case the resulting distribution can originate from a bimodal coupling to a lower frequency, or to a unimodal coupling of the double of that same frequency. As there is no way to distinguish between the unimodal coupling lf1 *2 and a bimodal coupling of lf, we decided to only look at unimodal couplings. In Study 2, we computed the MVL of the mean distributions for each patient and for each pair of frequency within our interest (phase 4-12Hz, amplitude 30-140Hz).

3.6.3. Single trial PAC and averaging over trials

In the study of Phase-Amplitude Coupling, we saw various types of analysis. One of them is to analyze PAC for each trial and then to average the values of coupling over trials. The other, the one we used, is to average the distributions over trials and then obtain a single PAC value.

These two methods are both valid but they are aimed to explore different questions. On one hand, we explore the coupling of each single trial, therefore the hypothesis is not linked to a particular or common phase preference of the data, but only to a coupling mechanism that can happen with any phase.

This distinction is important, because we can obtain significant results of PAC by studying individual trials if all trials exhibit a significant coupling but are coupled to a different phase. In this case, it means there is a phase-amplitude coupling mechanism going on but no common phase preference. If we analyzed the same data with the other method, we would likely find no significant coupling, because the average distribution would have no clear phase preference, although all trials exhibit PAC individually.

If we are interested in common effects, and the hypothesis, as in the case of our study, is that trials are coupled on average to the same phase, then looking at an average distribution makes more sense. If however, we are interested only in coupling effects and their functioning, independently of the phase preference, the first method is better.

In our case, we chose to average over trials the distributions prior to the calculation of the modulation index, because our hypotheses included a common directionality and phase preference of the effect.

3.6.4. PAC Summary

For our data in Study 1 and to study PAC we filtered low frequencies adding or subtracting 0.2 times the low frequency of interest, and for high frequency adding or subtracting 0.7 times the frequency of interest. We then binned the data into 18 equal bins of 20 degrees obtaining a distribution of mean amplitude per phase bin, and averaged over trials. Then we extracted the mean vector length of the resulting distribution. We corrected our modulation index with time-shuffled surrogate trials.

3.7.Phase Opposition and phase preferences

3.7.1. Studying phase opposition: existing methods

When studying phase coupling we also wondered about common phase preferences. Coupling of high frequencies to different phases of theta, could underlie different mnemonic mechanisms (Heusser et al., 2016), or be reflective of a particular communication between brain areas (Bonnefond et al., 2017). In this case, several methods can detect angular

differences in distributions or in datasets. One way to analyze differences in phase preference is to use Circular statistics (Berens, 2009), and the study of frequency of angles. This technique works much like a t-test but for angular distributions on a polar plane. It takes the frequency of apparition of an angle for a subset of subjects or trials and tests whether the average angular preference of two conditions differ. The disadvantages of this method is that it relies heavily on the number of trials or occurrences of a specific event or condition, and therefore this analysis can create false negatives for experiments with a low number of trials. Additionally, it only has the angle component, which means that each trial or occurrence is summarized to its angle of preference, without taking into account coupling strength. This means that trials with a very low coupling can show a phase preference that could be solely explained by random or common factors in the data.

Another possible method of analysis is Pairwise Phase Consistency (PPC) (Vinck, van Wingerden, Womelsdorf, Fries, & Pennartz, 2010). This method is usually used to measure the consistency of phase consistency or relationship across brain regions but can be used in a variety of ways. It studies the consistency of phase relationships, but in the way that it is calculated, it brings similar challenges than circular statistics. Trials are prepared by transforming them into vectors, and then are unit normalized, meaning that the amplitude of each trial vector becomes unified or equal to 1. By doing so, we suppress again the coupling characteristic of the data.

Similarly, Inter-Trial Coherence (ITC) (VanRullen, 2016) examines the consistency of phase synchronization of oscillatory brain activity across trials or repetitions. But this technique too focuses solely on the phase component, and although it gives a very enlightening insight on the consistency of phase preference across trials, it does not consider coupling strength. This means that it can be used on datasets where experimenters know already that there is a strong coupling happening, but it cannot be used in an exploratory way.
Similarly, Phase-Amplitude-Coupling Opposition Index (PACOI) (Costa et al., 2022) uses an adaptation of the PPC to assess the difference in phase preference between two conditions. PACOI is calculated as such:

$$PACOI = PPC(A) + PPC(B) - 2 * PPC(A + B)$$

Since PPC evaluates the phase consistency of a subset of trials, if datasets A and B have similar phase preferences, then the joint dataset (A+B) will also have a similar phase preference, and PACOI will be closer to 0. On the other hand, if A and B have distinct phase preferences, PPC(A+B) will be closer to 0, and by extension, PACOI will have a higher value.

This technique is very elegant, and is stable with a lower number of trials, because of the properties of PPC (Vinck et al., 2010), but it also does not take into account PAC strength, and is adapted to datasets where we already know coupling is strong, or alternatively, adapted to hypotheses where coupling strength and phase preference are not necessarily connected.

We wanted to study opposition of phase preferences in a way that took into account PAC strength, we developed a method, underlined in Study 2 that answers this problem: The Mean Opposition Vector Index (MOVI), which we used in Study 1.

3.7.2. MOVI and the study of phase Opposition

In the case of our study and the way we computed PAC, we were interested not only in the modulation of our data, and in the study of non-uniformity, but also in the phase preference. The Hasselmo Model (presented in the introduction) states that memory processes might exhibit a gamma-theta phase preference in function of Encoding or Recall.

We aimed at testing this model in humans, and therefore wanted to see if the phase preference of the non-uniform distributions of Encoding had a different phase preference than the non-uniform distribution found during recall processes. To this end, we wanted to find an index that would allow us to explore this hypothesis but that took into account also coupling and non-uniformity of both datasets. We found several ways of comparing the angular preference of distributions but none of them were satisfactory to our goals (see above).

We explored a last method that seemed to reunite several of the criteria we wanted, divergence between two distributions while taking into account PAC strength: The Kullback-Leibler Divergence (KLD). Kullback-Leibler divergence is one of the most widely used methods to assess the distance between two probabilistic distributions and was used to compute the Modulation index (Tort et al., 2010). It calculates the distance between two distributions in the following way:

$$DKL\ (P{:}\ Q) = \sum \mathrm{p(x)} * \log \frac{p(x)}{q(x)}$$

Where p(x) is the value of each bin of distribution P, q(x) is the value of each bin of the distribution Q.

This measure, however, is asymmetrical, meaning that the distance between P and Q is not the same as the distance between Q and P, and it is possible to make it symmetrical considering the Jeffrey's Divergence with the following formula:

$$DKL_{sym} = \frac{DKL(P{:}\ Q) + DKL\ (Q{:}\ P)}{2}$$

This symmetrisation however has been shown to have numerical issues where resulting values were either too high or too low (Nielsen, 2019) and an alternative way to make the measure symmetrical was found.

The Jansen-Shannon Divergence uses DKL formulas to estimate the distance of each distribution to the average between the two distributions in the following way:

$$JSD = \frac{DKL\left(P{:}\ \frac{P+Q}{2}\right) + DKL\left(Q{:}\frac{P+Q}{2}\right)}{2}$$

Where $\frac{P+Q}{2}$ is the average distribution of P and Q. This distance can be interpreted as the total divergence from the average distribution. The important property of the Jensen-Shannon divergence compared to the Jeffrey Divergence is that this distance is always bounded $0 \leq JSD \leq log2$ and solves possible numerical problems given by the symmetrical DKL. In the case of iEEG data and neurophysiological signals we tested JSD (see Study 2) (Nielsen, 2019).

We therefore developed our own index for calculating opposition that relies on an intuitive functioning and that we called Mean Opposition Vector Index (MOVI).

In the case of MOVI, we took the two distributions A and B and created an alternative distribution of amplitude per phase bin based on the difference between the two original distributions with the following formula:

$$D_{alt} = \frac{(D_A - D_B + \frac{2}{nbins})}{2}$$

Where D_A is distribution A, D_B is distribution B and nbins is the number of bins (18 in this case). We then applied the MVL (Canolty et al., 2006; Cohen, 2008) measure to the alternative distribution to assess the strength of opposition between the two distributions for each trial with:

$$MVL = \left| \frac{\sum(amp(x) * e^{i*\theta(x)})}{N} \right|$$

Where amp(x) is the amplitude of each phase bin (x), θ(x) being the phase of each bin (x) and N the number of bins. This vectorized each phase bin and extracted the absolute value of the mean vector which gives the vector length. The longer the vector, the higher the coupling, or in the case of MOVI, the opposition.

We added twice the value of the uniform distribution ($\frac{2}{nbins}$) to avoid having negative values and then divided everything by 2 to have an alternative distribution D_{alt} that had a magnitude of peak to through difference that was the average of the peak to through distance of both distributions. In the case of an opposition of phase preference, the alternative distribution would have a non-uniformity score equal to the sum of the MVL of both distributions, by dividing the alternative distribution by 2 we ensure that the MVL magnitude of this alternative distribution is instead between the MVL of both distributions. This way, we ensure that PAC strength is taken into consideration and we lower the risk of having false positives by not increasing the peak to through difference.

We hypothesized that if two distributions have opposed phase preference the alternative distribution will be unidirectional and non-uniform and will exhibit a strong MVL. On the other hand, if two distributions have the same phase preference, the alternative distribution will be flat and the MVL will be 0. Finally, we ensure to avoid false positives and to take PAC into account because with a lower PAC of both or either distribution, the alternative distribution will also lose in non-uniformity and the MVL will be lower. Finally, MOVI alone could still detect false positives, so we compared its experimental value to surrogate trials. The advantage of using surrogate trials with either MOVI or JSD is that it gets rid of common effects that may be due to an ERP or to phase reset mechanisms, when using a label shuffling procedure (See section on surrogate trials). In this sense, it picks up on opposition of distributions that is specific to the dataset, more so than previously described methods. For the study of phase opposition, we also used surrogate trials. To do so we computed the surrogate trials of each distribution separately and then compared the two surrogate distributions in the same way as the experimental one.

4. Chapter 4: Study 1

Measuring phase-amplitude coupling opposition in neurophysiological signals with the Mean Opposition Vector Index (MOVI)

Please Note: This study has been published on BioRxiv on the 4th of August 2023
https://www.biorxiv.org/content/10.1101/2023.08.04.551929v1

4.1.Abstract

Background: The phase–amplitude coupling (PAC) opposition between distinct neural oscillations is critical to understanding brain functions. Available methods to assess phase-preference differences between conditions rely on density of occurrences. Other methods like the Kullback-Leibler Divergence (DKL) assess the distance between two conditions by transforming neurophysiological data into probabilistic distributions of phase-preference and assessing the distance between them. However, these methods have limitations such as susceptibility to noise and bias.

New Method: We propose the "Mean Opposition Vector Index" (MOVI), a parameter-free, data-driven algorithm for unbiased estimation of PAC opposition. MOVI establishes a unified framework that integrates the strength of PAC to account for reliable unimodal differences in phase-specific amplitude coupling between neurophysiological datasets.

Results: We found that MOVI accurately detected phase opposition, was resistant to noise, and gave consistent results with a low or asymmetrical number of trials, therefore in conditions more similar to experimental studies.

Comparison with existing methods: MOVI outperformed Jensen-Shannon Divergence (JSD), an adaptation of the DKL, in terms of sensitivity, specificity, and accuracy to detect phase opposition.

Conclusions: MOVI provides a novel and useful approach to the study of phase-preference opposition in neurophysiological datasets.

4.2.Introduction

Neurophysiological data exhibits oscillations of different frequencies, which may co-occur and also interact with one another (Hyafil et al., 2015; Jensen & Colgin, 2007; Tort et al., 2010). Among the various forms of coordination, phase-amplitude coupling (PAC) stands out as the most widely acknowledged as it can be detected throughout the brain in animal studies (Jensen & Lisman, 1996; Pavlides et al., 1988; Tort et al., 2008) and human brain recordings, using techniques such as electroencephalography (EEG) (Axmacher et al., 2010; Canolty et al., 2006; Tort et al., 2009), magnetoencephalography (MEG) (Fuentemilla et al., 2010) and local field potential (LFP) recordings (Rutishauser et al., 2010; Saint Amour di Chanaz et al., 2023). PAC involves the interaction between the phase (the timing) of low-frequency brain oscillations and the amplitude (the strength) of higher-frequency oscillations and outlines that information coding in the brain involves more than just individual neuron action potential firing, but the brain's extracellular field potential oscillations serve as temporal reference to aid efficient information processing by the spiking activity of the neural ensembles.

The best studied-example is the coupling of the ongoing theta (3-8Hz) and the amplitude of gamma oscillations (>30Hz) (Bragin et al., 1995; Buzsaki, 2002; Tort et al., 2008) Theta-gamma PAC has been reported in a variety of species, brain regions and experimental conditions (Axmacher et al., 2010; Giraud & Poeppel, 2012; J. E. Lisman & Jensen, 2013), and theoretical work has suggested hippocampal theta-gamma PAC supports a neural coding regime to support mnemonic operations (Colgin, 2015b) and spatial navigation (Huxter et al., 2008; Jensen & Lisman, 1996; O'Keefe & Burgess, 2005; Tsodyks, Skaggs, Sejnowski, & McNaughton, 1996). The importance of theta-gamma PAC is that the mechanisms behind it provide valuable insights into how the brain processes and represents information. For example, influential computational models, supported by empirical findings in rodents (Bragin et al., 1995; Colgin et al., 2009) and in humans (Kunz et al., 2019; Pacheco Estefan et al., 2021) posit that theta-nested gamma oscillations may allow the hippocampal network to temporally organize sequences of events within each theta cycle (J. Lisman, 2005; J. E. Lisman & Idiart, 1995; J. E. Lisman & Jensen, 2013; O'Keefe & Recce, 1993) Other models, also supported by empirical data in rodents (Bieri et al., 2014; Colgin et al., 2009; Douchamps, Jeewajee, Blundell, Burgess,

& Lever, 2013; Fernandez-Ruiz et al., 2017; Lever et al., 2010; Manns et al., 2007; Pavlides et al., 1988; Poulter, Lee, Dachtler, Wills, & Lever, 2021) and in humans (Saint Amour di Chanaz et al., 2023), propose that gamma couples to opposed-phase states of the ongoing hippocampal theta rhythm activity during memory encoding and during retrieval (Hasselmo et al., 2002). Together, these findings underscore that neural oscillations have broader implications than just PAC alone. Taking the phase preference of PAC into account is critical, as it significantly influences the organization and processing of mnemonic information in the brain. Therefore, it becomes essential to incorporate analytical tools that can effectively characterize differences in phase preference within PAC across neural states.

There are several quantitative approaches to identifying phase preference within PAC and how phase preference within PAC differs or opposes across neural states or experimental conditions. Some of these methods rely on the existence of PAC and aim at detecting phase-preference differences between two conditions. Analytically, these methods, such as the Inter-Trial Phase Coherence (ITPC); (VanRullen, 2016), are used to estimate the average angular degree of incidences in which each trial is summarized into a single vector with a phase preference and then the angles of the vectors are compared to a uniform polar distribution or to another subset of trials. These methods rely, therefore, on density of occurrences. An important limitation in the context of detecting phase preference within PAC, however, is that these approaches do not consider coupling strength of angle preference as each trial, or observation is summarized into a unit-normalized vector. Thus, while these methods are suitable to quantify phase clustering across trials or observations, they undermine the possibility that phase preference could be brought by weak or even non-meaningful amplitude modulations. In these cases, these indexes could still provide non-random phase clustering values but that would compromise the interpretability of the underlying neural mechanisms.

Neurophysiological data can also be analyzed using PAC methods implemented separately into equal phase bins. In PAC analysis, phase bins are used to divide the phase values of low-frequency oscillations (e.g., theta) into equal intervals or segments. These intervals represent different phase angles that cover the entire 360-degree range of a circular distribution. For

each bin, the mean amplitude is calculated, resulting in a distribution of amplitude per phase. This process combines the time series of phase and amplitude into a single distribution of amplitude per phase, capturing both components without losing information about the variability of amplitude phase-preference. The method involves taking the time-series of the filtered amplitude and phase, identifying time-points corresponding to specific phase ranges based on the number of bins, and then averaging the amplitude time-points to obtain a single average amplitude measure for each phase bracket. The distributions obtained from the data can be studied using different methods, such as the Kullback-Leibler Divergence (DKL). DKL is a commonly used method in fields like genetics (Akhter et al., 2017) and engineering (Ji et al., 2022) to measure the distance between two probabilistic distributions. However, a limitation of DKL is that it is not symmetric in comparing distributions (Nielsen, 2019). This means that the distance between distribution A to B is not the same as the distance from distribution B to A, which can lead to asymmetrical results when comparing distributions using DKL.

The Jensen-Shannon Divergence (JSD) overcomes the asymmetry limitation of the DKL by providing a symmetrical measure (Nielsen, 2019). It calculates the distance between the mean distribution of two datasets (A and B) and then compares each dataset to the mean distribution, resulting in a symmetrization of the DKL. However, JSD uses a logarithmic transformation, making it more suitable for detecting average differences between distributions rather than those driven by a single-phase preference. Another shortcoming of JSD is it has the capability to detect multimodal differences in phase preference, which can be problematic. If one or both distributions exhibit multiple peaks of phase preference (multimodal), JSD might identify a difference even in situations where it may not reflect a clear phase preference. For example, if high-frequency activity is coupled to 8Hz at one specific phase (unimodal), JSD may erroneously indicate a bimodal coupling at 4Hz with two peaks of phase preference. This sensitivity to multimodal distributions is not ideal when assessing phase-preference differences, as it can lead to misinterpretations and biases, especially towards lower modulating frequencies.

To address the limitations of the JSD in assessing uniform and unimodal opposition in phase preference, we developed a new algorithm that uses the Mean Vector Length (MVL) measure (Canolty et al., 2006) and creates an alternative distribution from the difference of the two

distributions being compared. By applying the MVL to this new distribution, we can detect a uniform and unimodal opposition in phase preference while considering phase-amplitude coupling strength. We refer to this index as Mean Opposition Vector Length (MOVI), and we will detail below its premises, assumptions, and usefulness when working with neurophysiological data. In this study, we will compare MOVI against JSD, which encompasses most of the criteria we wanted to assess phase-opposition by considering coupling strength, not risking having abnormally high or low numerical values like Jeffrey's Divergence, and symmetry in the sense that the distance between A and B would be the same as the distance between B and A. We will contrast their differences in terms of sensitivity and specificity (Trevethan, 2017), calculate their predictive value, and assess accuracy and Matthews Correlation Coefficient (MCC) (Chicco, Totsch, & Jurman, 2021) on simulated data, where we will manipulate different variables and parameters that can be found in neurophysiological data such as PAC strength, noise, opposition angle, number of trials, and inter-trial phase coherence. Matlab scripts to produce the simulations and perform the analyses described in this paper are available at Github: https://github.com/DMFresearchlab/MOVICode

4.3.Material and Methods

4.3.1. Synthetic data generation

We simulated datasets containing two phase-coupled trial distributions. For both distributions, we simulated a time series of coupled low and high frequencies. The frequency sampling of these time-series was of 1000 Hz and we simulated 2500 time points, or the equivalent of 2.5 sec epochs. When generating our datasets we simulated each trial independently using the formulas provided by (Tort et al., 2010) and adding variable parameters to control for coupling angle for each distribution. We simulated a baseline of 50 trials, and each trial was composed of a pair of frequencies, a frequency for phase ($f(p)$) and a frequency for amplitude ($f(a)$). We also took into account the filtering parameters, and hence simulated the central frequencies of interest (f) as well as the low and high limits of the frequency window $f(a) \pm f(a) * 0.35$ for amplitude and $f(p) \pm f(p) * 0.2$ for phase. All trials were simulated in the following way:

$$Raw\ Data = Signal(p) + Signal(amp) * Signal(mod) + noisephy + pinknoise$$

where

$$Signal(p) = f(p) * \sin(Ang_{start(p)} + 2 * \pi * f(p) * time)$$

and

$$Ang_{start} = A_s + R_a[a_l : a_h]$$

The starting angle of each frequency was determined by the sum of a fixed starting angle A_s and a random angle R_a between a lower limit a_l and a higher limit a_h. The random angle made each trial slightly different within each condition but within a fixed angle range. We wilfully introduced this noise to have a similar phase preference across trials and to try to replicate real neurophysiological data where different trials do not have the exact same characteristics. It also helped to ensure that each trial was different to justify correction by surrogate trials. Without the random angle, all trials would have been identical, and averaging over trials would be the same as having one single trial. In this case, the correction by surrogate trials would also have been unnecessary.

$Signal(amp)$ was generated in the same way as $Signal(p)$ but with a beginning angle specific to amplitude $Ang_{start(amp)}$.

$Signal(mod)$) is the modulatory signal of amplitude responsible for cross-frequency coupling mechanisms and it was defined in the following way:

$$Signal(mod) = \frac{\sin\left(A(p) + Ang_{start(mod)} + 2 * \pi * f(p) * time\right) * (1 - \chi) + 1 + \chi}{2}$$

where $A(p)$ is the fixed starting angle for phase to ensure that the modulation of the signal is locked to the phase for each trial. $Ang_{start(mod)}$ is the starting angle specific to modulation and relative to the phase angle where the modulation can happen in phase or out of phase with the low frequency. χ is a coupling factor between 0 and 1, where 1 is no coupling and 0 is perfect coupling. The modulatory *sin* wave always ranges between 0 and 1 and by multiplying the amplitude time series with the modulatory time series we ensure that we obtain a high frequency coupled to the frequency of the modulatory wave.

Noise adding uncoupled low and high frequencies to simulate as closely as possible noise that is likely to be found in real neurophysiological data. First, we ensured that the raw signal was slightly different for every trial by adding a low-frequency wave with a random starting angle, and a non-modulated high frequency wave. Then, pink noise (van Driel et al., 2015) was added with an amplitude of the noise signal being equivalent to the amplitude of the coupled high-frequency signal. We then computed MOVI and JSD on simulated data with these characteristics 100 times, which emulated an experiment with 100 synthetic participants, each with the same number of trials and the same settings. Knowing beforehand the degree of coupling and opposition allowed us to know the ground truth and benchmark the different methods used to assess for opposition. Since within the settings, there was randomness added with a random starting angle within a fixed angle window or with physiological-like noise it ensured that each synthetic participant was different. This allowed us to have a distribution of the MOVI and JSD scores to assess also how much variability there was in the indexes and if any factor or setting particularly influenced sensitivity or specificity. When the degree of angle opposition was not parametrically manipulated, the two datasets had an

opposition of 0° (non-opposed) or 180° (completely opposed). When not manipulated, PAC strength of both distributions was average and fixed, both distributions had 50 trials and each trial had a randomness of inter-trial coherence of 180°, meaning that all trials had a phase preference that was within ±90 degrees from the manually determined angle of coupling.

4.3.2. Pre-processing of the signal

Each trial of raw data was filtered using the eegfilt function of EEGlab (Delorme & Makeig, 2004). The window of the frequency of interest (f) was determined as well as $f(a) \pm f(a) * 0.35$ for amplitude and $f(p) \pm f(p) * 0.2$ for phase. Filtering was done on longer epochs that were then cut to fit the desired number of time points, removing any filtering artifacts. The filtering window increased with frequencies for both phase and amplitude extraction in order to avoid biases toward lower modulating frequencies and ensuring that the window of filtered high frequencies was always superior to twice the phase of locking: $\Delta_{amp} > 2 * phase$ (Aru et al., 2015). Then we extracted angles of phases for low-frequencies, and we extracted the absolute value of the square of the Hilbert envelope of amplitudes for high frequencies. Epochs were then binned in 18 equal bins of 20° (Tort et al., 2010). Each trial was then converted to a probabilistic distribution where sum = 1 by dividing the amplitude of each bin by the sum of all bins. Subsequently, we used these bins to calculate JSD and MOVI between different trial conditions.

4.3.3. JSD calculation

JSD requires the extraction of the DKL index, which is described as follows:

$$DKL\ (P{:}\ Q) = \sum \mathrm{p(x)} * \log \frac{p(x)}{q(x)}$$

where $p(x)$ is the value of each bin of distribution P, $q(x)$ is the value of each bin of the distribution Q. This measure, however, is asymmetrical, in the sense that $DKL\ (P{:}\ Q)$ is different than $DKL\ (P{:}\ Q)$. This is problematic in the sense that to assess distance or opposition of angles it is important that the choice of comparison order (distance from P to Q or from Q to P) does not alter the results. It is possible to make DKL symmetrical considering Jeffrey's Divergence (Nielsen, 2019) with the following formula:

$$DKL_{sym} = \frac{DKL(P:Q) + DKL\,(Q:P)}{2}$$

This symmetrization, however, has been shown to have numerical issues where resulting values were either too high or too low (Nielsen, 2019) and an alternative approach to make the measure symmetrical was developed using the Jensen-Shannon Divergence. The Jansen-Shannon Divergence uses DKL formulas to estimate the distance of each distribution to the average between the two distributions in the following way:

$$JSD = \frac{DKL\left(P:\frac{P+Q}{2}\right) + DKL\left(Q:\frac{P+Q}{2}\right)}{2}$$

where $\frac{P+Q}{2}$ is the average distribution of P and Q. This distance can be interpreted as the total divergence from the average distribution. The important property of the Jensen-Shannon divergence compared to the symmetrical DKL is that this distance score is always bounded $0 \leq JSD \leq log2$ and reduces biased opposition estimated given by the symmetrical DKL.

4.3.4. MOVI calculation

To calculate MOVI, like in JSD, we used the MVL on an alternate distribution made with the distributions A and B as explained below. First, we averaged the trial distributions of A and B to have a single distribution that was descriptive of common PAC effects and that shared a common direction. By doing so, if all trials exhibited strong PAC but each of them had their amplitude coupled to a different phase of low frequencies, the average distribution was flat, and no PAC would be detected. Measuring PAC on the average distributions instead of doing it at the trial level allows for a measure of phase-amplitude coupling across trials that share a direction preference and prevent sensitivity to spurious trial-level PAC that might not systematically rely on the same phase preference. In sum, averaging over trials is important because MOVI aims to detect phase-preference opposition between two conditions, and we need common directional effects of two distributions to assess opposition. For MOVI to be significant there needs to be a consistency in phase preference across trials (ITC) but also a

consistency of coupling strength (PAC), and that this be the case for both compared distributions. If all trials are strongly coupled but each to a different phase in one or both distributions, MOVI will not be significant. Similarly, if all trials have a consistent phase preference in both distributions but a weak coupling, MOVI will also not detect opposition. We performed these steps for two distributions that had either similar or opposed angles of phase preference. Both averaged distributions were then converted to a probabilistic distribution (sum = 1) before comparing them with the different techniques.

To compute MOVI, we took the two distributions A and B obtained after the implementation of pre-processing stage and created an alternative distribution (D_{alt})of amplitude per phase bin based on the difference of the two original distributions with the following formula:

$$D_{alt} = \frac{(D_A - D_B + \frac{2}{nbins})}{2}$$

where D_A is the distribution of A trials, D_B is the distribution of B trials and $nbins$ is the number of bins (18 in this case).

We then obtained the MVL measure (Canolty et al., 2006; Cohen, 2008) to the alternative distribution D_{alt} to assess the strength of opposition between the two distributions averaged over trials.

$$MVL = \left| \frac{\sum(amp(x) * e^{i*\theta(x)})}{N} \right|$$

where $amp(x)$ is the amplitude of each phase bin (x), $\theta(x)$ being the phase of each bin (x) and N the number of bins. This process vectorized each phase bin and extracted the absolute value of the mean vector, which gives the vector length. The longer the vector, the higher the coupling, or in the case of MOVI, the opposition.

We added twice the value of the uniform distribution ($\frac{2}{nbins}$) to avoid having negative values and facilitate the normalization of the distribution into a probabilistic one (sum = 1). Then, we divided everything by 2 to have an alternative distribution D_{alt} that had a peak to through difference magnitude equivalent to either distribution. In the case of opposition in phase

preference, D_{alt} would have a non-uniformity score equal to the sum of the MVL of both distributions, by dividing the alternative distribution by 2 we ensure that the MVL magnitude of this alternative distribution is instead between the MVL of both distributions. This way, we ensure that PAC strength is taken into consideration, and we lower the risk of having false positives by not increasing the peak to through difference.

We hypothesized that if A and B distributions have opposed phase preferences, the alternative distribution would be unidirectional and non-uniform and would exhibit a strong MVL (Figure 4-1 A). On the other hand, if distributions A and B have the same phase preference, the alternative distribution would be flat and the MVL would be 0 (Figure 4-1 B). In the case of both A and B distributions showing a weak PAC, even in conditions where the phase preferences were opposed between two, MOVI would be small. MOVI, therefore, ensures that phase opposition would be statistically significant only when the two distributions showed a solid phase opposition and a strong PAC.

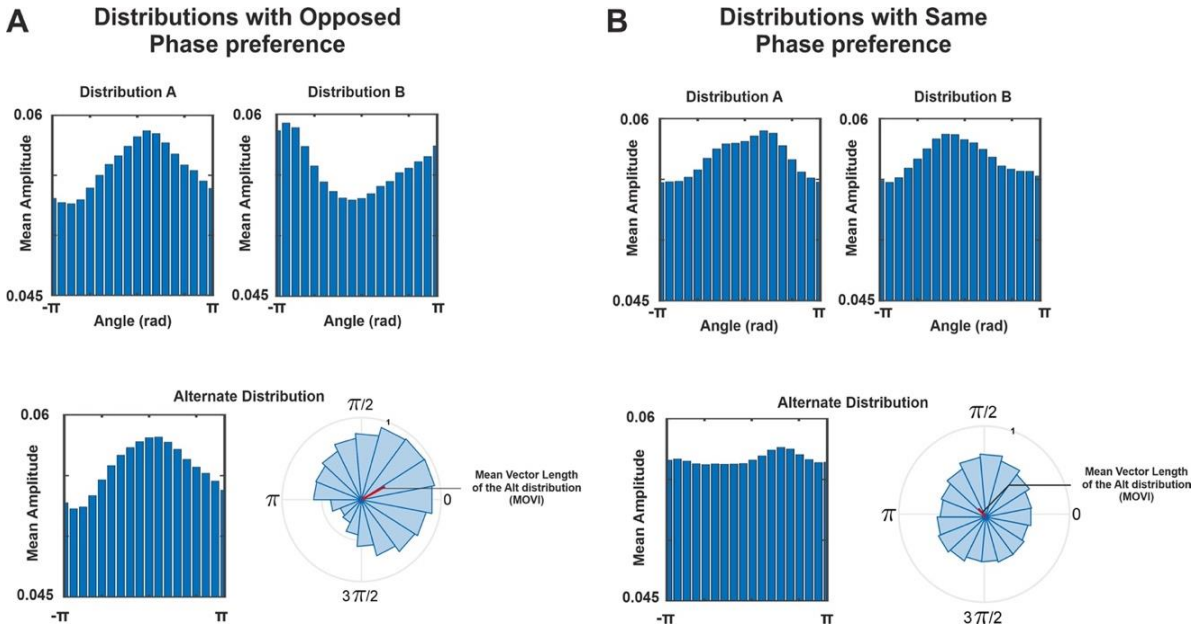

Figure 4-1: Schematic representation of MOVI

*(**A**) Distributions A and B exhibit high PAC and opposed phase preference. The alternate distribution exhibits a strong preference. The high MVL value of the alternative distribution indicates opposition of phase preference between distributions A and B. (**B**) Distributions A and B exhibit high PAC but the same phase preference. The alternate distribution thus shows no phase preference and is flat. MOVI has a low value and indicates that distributions A and B are not opposed.*

4.3.5. Statistical analyses

The statistical assessment of MOVI and JSD involves constructing a null distribution employing surrogate trials, which are alternative trial distributions with shared variance. These surrogate trials are utilized to consider any common effects observed in the experimental data. This non-parametric approach results in surrogate trials having a MOVI or JSD score that is normally distributed around a mean. The assessment of the significance of the experimental value is done by comparing that experimental value to the distribution of the surrogate values.

For each comparison of A and B using either MOVI or JSD, where a comparison is made for every specific set of variables (angle, PAC strength, frequency, ITC, etc) we computed 1000 surrogate trials for each condition A and B. Surrogate trials may be calculated in two ways. First, label shuffling, which consists of shuffling the labels of amplitude trials before binning. Label shuffling creates a surrogate distribution that corrects for neural responses not necessarily related to phase-amplitude coupling (e.g., ERPs or phase resetting) but loses individual coupling that is more specific to each trial. Second, time-shuffling, which involves the random division of each amplitude trial into two segments, with the subsequent inversion of the order of the time-series chunks within the trial. This way a random coupling would be created. However, this method is less conservative, as it does not account for effects that might be driven by an ERP or a phase reset mechanisms. In general, both of these surrogate trial creation methods yield highly comparable outcomes, and the decision to prefer one over the other primarily depends on the extent to which one desires or requires control over ERP or phase-reset driven effects. Although we did not expect to observe results driven by phase-reset in synthetic data, we here used the label-shuffling method as this would control for these effects on real neurophysiological data. Therefore, we shuffled the labels of amplitude trials and randomly matched them with phase trials before binning and averaging the binned distributions over trials. Once an average null distribution was generated for each of the two experimental conditions, we calculated the MOVI and JSD index in the same way as for the non-shuffled trials.

When conducting a test for MOVI or JSD statistical significance for a single pair of frequencies, we compared the experimental value of MOVI or JSD to the respective distributions of surrogate scores. We considered a test to be significant if the experimental score was higher than 95% of the surrogate scores. The p-value was calculated as 1 minus the proportion of surrogates lower than the experimental value. We computed this for 100 artificial subjects to see consistency of testing and false alarm or false negative rate when varying parameters in the simulation like PAC strength, or opposition angle.

4.3.6. MOVI and JSD comparison

Using synthetic data is useful to quantify the efficacy of MOVI against the JSD approach because it allows us to predefine the ground truth (i.e., opposition or not) and objectively estimate the difference in sensitivity (proportion of positive tests for truly opposed distributions) and specificity (percentage of negative tests for non-opposed distributions) for both methods of analysis as a function of different parameter manipulations. We compared MOVI and JSD by calculating the proportion of hits (significant opposition when actual opposition exists) and the proportion of false alarms (significant opposition when no actual opposition exists), as a function of the manipulation of i) PAC strength of both or either distribution, ii) angle of opposition between the two distributions, iii) a number of trials, iv) inter-trial coherence, and v) noise strength.

Results are displayed using a 2D matrix that shows the proportion of how often a test is significant given a specific set of variables for both MOVI and JSD. To estimate the sensitivity of a measure, we quantified how well MOVI or JSD identified true positives (characterizing type I error). To quantify the specificity, we quantified how well MOVI or JSD identified true negatives, or the absence of false positives (characterizing type II error). In other words, when we observe false positives, specificity decreases and type II error increases. The hits and false alarms matrices were then compared to see if there was a significant difference in sensitivity and specificity between both opposition measures using a binomial test. P-values were obtained for each combination of variables (PAC, Angle, number of trials, etc.). A $p < 0.05$ was used to threshold statistical significance. However, we used a Bonferroni correction to compensate for multiple comparisons, and showed only the values that survived the

correction. In the results section we report the minimum and maximum significant t and p-values in each matrix.

We also computed the average Positive Predictive Value (PPV) of the matrices for each index and generated a PPV and a Negative Predictive Value (NPV) matrix for each index and taking as observation the individual voxels of each matrix. We then compared these values with a t-test with the degrees of freedom being equal to the number of voxels per matrix -1 (in this case df = 24). PPV is the ratio of true positives over the number of total positive tests. It ensures that an increase in sensitivity in a test that likely induces more false positives does not result in a too steep decrease in specificity (Trevethan, 2017). PPV is the probability of having a real effect if the test is positive. For example, a PPV of 0.97 states that a positive test has a 97% chance of being a true positive rather than a false positive. PPV is linked with the false discovery rate (FDR) as FDR = 1-PPV and PPV = 1-FDR, where FDR is the ratio of true positives overall positive tests.

The PPV is calculated as:

$$PPV = \frac{True\ positives}{True\ positives + false\ positives}$$

The average PPV was calculated for both each value of the 2D result matrices that resulted from MOVI and JSD approach and then compared with a repeated measures t-test. Similarly, we calculated the NPV that assesses the probability of an effect being truly negative given a negative test. NPV is linked with the False Omission Rate (FOR) as NPV = 1-FOR and FOR = 1-NPV, where FOR is the ratio of False Negatives overall negative tests. To assess how a test correctly identifies positive and negative outcomes, we also calculated the Accuracy as:

$$Accuracy = \frac{TP + TN}{P + N}$$

Where TP are true positives, TN are true negatives, P are all positive tests and N are all negative tests. Finally, we can assess an index performance with Matthews Correlation Coefficient (MCC) (Chicco et al., 2021) that has a value between -1 and 1. Since MCC is a measure that encompasses performance and bias, a value of 1 would mean that the test

detects all the effects with no bias, while a value of -1 would be a test that does not detect effects at all and has only biases or false discoveries. MCC is calculated as follows:

$$MCC = \frac{Cov(c,l)}{\sigma_c * \sigma_l} = \frac{TP * TN - FP * FN}{\sqrt{(TP + FP) * (TP + FN) * (TN + FP) * (TN + FN)}}$$

where $Cov(c,l)$ is the covariance of true classes c and predicted labels l, and σ_c and σ_l are their standard deviations, respectively. The MCC is related to the other measures we explained below as:

$$MCC = \sqrt{PPV * TPR * TNR * NPV} - \sqrt{FDR * FNR * FPR * FOR}$$

where TPR is the true positive rate, TNR true negative rate, FNR is the false negative rate, FPR false positive rate (Chicco et al., 2021).

4.4.Results

We simulated different conditions that typically happen and constrain the capacity to detect phase opposition by inflating Type I or Type II error rates in experimental setups, like the number of total trials per condition and the asymmetry of number of trials between conditions. Additionally, we simulated different conditions by manipulating simulation parameters to affect PAC strength, noise strength, and angle of opposition.

4.4.1. Testing distance measures sensitivity as a function of PAC and noise strength

In our first simulation, we explored the effect of PAC strength and the strength of pink noise. In our first simulation, we calculated MOVI and JSD on a continuous scale of PAC strength and pink noise ranging from the no PAC to a strong PAC. Figure 4-2 shows the number of significant hits over 100 simulated participants in case of opposed or non-opposed datasets.

With perfectly opposed distributions, MOVI is significantly more sensitive, and detects more easily opposed distributions than JSD. MOVI is capable of detecting opposition at lower levels of PAC compared to JSD.

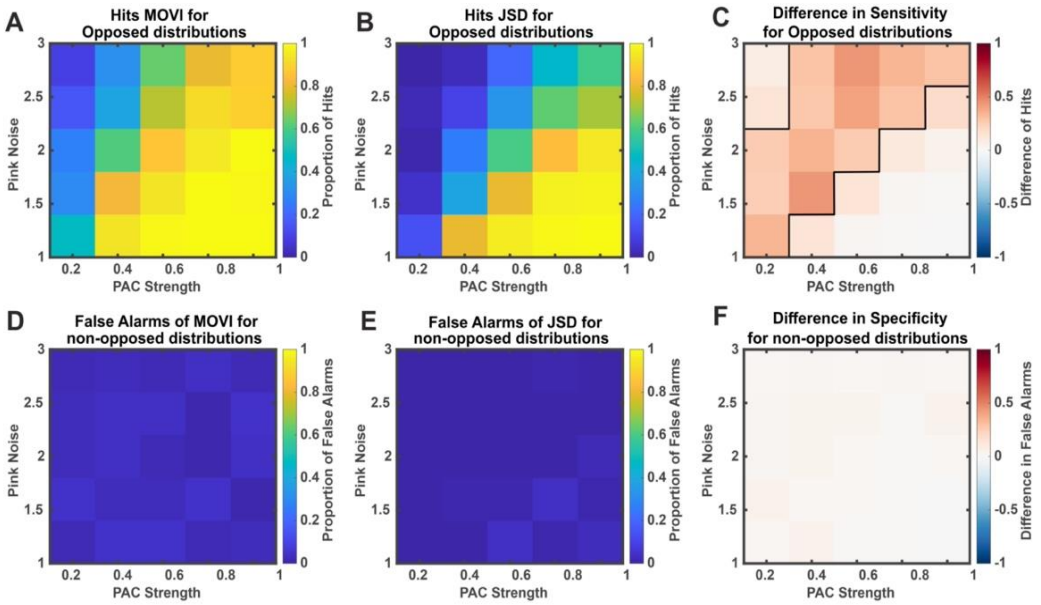

Figure 4-2: Hits and false alarms for MOVI and JSD in function of PAC and Pink Noise strength in Opposed and non-opposed distributions

*(**A**) Proportion of Hits for MOVI on opposed distributions as a function of PAC strength and Pink Noise Strength. (**B**) Proportion of Hits for JSD on opposed distributions as a function of PAC strength and Pink Noise strength. (**C**) Difference in sensitivity between MOVI and JSD. A Binomial test was performed, and p-values were corrected with a Bonferroni correction. Threshold of p-values was a 0.05. For Opposed Distributions, MOVI is significantly more sensitive than JSD for the settings within the cluster delimited by the dark line. (**D**) Proportion of False Alarms for MOVI for non-opposed distributions as a function of PAC strength and pink noise strength. (**E**): Proportion of False Alarms for JSD for non-opposed distributions as a function of PAC strength and pink noise strength. (**F**): Difference in Specificity (1-False Alarms) between MOVI and JSD. No significant difference was detected between the two indexes.*

We observed that both MOVI and JSD detected opposition with strong PAC with low noise and opposition (Figure 4-2A and B**)** but not when the distributions have the same phase preference (Figure 4-2D and E). However, MOVI outperformed JSD to detect phase opposition at smaller PAC strength values and continued detecting phase opposition in conditions of

larger noise values. MOVI exhibited a significantly higher sensitivity than JSD in those higher noise conditions as shown by the black line delimiting the cluster of values that survived correction depicted in Figure 4-2C (within cluster, binomial test, t_{min} = 3.49, p = 0.018, t_{max} = 6.04, p < 0.01). Furthermore, we calculated the average Positive Predictive Value of both indexes (see Methods) and across the matrices both indexes did not differ significantly in the average PPV (average PPV for MOVI = 0.94, average PPV for JSD = 0.97, t-test: t = -1.5, p = 0.11, df = 24). However, MOVI had a significantly higher NPV (MOVI NPV = 0.81, JSD NPV = 0.72, t-test: t = 7.24, p < 0.01, df = 24), thereby indicating it detected less false negatives than JSD. The accuracy of MOVI and JSD was 0.84 and 0.75 respectively, meaning that MOVI was more accurate in the detection of true positives and true negatives than JSD. The MCC of MOVI and JSD was 0.80 and 0.70 respectively. In these simulated conditions, a result from MOVI is more likely to detect a real effect and is less biased than JSD.

4.4.2. Testing distance measures sensitivity as a function of angle difference and noise strength

In the previous test, we showed that MOVI was more sensitive in identifying phase opposition compared to JSD with lower levels of PAC and at lower signal-to-noise ratio. Here, we examined whether these two methods differed in their sensitivity to phase opposition as a function of the degree of angle difference between two distributions and noise. To test this issue, we fixed PAC strength at a value of 0.4 where MOVI and JSD had a sensitivity and specificity that did not significantly differ (Figure 4-2C and F) and took angle difference as a variable. We generated various datasets by simulating angle differences in steps of 45 degrees, ranging from 0 to 180. Consequently, when the angle difference was 0, the distributions exhibited an identical phase preference, whereas with an angle difference of 180, the distributions displayed an opposite phase preference.

Results are depicted in Figure 4-3, where statistically significant differences (p < 0.05, corrected) between MOVI and JSD are outlined with a black line. Our results showed that MOVI was significantly better than JSD in detecting phase opposition, particularly when the angles of difference were smaller and in conditions of greater noise in the signals (within cluster, t_{min} = 3.39, p = 0.017, t_{max} = 5.25, p < 0.01, df = 24). Neither MOVI nor JSD detected

phase opposition when there was none (Figure 4-3A and B), but JSD required less noisy data and greater angle difference between the distributions to detect phase opposition (Figure 4-3C). For higher noise values and phase preference differences starting at 90 degrees, MOVI exhibited greater sensitivity compared to JSD. In this test, we refrained from calculating the PPV, NPV, Accuracy, and MCC of the indexes. This decision was based on the difficulty of determining what constitutes a true positive or a true negative in the context of angle opposition variations. For instance, when the distance is 90 degrees, it is not possible to definitively classify the distributions as opposed or non-different.

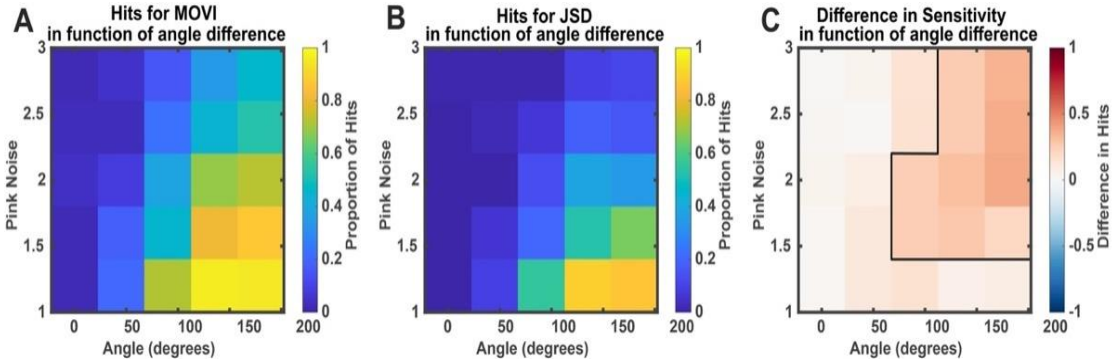

Figure 4-3: Hits for MOVI and JSD in function of angle difference between two distributions.

*(**A**) Proportion Of positive tests for MOVI as a function of angle difference between the two distributions and pink noise strength. (**B**) Proportion Of positive tests for JSD as a function of angle difference between the two distributions and pink noise strength. C: Difference in sensitivity between MOVI and JSD. A Binomial test was performed and p-values were corrected with a Bonferroni correction. Threshold of p-values was set at 0. For Opposed Distributions, MOVI is significantly more sensitive than JSD for the settings within the cluster delimited by the dark line that are higher noise strength and lower angle differences.*

4.4.3. Are the number of trials important for MOVI and JSD?

We examined whether the sensitivity of MOVI and JSD changed as a function of number of trials. We simulated datasets with an increasing number of trials in both conditions (from 10 to 50 with increments of 10 trials) and calculated MOVI and JSD accordingly.

Results are depicted in Figure 4-4, where statistically significant differences at the cluster level ($p < 0.05$, corrected) between MOVI and JSD are outlined with a black line. Our findings revealed that MOVI was capable of detecting phase opposition even with a smaller number of trials (Figure 4-4A), whereas JSD necessitated a higher number of trials in both conditions to detect phase opposition (Figure 4-4B). However, both indexes faced challenges in detecting phase opposition when both distributions consisted of only 10 trials. This implies that despite the superior sensitivity of MOVI compared to JSD, a substantial number of trials is still necessary to conduct the test effectively with MOVI. This observation could be attributed to the increased significance of factors like noise and random coupling between low and high frequencies, which are less likely to be mitigated through the computation of surrogate trials. Here too MOVI exhibits a significantly higher sensitivity than JSD (Figure 4-4C) as shown by the black line delimiting the cluster of values that survived correction (within cluster, t_{min} = 3.22, $p = 0.031$, t_{max} = 6.58, $p < 0.01$). In this case too, PPV did not differ significantly between MOVI and JSD (mean PPV for MOVI = 0.81, mean PPV for JSD = 0.87, t-test: $t = -1.69$, $p = 0.10$, $df = 24$). MOVI however had a significantly higher NPV than JSD (MOVI NPV = 0.57, JSD NPV = 0.52, t-test: $t = 4.95$, $p < 0.01$, $df = 24$), meaning that MOVI produced fewer false negatives (Figure 4-4D, E and F). Additionally, the Accuracy of MOVI was 0.61 and the accuracy of JSD was 0.53. The MCC of MOVI and JSD was respectively 0.40 and 0.21, showing that MOVI was more likely to detect a real effect than JSD.

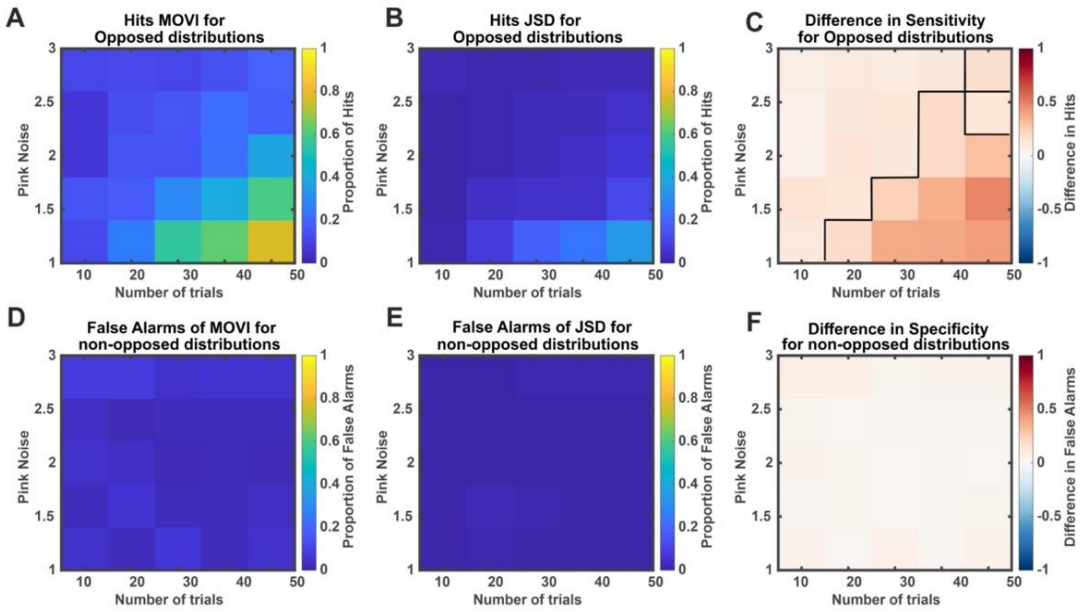

Figure 4-4: MOVI and JSD as a function of number of trials and noise.

*(**A**) Proportion of Hits for MOVI on opposed distributions as a function of number of trials and Pink Noise Strength. (**B**) Proportion of Hits for JSD on opposed distributions as a function of number of trials and Pink Noise strength. (**C**) Difference in sensitivity between MOVI and JSD. A binomial test was performed, and p-values were corrected with a Bonferroni correction. Threshold of p-values was a 0.05. For Opposed Distributions, MOVI is significantly more sensitive than JSD for the settings within the cluster delimited by the dark line, where MOVI has a lower false omission rate even with a lower number of trials. (**D**) Proportion of False Alarms for MOVI for non-opposed distributions as a function of number of trials and pink noise strength. (**E**) Proportion of False Alarms for JSD for non-opposed distributions as a function of number of trials and pink noise strength. (**F**) Difference in Specificity (1-False Alarm Rate) between MOVI and JSD. No statistically significant difference was detected between the two indexes (all, p > 0.05).*

4.4.4. Does asymmetrical number of trials between conditions influence MOVI and JSD?

In the previous test, we assessed both indexes using a symmetrical number of trials for each condition, ensuring that both conditions had an equal number of trials. However, we also wanted to investigate whether the indexes could detect opposition when there was an

uneven number of trials between conditions. Furthermore, we sought to determine the extent to which this asymmetry could impact the sensitivity of both indexes. To this end, we varied the number of trials of only one distribution (between 10 and 50 with steps of 10) and the other distribution had a fixed number of 50 trials and a fixed PAC strength of 0.4.

Results are depicted in Figure 4-5, where statistically significant differences ($p < 0.05$, Bonferroni corrected) between MOVI and JSD are outlined with a black line (Figure 4-5C). What is observed is that it is generally not advised to work with a very low number of trials where false alarms appear in both MOVI and JSD for less than 20 trials in a single condition (Figure 4-5D, E, and F) as this could account for false positives. Overall, MOVI showed higher sensitivity than JSD with an uneven number of trials (within cluster, Binomial test, $t_{min} = 3.48$, $p = 0.012$, $t_{max} = 6.52$, $p < 0.01$). Through the calculation of the mean PPV, we found that a positive test result using JSD was more likely to be a true positive compared to MOVI (MOVI PPV = 0.85, JSD PPV = 0.92), and that this difference was statistically significant (t-test: $t = -3.31$, $p = 0.01$, $df = 24$). Additionally, we computed the average NPV for both indexes (MOVI: NPV = 0.65; JSD: NPV = 0.56) and found that MOVI was significantly less prone to false negatives (t-test: $t = 8.27$, $p < 0.01$, $df = 24$). we obtained an Accuracy value of 0.70 for MOVI and 0.59 for JSD, while their MCC were 0.57 and 0.41, respectively. Once again, in this test, MOVI demonstrated a greater likelihood of detecting genuine effects compared to JSD.

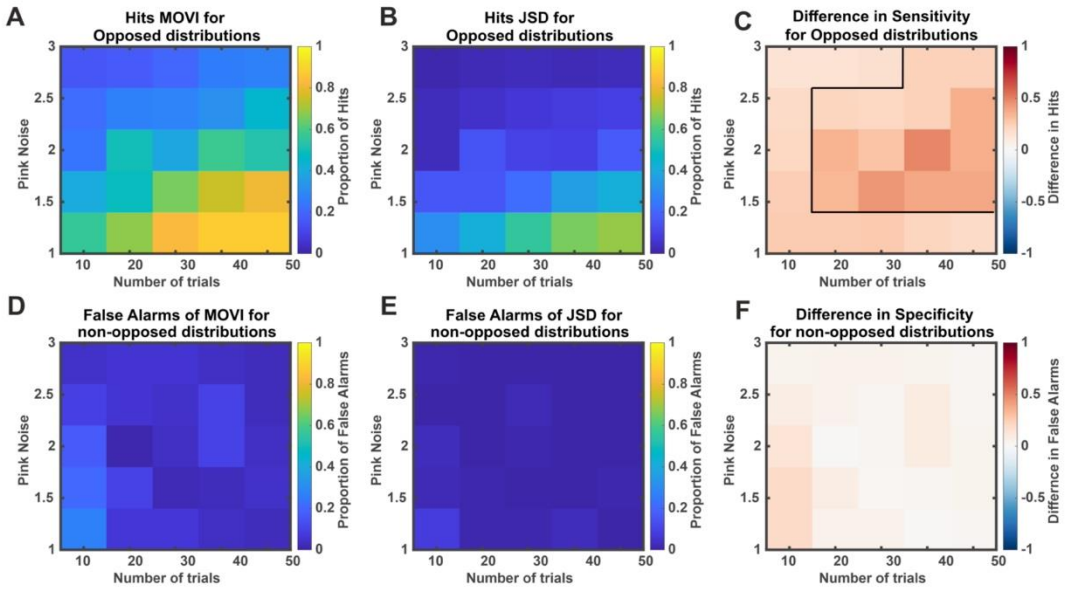

Figure 4-5: MOVI and JSD as a function of asymmetrical number of trials.

*(**A**) Proportion of Hits for MOVI on opposed distributions as a function of number of trials in only one distribution (asymmetrical number of trials) and Pink Noise Strength. (**B**) Proportion of Hits for JSD on opposed distributions as a function of number of trials for one distribution and Pink Noise strength. (**C**) Difference in sensitivity between MOVI and JSD. A Binomial test was performed, and p-values were corrected with a Bonferroni correction. Threshold of p-values was set at 0.05. For Opposed Distributions, MOVI was significantly more sensitive than JSD for the settings within the cluster delimited by the dark line, where MOVI has a lower false omission rate even with a lower number of trials in only one condition. (**D**) Proportion of False Alarms for MOVI for non-opposed distributions as a function of number of trials and pink noise strength. (**E**) Proportion of False Alarms for JSD for non-opposed distributions as a function of number of trials and pink noise strength. (**F**) Difference in Specificity (1-False Alarm Rate) between MOVI and JSD. No significant difference was detected between the two indexes, although one value almost survived Bonferroni correction with pink noise = 1 and 10 trials in only one condition (binomial test: t = 3.32, p = 0.063).*

4.4.5. Does inter-trial coherence affect MOVI and JSD?

Here, while keeping the Phase-Amplitude Coupling (PAC) strength fixed, we assessed whether different degrees of coherence in phase preference for each individual trial influenced MOVI

and JSD indexes. Thus, in this analysis, every trial is expected to display PAC, albeit with varying levels of inter-trial phase preference. Consequently, in scenarios where there is a high variability in inter-trial phase preference, measuring the coupling strength of each individual trial would likely yield significant coupling. However, if we were to average the distributions of all trials and then measure the coupling strength of the average, it is probable that we would not observe significant coupling. This distinction is relevant, for example, in cases where experimenters preferred to test PAC on each trial individually (Axmacher et al., 2010).

Results are depicted in Figure 4-6, where statistically significant differences at cluster level ($p < 0.05$, corrected) between MOVI and JSD are outlined with a black line. Our findings revealed that both MOVI and JSD detected shared and consistent differences in phase preference (Figure 4-6A, B, D, and E) However, MOVI exhibited greater sensitivity in cases of higher inter-trial variability in angle preference and higher levels of pink noise (Figure 4-6C) (within cluster, binomial test, $t_{min} = 3.20$, $p = 0.034$, $t_{max} = 5.84$, $p < 0.01$). We also found that although MOVI showed slightly more false positives this decrease in specificity was not significant compared to JSD (Figure 4-6F). Additionally, we calculated the average PPV of both indexes (PPV for MOVI = 0.90, PPV for JSD = 0.96) and compared them. This analysis determined that a positive test result with JSD was more likely to represent a true positive compared to MOVI under these simulation conditions (t-test, $t= -3.75$, $p = 0.01$, $df = 24$).

We computed the NPV for both indexes, resulting in an NPV of 0.65 for MOVI and 0.55 for JSD. A direct comparison of the two showed that a negative result by MOVI was significantly (t-test, $t = 9.65$, $p < 0.01$, $df =24$) more likely to be truly negative, while JSD exhibited a significantly higher rate of false negatives. Average Accuracy for MOVI was 0.70 and for JSD 0.59. The MCC for MOVI was 0.59, and for JSD it was 0.40. In sum, these results demonstrate that MOVI displayed superior accuracy in detecting real positive or negative effects and produced fewer false results compared to JSD.

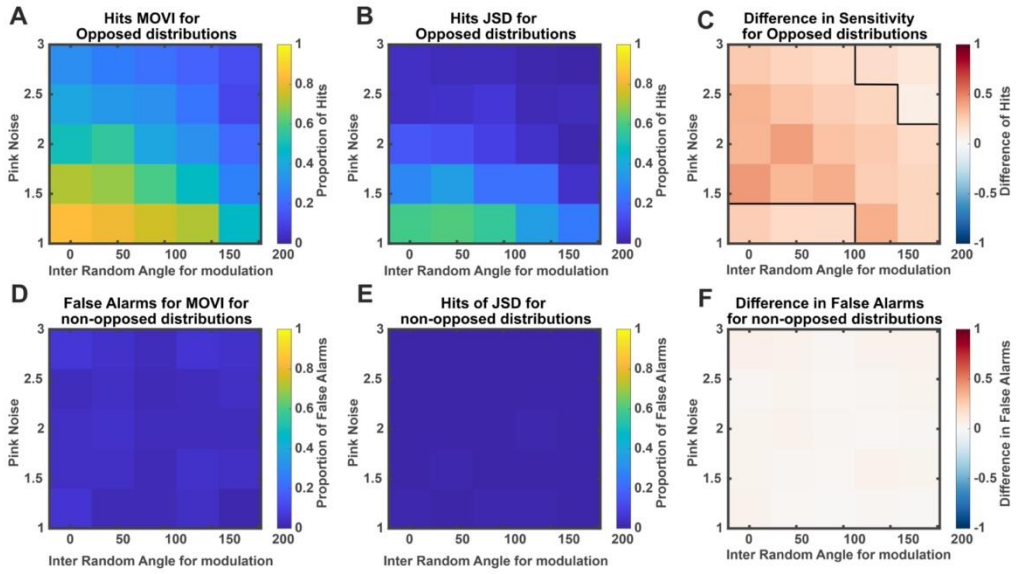

Figure 4-6: MOVI and JSD as a function of Inter-Trial phase-preference variability

*(**A**) Proportion of Hits for MOVI on opposed distributions as a function of Inter-trial coherence of angle preference and Pink Noise Strength. (**B**) Proportion of Hits for JSD on opposed distributions as a function of Inter-trial coherence of angle preference and Pink Noise strength. (**C**) Difference in sensitivity between MOVI and JSD. A binomial test was performed, and p-values were corrected with a Bonferroni correction. Threshold of p-values was a 0.05. For Opposed Distributions MOVI is significantly more sensitive than JSD for the settings within the cluster delimited by the dark line, where MOVI has a lower false omission rate with higher inter-trial variability in angle preference. (**D**) Proportion of False Alarms for MOVI for non-opposed distributions as a function of Inter-trial coherence of angle preference and pink noise strength. (**E**) Proportion of False Alarms for JSD for non-opposed distributions as a function of Inter-trial coherence of angle preference and pink noise strength. (**F**) Difference in Specificity (1-False Alarm Rate) between MOVI and JSD. No significant difference was detected between the two indexes.*

4.5. Discussion

Phase-amplitude coupling (PAC) is a widely studied phenomenon in the brain, and its mechanisms offer insights into how the brain processes and represents information. Computational models propose that nested gamma oscillations within theta cycles may organize sequences of events, while other models suggest gamma couples to opposed-phase states during memory encoding and retrieval. Characterizing differences in phase preference in PAC analysis between neural states or experimental conditions is crucial for understanding neural coding and mnemonic operations. In the current study, we presented MOVI, an analysis method for detecting phase preference difference within PAC between two datasets. Using synthetic data, we showed that MOVI is more tolerant to low signal-to-noise ratio, lower levels of angle differences and trial number asymmetry between conditions than other robust phase-opposition indexes like JSD.

We found that MOVI is more sensitive than JSD in detecting phase opposition. MOVI can detect phase differences even when PAC is weaker, with fewer or unevenly distributed trials, and smaller angle variations between distributions. It is also more resilient to noise and variations in angle preference across trials. While this higher sensitivity may lead to more false negatives, it does not significantly impact the overall accuracy of the Matthews Correlation Coefficient (MCC), a measure of performance in binary classification tasks. In fact, in all tests conducted, MOVI consistently outperformed JSD in terms of accuracy and MCC, demonstrating its superior sensitivity to real differences and its ability to effectively detect true positive and negative effects, primarily by reducing the number of false negatives compared to JSD. These findings highlight the advantages of using MOVI over JSD for quantifying phase opposition in neurophysiological data, particularly when dealing with complex and noisy signals. MOVI's ability to detect smaller phase differences and handle varying trial conditions makes it a valuable tool for understanding phase-preference patterns and phase-amplitude coupling in the brain.

While MOVI proves highly effective in detecting phase opposition and capturing phase-amplitude coupling patterns, it may not be the ideal choice for analyzing event occurrences like spiking frequency (Rutishauser, 2019; Rutishauser et al., 2010) or ripple counts (Norman

et al., 2019) These scenarios involve instances that do not necessarily follow a probabilistic distribution shape, and circular statistics (Berens, 2009) PPC (Vinck et al., 2010), ITC (VanRullen, 2016), or PACOI (Costa et al., 2022) might offer more suitable alternatives. These methods consider different aspects of neural activity and are better suited to address specific research questions where the distribution shape might not be appropriate for MOVI analysis.

However, one key advantage of MOVI compared to other methods is its adaptability to studying phase-amplitude phenomena without the need to summarize the power dimension of amplitude as unit-normalized vectors. MOVI and JSD both allow the treatment of amplitude data without any loss of information by modifying the neurophysiological data into another form. However, MOVI stands out as being more sensitive and capable of accurately discriminating phase-preference opposition or its absence within PAC between conditions.

Another beneficial aspect of MOVI is that it generates an index of opposition for each observation or subject. This feature facilitates a smoother transition to second-level statistics, where experimental MOVI values can be compared to surrogate MOVI values. Consequently, MOVI can serve as an effective exploratory method in the study of phase opposition within PAC distributions, enabling researchers to investigate previously unknown interactions between mechanisms in neurophysiology and experimental settings or neural states.

One limitation of our study is that we evaluated the MOVI and JSD methods using a 2.5s segment of artificial data. While this segment is suitable for most task-induced research in humans and animals, it may not fully capture the dynamics of neural activity during extended periods or other types of research focusing on phase-preference within PAC over longer time frames. For instance, in animal studies, researchers often record neural activity over extended periods to capture a comprehensive view of brain dynamics while navigating in a maze or during states of quiescence. Similarly, during sleep studies, neural data is typically recorded over hours to observe the brain's activity during different sleep stages. Nevertheless, while our study did not specifically test MOVI for long time segments, we believe that MOVI, given its sensitivity to phase-preference opposition and its adaptability to various data lengths, would still be a valid approach to assess phase preference differences in such scenarios.

In conclusion, MOVI stands out as a powerful and versatile tool in the neuroscientific field. Its unique ability to combine coupling strength and opposition measures makes it an attractive choice for analyzing complex neural interactions and mechanisms in neurophysiology signal datasets. Unlike other indexes, MOVI does not necessitate additional verification of coupling strength, allowing for a more straightforward exploration of phase-preference differences between datasets. Furthermore, the user-friendly nature of MOVI makes it intuitive and easy to use, providing a comprehensive summary of unidirectional phase-preference differences between datasets. Overall, MOVI's capabilities make it a valuable addition to the neuroscientific toolbox, facilitating the exploration of phase-preference patterns and the investigation of neural dynamics in diverse experimental settings.

4.6.Conclusions

In this paper, we introduced a novel method to analyze phase-preference variations within PAC in neurophysiological data: the Mean Opposition Vector Length Index. Our approach involved creating an alternate distribution and measuring its non-uniformity using the Mean Vector Length method. Through synthetic experiments, we demonstrated that MOVI showed superior sensitivity compared to a conventional measure (JSD) in various settings. We suggest that MOVI offers greater flexibility and adaptability to neurophysiological data and practical experiments. It proved to be more robust against low number of trials, noise, and asymmetrical numbers of trials that commonly occur in experimental conditions and neurophysiological recordings. We conclude that MOVI is well-suited for real-world research scenarios, enabling more accurate and comprehensive analysis of phase-preference differences within PAC patterns between diverse neurophysiological datasets.

5. Chapter 5: Study 2

Gamma amplitude is coupled to opposed hippocampal theta-phase states during the encoding and retrieval of episodic memories in humans

Please Note: This study was published in Current Biology on the 14th of April 2023 *https://www.cell.com/current-biology/pdf/S0960-9822(23)00393-7.pdf*

5.1.Summary

Computational models and *in vivo* studies in rodents suggest the emergence of gamma activity (40-140Hz) at memory encoding and retrieval is coupled to opposed phase states of the underlying hippocampal theta rhythm (4-9Hz) (Bieri et al., 2014; Colgin et al., 2009; Fernandez-Ruiz et al., 2017; Hasselmo et al., 2002; Manns et al., 2007). However, direct evidence for whether human hippocampal gamma-modulated oscillatory activity in memory processes is coupled to opposed phase states of the ongoing theta rhythm remains elusive. Here we recorded local field potentials (LFP) directly from the hippocampus of ten epileptic patients with in-depth implanted electrodes. We used a memory encoding and retrieval task whereby trial unique sequences of pictures depicting real-life episodes were presented and 24h later, participants were asked recalled them upon the appearance of the first picture of the encoded episodic sequence. We found hippocampal-specific theta-to-gamma cross-frequency coupling during the encoding and retrieval of episodic memories. We also showed that during encoding gamma oscillations were coupled to the peak of the ongoing theta rhythm, while at retrieval, gamma was coupled to the trough of the hippocampal theta. Furthermore, we found that the degree of theta-gamma phase opposition between encoding and recall was associated with participants' memory performance so that those episodes that were successfully recalled showed greater theta-gamma phase opposition than forgotten ones. The current results are the first direct empirical evidence in support of hippocampal theta-gamma phase opposition models in human long-term memory and provide fundamental insights into mechanistic predictions derived from computational and animal work, thereby contributing to establishing similarities and differences across species.

5.1.1. Results

Ten participants (6 females, age 29.5 ± 11.7 years - mean ± SD) with drug-resistant epilepsy participated in a 2-day encoding and recall episodic memory task (Figure 5-1A). Participants studied a series of 60 different episodes of 4 picture image sequences each depicting a plausible succession of instances of a real-life episode that they had to recall immediately (recall day 1), and then again 24 hours later (recall day 2), cued with the first image of each episode. Memory accuracy was assessed by counting the number of pictures from each

episode that were correctly included in the recall phase (3 being the maximum value to reach per episodic series). We then obtained a memory score for each episode that ranged from 0 (i.e., no pictures included in the recall) to 3 (i.e., all pictures included in the recall), given that the recall of the first picture was non-informative of memory retrieval as it was always displayed as a cue during the recall. The total number of recalled pictures for each episode was then used to categorize whether that episode was remembered or forgotten. We categorized episodes that included 2 or 3 pictures in their recall as "remembered" and when participants recalled 0 or 1 pictures from the episode, we categorized those as "forgotten". As expected, participants remembered on average more episodes in the recall task on day 1 (mean $\pm$ SD, 64.9% $\pm$ 18.1%) than in the recall task on day 2 (mean $\pm$ SD, 53.2% $\pm$ 16.5%) (paired t-test, $t(9) = 2.89$, $p = 0.02$) (Figure 5-1B; Supplemental Results; Table 5-1). We also observed that the number of cases in which pictures from an episode were recalled in an incorrect order or when these included pictures from other episodes was infrequent, both in the recall day 1 (6.0% $\pm$ 4.10%) and at the recall day 2 test (5.83 % $\pm$ 2.97%), and the number of errors in their recall did not differ between the two tests ($t(9) = 0.16$, $p = 0.87$), thereby indicating that participants were accurate in their remembered episodes.

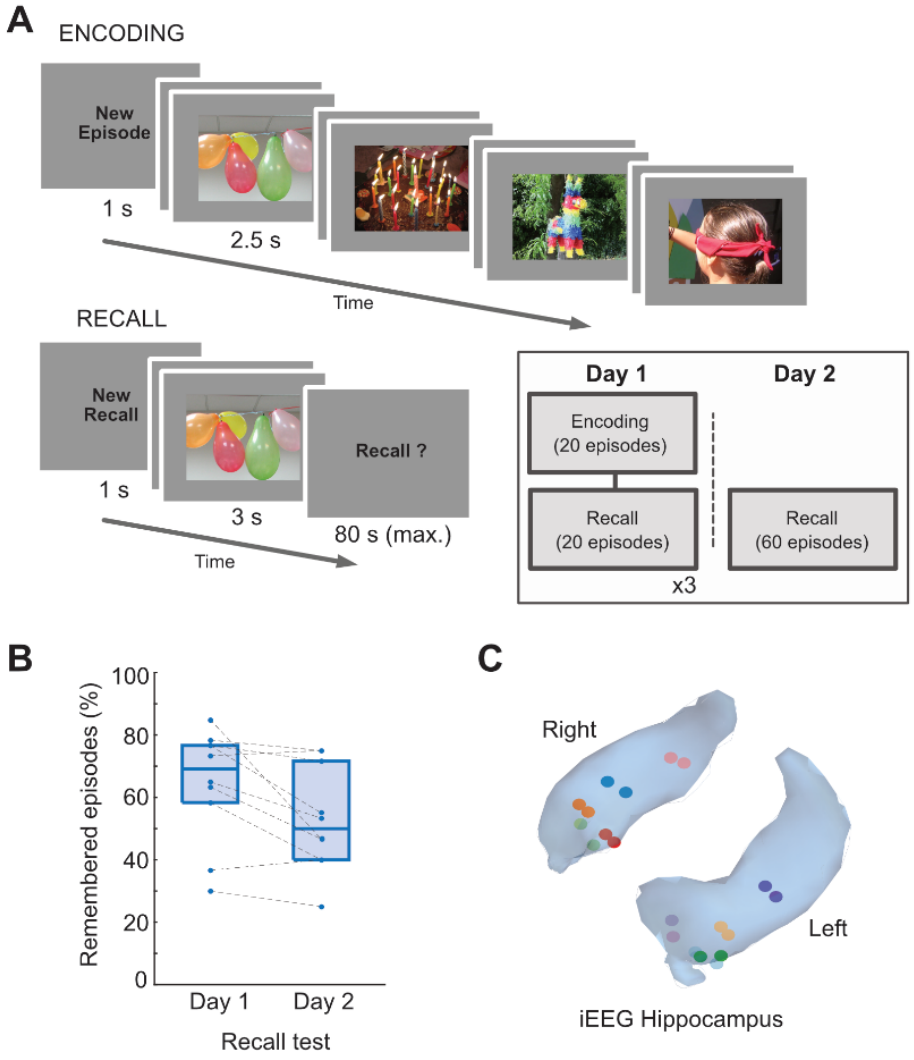

Figure 5-1: Experimental design and recording locations.

(A) On day 1, participants were presented with 3 blocks of 20 different picture series each including 4 pictures depicting a plausible succession of instances of a real-life episode (encoding phase). Participants were informed that memory of the encoded episodes would be tested after each encoding block on the same day (recall day 1) and again 24h later (recall day 2). Participants were informed that the recall phase consisted of the presentation of the first picture of each of the series and that they should verbally recall the pictures associated with each of them. They were asked to be as specific and precise as possible, and to try to recall the events in order, mentioning the first image as the beginning of their story. (B) Participants' proportion of episodes that were successfully remembered in the day 1 and day 2 recall tests. In the box plots the central mark is the median, and the edges of the box

are the 25th and 75th percentiles. Each dot on both plots represents a single participant. Dashed lines on the boxplot connect the value of an individual in the two conditions. (C) Hippocampal electrode localizations from all the participants, shown on a three-dimensional hippocampus model. Each pair of color dots indicate the two electrodes from the participants used for this study, which was used for bipolar referencing, resulting in one trace per patient.

While participants performed the task, we recorded direct hippocampal activity via implanted depth-electrodes (Figure 5-1C), thereby allowing us to examine hippocampal neurophysiological mechanisms that supported episodic memory encoding and retrieval in humans. Previous work using intracranial electroencephalographic (iEEG) recordings from human hippocampus revealed increases in high-frequency gamma power (~ 40 - 120 Hz), an established correlate of firing rates of individual neurons (Hirabayashi et al., 2014; Jacobs, Kahana, Ekstrom, & Fried, 2007; Manning, Polyn, Baltuch, Litt, & Kahana, 2011), increases during encoding (Sederberg et al., 2007) and retrieval, either in recognition (Staresina et al., 2016) or in recall (Burke, Long, et al., 2014; Burke, Sharan, et al., 2014) memory tasks. We thus carried out a single-trial time-frequency analysis on hippocampal EEG data during the encoding of episodes and at their recall on day 2 and computed the relative gamma power increases and decreases corrected with respect to a 0.5 s baseline window (see Methods). This analysis revealed marked gamma band (~ 40 – 140 Hz) power increase from ~ 0.3 to 1.3 s during memory encoding and recall (Figure 5-2A and Figure 5-5) which proved to be statistically significant (cluster statistics at encoding: t_{sum} = 1699.1, t_{peak} = 5.97, p = 0.002; cluster statistics at recall: t_{sum} = 2503.0, t_{peak} = 6.8, p = 0.006) after correcting for multiple comparisons using a cluster-based non-parametric method (Figure 5-2B; see Methods). However, a comparison of the cluster-averaged gamma power increase for episodes that were remembered and forgotten revealed that the magnitude of the increase was similar between conditions (repeated measures ANOVA, all Fs < 0.5), both during memory encoding (paired t-test: t(9) = -0.48, p = 0.64) and recall (t(9) = 1.35, p = 0.21) (Figure 5-2C). Additional analysis accounting for picture order within the episode confirmed that gamma power increase was consistent throughout encoding and similarly elicited by episodes that would be

later remembered or forgotten. This contrasts with earlier findings that showed greater hippocampal gamma power response during the encoding of words from a list that were later remembered compared to those that were forgotten (Sederberg et al., 2007), or the correct identification of a color associated background of a word during a recognition task (Staresina et al., 2015). While it would be reasonable to expect performance-dependent hippocampal gamma power modulations in our study too, there are important differences between the previous and our task design. Here, we asked participants to encode and recall the complete sequence of visual pictures depicting the unfolding of a realistic and schema-consistent episode, and we distinguished between remembered and forgotten episodes based on the participant's ability to recollect the pictures verbally, remaining agnostic to the likely possibility that they successfully recognized the picture cue even in the forgotten trials. Thus, our task design may be less sensitive isolating the gamma power differences between successful and unsuccessful memory performance revealed in previous studies.

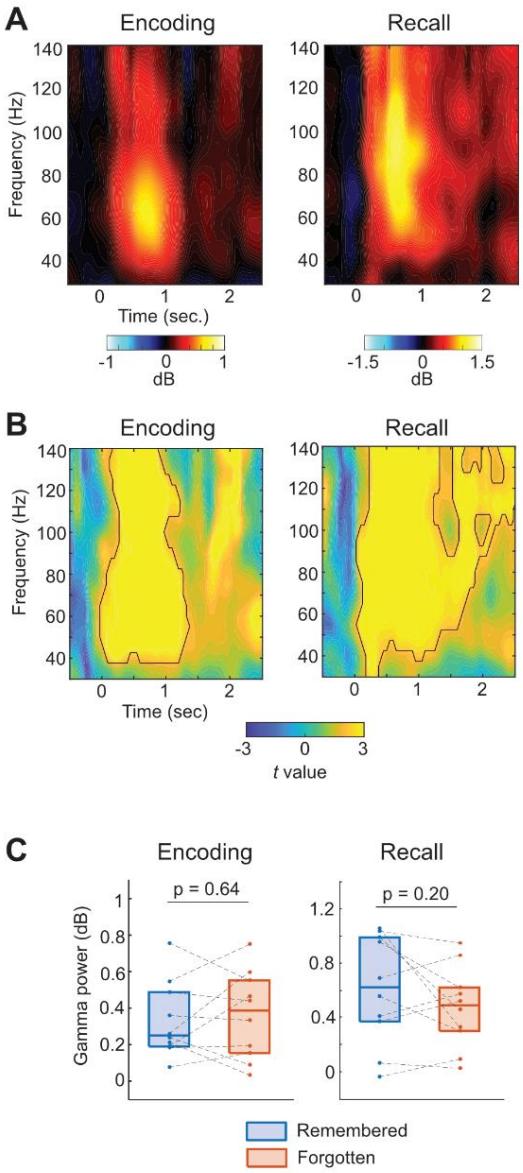

Figure 5-2: Hippocampal gamma power during memory encoding and recall.

(A) Group-averaged changes in spectral power elicited during memory encoding and recall. (B) Time-frequency t-value map of gamma power in- and decrease at encoding and at recall. Thick black lines depict the cluster that resulted as being statistically significant at encoding and at recall ($p < 0.05$, cluster statistics). (C) Cluster-averaged gamma power at encoding and recall for remembered and forgotten episodes. Paired t-test associated p values between conditions associated are displayed. For all box plots in (C), the central mark is the median, and the edges of the box are the 25th and 75th percentiles. Each dot represents the value for an individual participant in each condition. Dashed lines on the boxplots connect the value of an individual in the two conditions.

We next asked whether the increase in gamma power seen during episodic encoding and during recall was coupled to the ongoing hippocampal theta phase states. Hippocampal theta oscillations have been related to the dynamics of memory function (Buzsaki, 2002; Huxter et al., 2008; Jezek, Henriksen, Treves, Moser, & Moser, 2011; Jones & Wilson, 2005; Kunz et al., 2019; O'Keefe & Conway, 1978; O'Keefe & Dostrovsky, 1971; Reddy et al., 2021; Tort et al., 2009), and specifically to the interplay between encoding and retrieval (Hasselmo et al., 2002; Kunec, Hasselmo, & Kopell, 2005). In theta-based hippocampal models, the phase of ongoing theta oscillations separates encoding and retrieval and determines the different plasticity regimes that memory encoding, and retrieval require (Hasselmo et al., 2002). Prior rodent studies reported evidence that modulations within the gamma band distinguishing encoding from retrieval (Bragin et al., 1995; Colgin, 2015b), and the study of theta on humans showed a preferential phase for encoding and recall (Kerren et al., 2018; Rizzuto, Madsen, Bromfield, Schulze-Bonhage, & Kahana, 2006; Ter Wal et al., 2021), highlighting the intrinsic property of the hippocampus to shift its dynamics towards encoding and retrieval, even when the same perceptual experience is present during the two tasks (Long & Kuhl, 2021); however, direct evidence of whether human hippocampal gamma-modulated activity in memory processes is coupled to opposed phase states of the ongoing theta rhythm remains elusive.

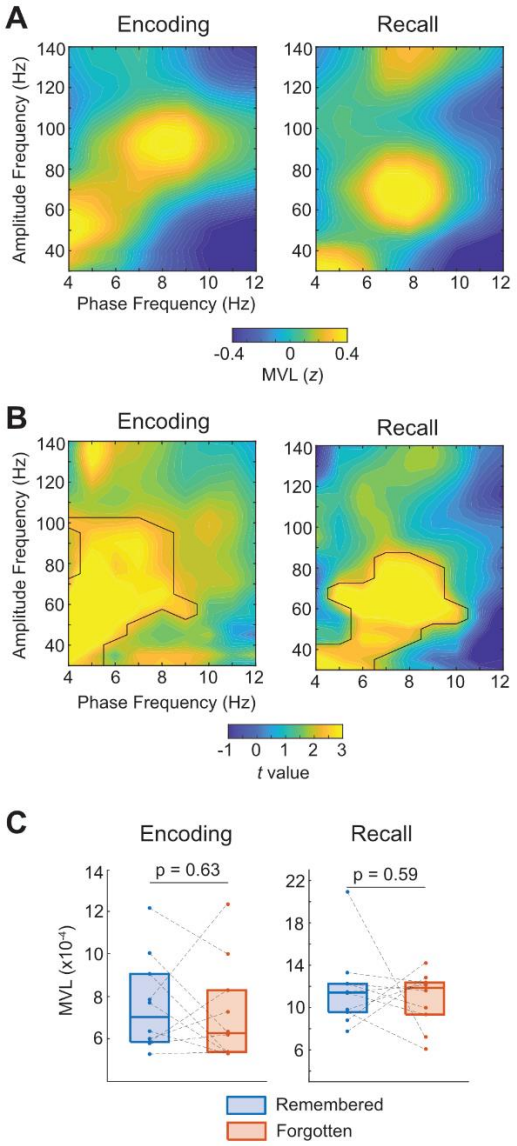

Figure 5-3: Hippocampal theta-gamma phase-amplitude coupling during memory encoding and recall.

(A) Group-averaged of phase-amplitude comodulogram computed during memory encoding and recall. X-axis indicates phases modulating the signal and the Y-axis represents the modulated amplitude. (B) Phase-to-amplitude t-value map during encoding and recall. Thick black lines depict the cluster that resulted statistically significant during encoding and recall ($p < 0.05$, cluster statistics). (C) Cluster-averaged PAC strength for remembered and forgotten episodes during encoding and recall. Paired t-test associated p values between conditions associated are displayed. For all box plots in (C), the central mark is the median, and the edges of the box are the 25th

and 75th percentiles. Each dot represents the value for an individual participant in each condition. Dashed lines on the boxplots connect the value of an individual in the two conditions.

To address this issue, we first examined whether hippocampal gamma oscillations exhibited phase amplitude coupling (PAC) with ongoing theta phase during encoding and during retrieval in our data. We assessed the existence of theta-gamma PAC by using a comodulogram method as described in (Tort et al., 2009), which allows PAC to be scanned from several narrow-filtered frequencies within the theta and gamma frequency bands. We then quantified the magnitude of PAC in each frequency pair by using the co-called Mean Vector Length (MVL) method (Canolty et al., 2006) (see Methods), which has been found to be relatively robust to signal-to-noise over time for EEG segments of few seconds (Tort et al., 2010). The results of this analysis revealed that hippocampal gamma band amplitude during memory encoding and during memory recall was modulated by the ongoing theta phase state (Figure 5-3A , also see Figure 5-6). Cluster-based statistics confirmed a statistically significant theta-gamma PAC cluster, comprising amplitude modulations in the ~ 40 – 110 Hz frequency range that were coupled to ~ 4 – 9 Hz phases during encoding (cluster statistics: t_{sum} = 181.7, t_{peak} = 5.51, $p < 0.001$) and amplitude modulations at ~ 50 – 90 Hz frequency range that were coupled to the ongoing theta phases within the ~ 4 – 10 Hz frequency range during recall (cluster statistics: t_{sum} = 139.9, t_{peak} = 5.48, $p < 0.001$) (Figure 5-3B). Theta-gamma PAC was also detected during recall on day 1 (i.e., in the test that took place a few minutes after encoding) (Figure 5-12). However, the degree of PAC between memory conditions did not differ statistically (repeated measures ANOVA, all Fs < 0.3; encoding: $t(9) = 0.49$, $p = 0.63$; recall: $t(9) = 0.54$, $p = 0.60$) (Figure 5-3C). Additional control analyses showed that theta oscillations were present during encoding and recall (Figure 5-5), that encoding theta-gamma PAC was similar throughout the sequence of encoded pictures and between memory conditions (also see Figure 5-7), that theta-gamma PAC could not be identified in other brain regions outside the hippocampus, such as in the middle temporal gyrus (also see Figure 5-9) and that the lack of theta-gamma PAC differences could not be explained by signal-to-noise properties derived from hippocampal Evoked-Potential Responses elicited during encoding and recall in the task (also see Figure 5-8 and Figure 5-10).

The results presented thus far show that hippocampal gamma is effectively coupled to the ongoing theta phase state, but it is not predictive of episodic memory formation and retrieval. Our analysis, however, does not account for the possibility that gamma amplitude modulation to theta phases occurs at distinct phases at encoding and at recall, as it would be predicted by theta-phase hippocampal models[1]. To test theta phase opposition, we developed an index, the Mean Opposition Vector Index (MOVI), allowing us to statistically assess the existence of PAC opposition between two experimental conditions (See Methods). Briefly, MOVI is the MVL of an alternate distribution, calculated as the difference between the two compared distributions. Each participant had an experimental MOVI value that was tested against 1000 surrogate values after shuffling across trials. These experimental values were averaged as well as the surrogate values and we obtained an experimental MOVI value to test against a distribution of surrogates. We z-scored the experimental value and obtained a p-value by identifying the fraction of surrogate MOVI values that were smaller than the experimental value (see, Methods).

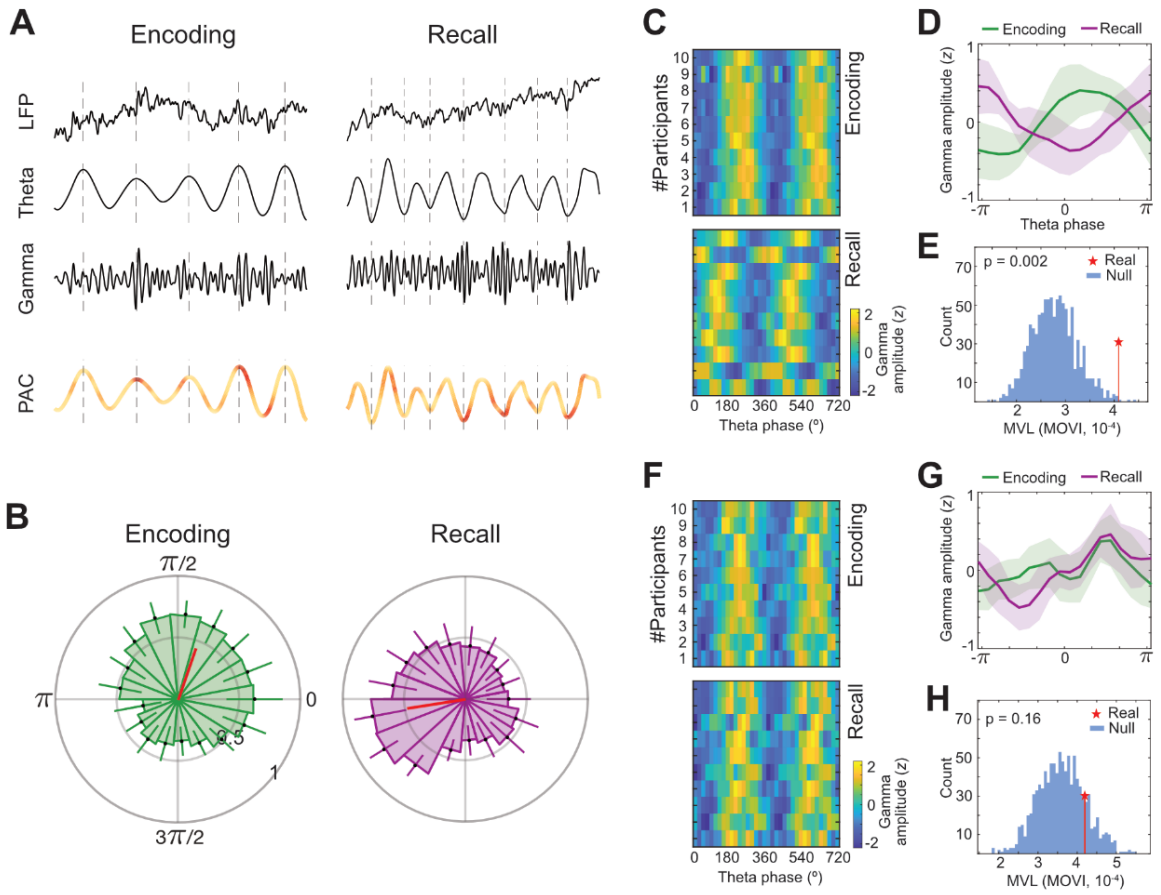

Figure 5-4: Hippocampal theta-gamma phase preference and Mean Opposition Vector Index (MOVI).

(A) Representative example of raw (LFP) and filtered (theta and gamma) hippocampal recordings from one of the participants of the study during encoding and at recall. The PAC wave shows where on the theta cycle there is an increase in gamma activity for the example trial. (B) Polar distribution of averaged gamma amplitude (z) across participants over theta phases within the significant cluster of PAC found at encoding and at recall. Error bars represent standard error across participants. Grand average across participants is depicted by the thick red line. (C) Individual distribution of hippocampal gamma amplitude over a cycle of theta at encoding and recall for remembered trials. Participants' distributions have been realigned to the mean angle direction of encoding and the recall distributions have been realigned relative to each participant's encoding distribution for this figure only. (D) Average distribution of hippocampal gamma amplitude over theta phase for all patients for remembered trials. Shaded area represents the SEM across participants. (E) Experimental value of MOVI (red star) compared to surrogate value for all participants for remember trials.

(F) Individual distribution of hippocampal gamma amplitude over a cycle of theta at encoding and recall for forgotten trials. Participants' distributions have been realigned to the mean angle direction of encoding and the recall distributions have been realigned relative to each participant's encoding distribution for this figure only. (G) Average distribution of hippocampal gamma amplitude over theta phase for all participants for forgotten trials. Shaded area represents the standard error across participants. Note that the lack of phase preference in the plot does not reflect a lack of PAC but the degree of variability in phase preference across participants. (H) Experimental value of MOVI (red star) compared to surrogate value for all participants for forget trials.

We found significant gamma band activity coupling to opposed theta phase states during memory encoding and recall ($z = 2.29$, $p = 0.02$) (Figure 5-4A and B; also see Figure 5-13). This theta-gamma PAC opposition was statistically significant for remembered episodes ($z = 2.85$, $p = 0.004$) (Figure 5-4C and D) but not for forgotten episodes ($z = 0.98$, $p = 0.32$) (Figure 5-4E and F) or for the interaction remembered vs. forgotten ($t(9) = 0.76$, $p = 0.47$). This result indicates that gamma power was modulated by theta phase for both remembered and forgotten trials, though only for remembered trials the dominant theta phase was different for encoding and recall trials.

5.1.2. Discussion

Taken together, the current study provides evidence in humans that hippocampal gamma couples to opposed phase states of the ongoing theta rhythm activity in episodic memory during encoding and during retrieval. The present findings thus constitute empirical support for the computational models that show that the emergence of gamma oscillations at opposed phase states of the underlying theta rhythms may be optimal for acquiring new memories and retrieving existing memories (Hasselmo et al., 2002; Hasselmo & Stern, 2014).

While hippocampal theta-gamma PAC is well documented in task-based mnemonic processing in rodents (Bragin et al., 1995; Douchamps et al., 2013; Hasselmo & Stern, 2014; Lever et al., 2010; Manns et al., 2007; Poulter et al., 2021; Siegle & Wilson, 2014), evidence in humans has been compromised by the limited access to the direct sampling of hippocampal

activity with intracranial EEG recordings. Notably though, the existing data converged in showing that hippocampal theta phase coding scheme is a core mechanistic conduit in memory function (Pacheco Estefan et al., 2021; Rizzuto et al., 2006; Solomon, Lega, Sperling, & Kahana, 2019; Ter Wal et al., 2021) and that human hippocampal theta-gamma PAC underlies working memory (Axmacher et al., 2010; Bahramisharif, Jensen, Jacobs, & Lisman, 2018) and the recall of list-words (Lega et al., 2016). The current findings further extend this literature by providing novel evidence that human hippocampal gamma activity functionally shifts to distinct theta phase states to support episodic encoding or retrieval.

In line with previous studies examining memory-based hippocampal activity from intracranial recordings in humans (Lohnas et al., 2018; Staresina et al., 2016), we found an increase in power for a broad high-frequency range (~ 40 – 120 Hz) activity at encoding and at retrieval. Rodent research studying the dynamic interaction of the entorhinal cortex and the CA1 and CA3 subfields within the hippocampal network identified that encoding and retrieval may, in fact, engage two distinct gamma bands, a slow (~ 30 – 50 Hz) and a fast (~ 60 – 100 Hz), each of them functionally locked to different theta phase states (Colgin, 2015a). In this study, the size of the intracranially implanted electrodes and the rare occasions whereby the entorhinal cortex is sampled in clinical settings challenges the possibility of reliably separating slow and fast gamma activity within the entorhinal – hippocampal CA1/ CA3 network in humans (Griffiths et al., 2019; Wang, Schmitt, Seger, Davila, & Lega, 2021)

Our findings also point to the possibility that gamma coupled to a lower and a higher hippocampal theta rhythm during encoding and recall, respectively (see Figure 5-3). Interestingly, human hippocampal theta has been reported to be slower than rodents' theta and there may be two functionally and anatomically distinct rhythms, a slower (~ 3 Hz) and faster (~ 7 Hz) theta (Goyal et al., 2020; Lega et al., 2016). We explored whether low theta was also coupled with gamma at different phases during encoding and recall, but we did not find evidence for theta phase-opposition at low theta (Figure 5-12). A recent study has shown that, in fact, human hippocampus exhibited oscillations at multiple frequencies within the theta range organized along the longitudinal axis, being theta activity slower at the anterior and faster at the posterior hippocampus (Goyal et al., 2020). Our study, which included hippocampal activity indistinctively from electrodes located at anterior and middle

hippocampal regions (see Figure 5-1C) may have, perhaps, blurred together the low and high theta oscillations. Nevertheless, the extent to which low and fast theta showed different theta-gamma phase-amplitude coupling dynamics in memory would be an interesting question to explore in future studies. Addressing this issue adequately, though, would require a rich recording sampling of the hippocampus activity along its longitudinal axis.

5.1.3. Conclusion

In sum, current findings provide new insights into the functional role of hippocampal theta-gamma cross-frequency coupling in human episodic memory. We report that gamma oscillations are coupled to the peak of the ongoing theta rhythm during memory encoding and to the trough of theta at its retrieval. Additionally, we show that the degree of theta-gamma phase opposition was associated with memory performance. Thus, our findings provide the first direct empirical evidence in support of hippocampal theta-gamma phase opposition models subtending human long-term episodic memory, bridging an important gap between existing computational, rodent, and human evidence.

5.2.Methods

5.2.1. Experimental Methods and Details

Ten epilepsy patients (6 females, age 29.5 $\pm$ 11.7 years - mean $\pm$ SD) implanted with depth electrodes as part of their diagnostic assessment for pharmaco-resistant focal epilepsy participated in our study. Recordings were performed in two hospitals: the Hôpital Pitié-Salpétrière in Paris (France) and the Hospital Clínic - IDIBAPS in Barcelona (Spain). Electrode placement was exclusively guided by the clinical needs of localizing the seizure onset zone and consider the indications and feasibility of ulterior surgical resections. Participant selection was based on the following inclusion criteria: 1) normal IQ; 2) electrodes implanted in the hippocampus contralateral to or outside of the epileptogenic region were included for the analysis of neurophysiology signals. The study was conducted according to the Declaration of Helsinki and approved by the local ethics committee, and all patients provided written informed consent.

5.2.2. Data collection

The experiment was conducted in a sound-attenuated room in the hospital, with participants sitting upright in a comfortable chair or on their bed. The stimuli were presented on a 13-inch portable computer, placed on an overbed table at approximately 60 cm distance in front of the patients. Patients used the keyboard of the laptop to complete the behavioral task, and their responses were recorded. Trial onsets and offsets TTL triggers were sent to the EEG amplifier via a parallel port or an Arduino simulating a parallel port. In Paris, the recordings were performed using the ATLAS amplifier (Atlas, Neuralynx®, Inc., Bozeman, MO; 160 channels at 4096 Hz; bandpass filter between 0.1 Hz and 1000 Hz). The macroelectrodes (AdTech®, Wisconsin) used consisted of 4-12 platinum contact electrodes with a diameter of 1.12 mm and length of 2.41 mm, with nickel-chromium wiring. The distance between the centre of 2 contacts was 5 mm. In Barcelona the recordings were performed using a clinical EEG system (Natus Quantum LTM Amplifier) with a 1024Hz sampling rate and an online bandpass filter from 0.1Hz to 4000Hz. Intracerebral electrodes (Microdeep, DIXI Medical) were used for recordings. Each multielectrode had 8 to 18 contacts, spaced 5 mm and 1 to 2 mm long with a diameter of 0.8 mm. Verbal recalls were recorded with an audio recorder placed on the overbed table next to the laptop computer used to record responses.

5.2.3. Experimental Design

The experiment was conducted on two consecutive days (Figure 5-1A). On day 1, participants were presented with 3 blocks of 20 different episodic sequences each including 4 pictures depicting a plausible succession of instances of a real-life episode (encoding phase). Participants were instructed to encode the temporally extended episodes, whereby each single-exposure episode was itself composed of four discrete and unique picture stimuli assembled into an unfolding episode. They were also informed that their memory of each of the pictures within the episodes would be tested briefly after each encoding block (recall day 1) on the same day and again 24h later (recall day 2).

In the encoding phase, participants were presented with a total of 60 different episodic sequences separated into 3 different blocks. Each episode included 4 different pictures

presented sequentially. The trial structure was as follows: each trial started with the text presentation of “New Episode” for 1 s which marked the start of a new encoding episode. Each picture was then sequentially presented on a grey screen for 2.5 s and preceded by a black fixation cross in the center of the screen for 1 s. A fixation cross was displayed again for 2 s after the 4th picture, after which participants were instructed to rate, on a keyboard (keys 1, 2, 3 and 4), how much the sequence was emotionally salient to them. The emotional salience had to be rated on a scale from 1 (no salience or boring) to 4 (very salient). An inter-trial interval of 2 s was inserted before the start of the next encoding trial.

After each encoding block of 20 episodes, participants had a short break and started the recall phase (day 1). Participants were informed that the recall phase consisted of the presentation of the first picture of each of the series and that they should verbally recall the pictures associated with each of them. They were asked to be as specific and precise as possible, and to try to recall the pictures in the exact same order as they were presented, and to mention the first image as the beginning of their recall. Patients answered in their native language which was French in the Hôpital Pitié-Salpétrière in Paris and Spanish or Catalan in the Hospital Clínic – IDIBAPS in Barcelona. Each recall trial event began with a 1 sec text presentation on the screen that depicted “New memory”. After a black fixation cross in the centre of the screen for 1 s, the first picture of one of the encoded episodes was presented for 3 s, serving as a cue to prompt the verbal recall of the rest of the pictures in that episodic sequence. Participants were instructed to withhold their recall of the associated episode until the picture image was replaced by a message saying, “Can you recall the episode?”, which lasted a maximum of 80 s to allow them to take their time to recall the episode if needed. An external recorder positioned on the table adjacent to the laptop was used to record their verbal responses; however, since it was not connected to the laptop, the reaction times for the answers were not obtainable. Participants could press the spacebar to end the trial when they had finished the recall. Participants were instructed beforehand to explicitly say “I do not remember” after the picture image disappeared if nothing could be remembered that was associated with the picture cue. A short break of 5-10 minutes separated the start of the new encoding-recall block.

On day 2, participants were instructed that the cued recall task would be repeated (recall on day 2) and it would follow the same trial structure as in the recall phase on day 1. All 60 first pictures from the encoded series were presented in blocks of 20 trials, which were separated by a short 5-10 minutes break.

The presentation order of the series in the encoding phase was randomized for each participant and presented in a shuffled order on each round of recall on day 1. The order of the presentation of the picture cues from the 60 episodes was also shuffled for each participant. The task was programmed on Matlab R2017b using the Psychtoolbox3 toolbox (Brainard, 1997).

5.2.4. Electrode selection

Based on anatomical and functional criteria, one pair of hippocampal depth electrode contacts per participant was selected for analyses. Depth electrodes were implanted stereotaxically, and laterally via the temporal lobe. The presence of electrodes in the hippocampus was assessed with the examination of a computed tomography (CT) and (post-electrode removal) Magnetic Resonance Imaging (MRI) T1 scans. Cerebral atlases of each patient were obtained with the parcellation of the preoperatory T1 using Freesurfer (https://surfer.nmr.mgh.harvard.edu). The CT was then co-registered to the T1 and contact tags and names were placed manually using fieldtrip toolbox for ECoG and sEEG recordings (https://www.fieldtriptoolbox.org/). Confirmation of contact placement was then obtained with a co-registration of the post-operatory T1 to the preoperatory T1 and via superposition of the electrode placement matrix to the realigned post-operatory T1, and manual correction of the misplaced contact tags. Selection of channels was done in native space to prevent errors due to distortions while converting in MNI space. MNI space conversion was then done to have a generalized view of the patient's channels of interest. Since channels were referenced to the adjacent more distal contact along the electrode (bipolar referencing) channels of interest were selected on the bases of three main criteria (in this order of decreasing importance): (1) the channel of interest or the referenced one had to be in the hippocampus; (2) if more than one channel was eligible, hence fulfilled the prior criterion, to avoid using white matter references, hence limit noise from other brain areas, we privileged

the channel that had an adjacent distal referencing contact also in the hippocampus (Michelmann et al., 2018); Finally, (3) if more than one pair of adjacent channels were eligible, we selected those that had the least amount of epileptic activity according to the Artifact Rejection procedure (please see section below for details).

To visualize the selected contacts across our sample, we normalized each participant's post-implantation MRI along with their co-registered pre-implantation MRI to MNI space using SPM12 (http://www.fil.ion.ucl.ac.uk/spm/). To facilitate the visualization of contacts across the group, a 5-mm-radius sphere was created around each contact's centre point and overlaid across participants (Figure 5-1C).

5.2.5. Data preprocessing and artifact rejection

We first down-sampled raw EEG data from all participants to 1000 Hz. Then, we extracted epochs of EEG data from -2 to +4 s from stimulus onset for all stimuli (picture images) and plotted each EEG trial data to perform a visual inspection to identify epileptic activity with the help of an epileptologist. We recognized interictal spikes and epileptic activity, characterized by high amplitude EEG signals that were disruptive of previously ongoing activity. We then plotted each trial's spectral power (30 – 140 Hz) to evaluate the presence of noise in the time-frequency domain. Trials containing epileptic activity or noise were removed from further analysis. This resulted in 47.8 ± 10.8 (Mean ± SD) trials for image 1, 48.5 ± 10.8 trials for image 2, 49.6 ± 8.3 trials for image 3, 50.8 ± 8.3 trials for image 4 and 52.9 ± 10.0 trials for recall, being kept for analysis on average across patients, for a total of 60 trials per stimulus. We then re-referenced each contact to the closest contact on the same electrode (bipolar re-referencing, details explained above) and performed a second visual inspection of the LFPs and the spectral power data to ensure all epileptic spikes had been successfully removed throughout our priori Artifact Rejection procedure.

5.3.Quantification and Statistical Analysis

5.3.1. Behavioural Analysis

Participants' memory accuracy was assessed by analysing the verbal recall on day 1 and day 2. For each episode, each picture was counted as remembered or forgotten. A picture was counted as remembered when participants mentioned an action or an item that clearly depicted the content of the picture. We then obtained a memory score for each episode that ranged from 0 (i.e., no pictures included in the recall) to 3 (i.e., all pictures were included in the recall), given that the recall of the first picture was non-informative of memory retrieval as it was always displayed as a cue during the recall. The total number of pictures correctly recalled for each episode was then used to categorize whether that episode was remembered or forgotten. We categorized episodes that included 2 or 3 correctly recalled pictures as 'remembered' and 'forgotten' when participants recalled either none or a single picture from the episode. When pictures were correctly recalled in an episode, we also assigned a number from 2 to 4 to each of them to index the correspondence to the order position in the sequence at encoding. This allowed us assessing for the possibility that remembered pictures were recalled in an incorrect order during the recall (e.g., permutation errors). We also coded if pictures from one encoded episode were erroneously recalled in another one at test (e.g., false alarms).

To evaluate the extent to which recalled episodes in the immediate test were consistent to those recalled in the delayed test, we performed a linear regression analysis at the individual level using the number of pictures recalled in the immediate test as a dependent variable and the number of pictures recalled in the delayed test as an independent measure. If the pictures recalled in the delay recall test from each of the episodes scaled according to the recalled pictures at the immediate test, then the slope of this relationship should be positive and differ from 0. This analysis revealed that this was the case, as the slopes were positive (mean $\pm$ SD, 0.73 ± 0.16) and significantly above 0 ($t(9) = 14.62$, $p < 0.001$). These results indicate that the number of recalled images per episode was consistent in the recall test on day 1 and on day 2.

On average, participants rated the encoded episodes as emotionally neutral (mean ± SD, 2.46 ± 0.69; Participant 9 had to be excluded from this analysis because of with the recording of button presses during the encoding phase). Ratings were similar for remembered and forgotten episodes as a function of memory accuracy in the immediate (remembered: 2.49 ± 0.73 and forgotten: 2.46 ± 0.68, paired t-test t(8) = 0.18, p = 0.86) and in delayed recall test (remembered: 2.47 ± 0.78 and forgotten: 2.46 ± 0.59, paired t-test t(8) = 0.05, p = 0.96). These results indicate that participants' episodic engagement did not affect successful memory accuracy in our experiment.

5.3.2. Number of iEEG trials included in the analyses

We quantified the number of trials from each of the 4 pictures at encoding and at recall that were included in the iEEG analyses after artifact rejection and have them compared across memory conditions for each of the recall tests. We statistically assessed this issue at encoding by running a repeated measures ANOVA including two within-subject factors, memory type (remembered, forgotten) and picture position (1^{st}, 2^{nd}, 3^{rd}, 4^{th} in the episodic sequence). We used a paired-t test at recall as a statistical test for this issue.

This statistical approach revealed that the number of iEEG trials included in the analysis of the immediate recall test was, as expected, greater in the 'remembered' than in the 'forgotten' condition (repeated measures ANOVA, main effect of memory F(1,9) = 5.25, p = 0.048). This analysis also showed a statistically significant memory × picture position interaction (F(3,27) = 3.81, p = 0.02; but not a main picture position effect F(3,27) = 0.84, p = 0.48), which indicated that the difference in the number of iEEG trials between conditions was not homogeneous throughout the picture sequence. Similarly, a paired t-test confirmed there were more trials in the 'remembered' than in the 'forgotten' conditions during the recall phase (t(9) = 2.71, p = 0.02). For completeness, we detailed the number of trials in the immediate recall test: 'remembered' condition: 29.7 ± 10.5 for image 1, 31 ± 12.4 for image 2, 32.2 ± 10.4 for image 3, 32.6 ± 11.5 for image 4 and 35.6 ± 9.66 for the recall phase. The number of trials included in the 'forgotten' condition was 18.1 ± 11 for image 1, 17.5 ± 5 for image 2, 17.4 ± 9.9 for image 3, 18.2 ± 9.2 for image 4 and 19.1 ± 10.01 for the recall phase.

However, the number of iEEG trials included in the analysis in the remember and forget condition in the delay recall test showed to be not statistically different (repeated measures ANOVA: main effect of memory $F(1,9) = 0.39$, $p = 0.55$; main effect of picture order $F(3,27) = 0.84$, $p = 0.48$; interaction memory $\times$ picture order $F(3,27) = 0.71$, $p = 0.55$). Similarly, the number of trials included in the iEEG analysis was equivalent in the recall phase for the remember and forget conditions ($t(9) = 0.81$, $p = 0.44$). For completeness, here we detail the number of iEEG trials in each condition for the delayed recall test: 'remembered' condition: 25.5 ± 11.5 for image 1, 22.3 ± 10.1 for image 2, 27 ± 11 for image 3, 27.4 ± 11.7 for image 4 and 28.9 ± 11.42 for the delayed recall phase. The number of trials included in the 'forgotten' condition was 22.3 ± 10.1 for image 1, 22.7 ± 8.7 for image 2, 22.6 ± 9.1 for image 3, 23.4 ± 8.6 for image 4 and 24 ± 10.16 for the delayed recall phase.

These results are important as they ensure that the iEEG findings reported in the current study, which compared hippocampus iEEG signals for encoding and delay recall phases, cannot be simply explained by the difference in the number of analysed trials between the remember and forgotten conditions.

5.3.3. Hippocampal gamma power analysis

Data analysis of spectral power was performed using Fieldtrip (Oostenveld, Fries, Maris, & Schoffelen, 2011) and standard MATLAB functions on the 6 s iEEG epochs selected during the preprocessing stage. The 6 s time window included -2 s from picture onset to avoid padding on low frequencies in the targeted smaller temporal window of 2.5 s from picture onset in subsequent analysis. Frequency decomposition of the data was performed via Fourier analysis based on sliding time windows (moving forward in 10 ms increments). We applied a multi-tapering procedure and a DPSS filter with a fixed window length of 500 ms and seven orthogonal Slepian tapers, resulting in a spectral smoothing of ~ $\pm$ 10 Hz. The resulting power maps were decibel corrected with the average of the -0.5 s prestimulus baseline. For statistical analysis of power maps, we used a non-parametric cluster-based permutation procedure implemented in FieldTrip (Maris & Oostenveld, 2007; Oostenveld et al., 2011) and searched for power fluctuations against artificial data created by time-shuffling the experimental data. We tested the experimental data against the time-shuffled data in a

cluster-based permutation test where labels of the experimental and artificial data were randomly shuffled across participants 1000 times without repetition of combinations. The alpha level was set to 5% across analyses, and parametric t-tests were two-tailed (Maris & Oostenveld, 2007). Spectral power (but also PAC and MOVI described below) was studied within a window of 2.5 s from picture onset. During encoding, the 2.5 s corresponded to the time window of each of the pictures in the sequence and, during recall, this time window corresponded to the time window where the cue picture was on the screen. This way, the results at encoding and recall could be comparable in terms of temporal signal-to-noise properties of the iEEG signal and frequency resolution of the analyses.

5.3.4. Phase-amplitude coupling (PAC) analyses

For the identification of PAC on EEG data elicited by picture encoding and at recall, we first filtered the epochs with the function 'eegfilt' from the EEGlab toolbox of Matlab (Delorme & Makeig, 2004). Low frequencies (4 – 12 Hz) were filtered with a window of 0.3 times the frequency of interest, centred on each frequency step. Similarly, high frequencies (30 – 140 Hz) were filtered with a window of 0.7 times the frequency of interest. This allowed for better sensitivity and allowed Δ(hf) to be always higher than the maximum phase of coupling (low frequency + delta (LF)). Variable bandwidth of phase and amplitude has been shown to increase sensitivity reducing false negatives. It also maintains the equilibrium between the bandwidth of high frequencies needing to be higher than twice the central low frequency, to avoid biases toward slow-modulating rhythms (Aru et al., 2015). Filtered data was z normalized to trial average to ensure that all observed effects were not driven by an Event-Related Potential (ERP). After filtering, we extracted the angle of the Hilbert transform of low frequencies and calculated the phase. High-frequency amplitudes were calculated by the square of the Hilbert envelope.

To quantify phase-amplitude coupling we calculated the mean amplitude of each high-frequency per low-frequency phase bin in 18 different bins of 20 degrees each (Heusser et al., 2016; Pacheco Estefan et al., 2021; Staresina et al., 2015; Tort et al., 2009; Tort et al., 2008) for each trial of each patient. Each trial was then transformed into a probabilistic distribution (sum = 1) by dividing each bin by the sum of all bins. We then averaged the distributions over trials and calculated the Modulation Index (MI) using the Mean Vector Length (MVL) method

(Canolty et al., 2006), which takes the absolute value of the mean complex vector of binned amplitudes to increase specificity towards unimodal phase-amplitude coupling. Similar results were obtained using the Kullback-Leibler Distance with Shannon's entropy approach as a measure of non-uniformity (Tort et al., 2009; Tort et al., 2008). However, we noted that this method could create a bias towards lower modulating frequencies by picking up on bimodal coupling events that originate from higher modulating phases. Therefore, the data reported in our study are the results obtained with the MVL approach. To create surrogate distributions, each amplitude trial was cut at a random timepoint –excluding the first and last 10% of timepoints - and the two obtained amplitude time series were permuted. The time-shuffled amplitude was then binned with its corresponding non-shuffled phase, hence leading to a random phase preference for each trial. The MVL of this random distribution was then calculated in the same fashion as for the experimental trials. We repeated this procedure 1000 times and stored the MVL values of each iteration and participant. We then demeaned PAC data, both real and surrogates in order to perform t-scoring and statistical testing. To confirm that this normalization procedure did not affect the statistical structure of the data we performed a correlation test and observed a rho value of 1 between the original PAC data and the demeaned PAC data.

For statistical testing, we t-scored the real PAC across patients and identified clusters of contiguous pair of frequencies that showed to be significant at a threshold set to 2.5%. We repeated the process for each surrogate matrix and obtained a distribution of 1000 t-sums representing the maximum possible cluster in surrogate data. We only considered significant clusters in the empirical data whose summed t-values exceeded 95% of the surrogate distribution of t-sums.

5.3.5. Mean Opposition Vector Index (MOVI)

To test whether PAC for the memory encoding and memory recall periods rested on different phases of theta, we used an adaptation of the MVL approach described elsewhere (Canolty et al., 2006) on the difference between two distributions of amplitude per phase bin. We denoted $Distrib_A$ and $Distrib_B$ two distributions of amplitude per phase bin. Distributions A and B were calculated in the following way: we denoted f_A and f_p as the frequencies for amplitude and phase respectively of one condition. Within the significant cluster of PAC of

the said condition, we filtered data for each pair of frequencies as following the same procedure implemented to estimate PAC and created a binned distribution of mean amplitude per phase bin, averaged over trials. The distributions of each pair of frequencies were normalized to a probabilistic distribution (sum = 1) to avoid having different magnitudes of amplitude in function of the different frequencies. Once we had a distribution for each pair of frequencies, we averaged all the distributions across frequencies to obtain one single distribution with the average phase preference of the PAC cluster. The second distribution was obtained the same way but by extracting pairs of frequencies from the PAC cluster of its specific condition. In this way, we obtained 2 distributions of mean amplitude per phase bin A and B that each represented the mean amplitude per phase bin of their PAC cluster.

We then calculated MOVI as follows:

1- First, we calculated the difference between $Distrib_A$ and $Distrib_B$.
2- We added to this difference twice the mean of a uniform distribution with the same number of phase bins noted as: $2 * \frac{1}{nbins}$ to have only positive values that were similar to a probabilistic distribution (sum = 1). However, since the resultant distribution came from the difference between two distributions, if opposed, the difference between the peak and the through of this new distribution would have twice the magnitude of either of the original distributions A and B.
3- To correct for this issue, we divided the result by 2 to keep the magnitude of modulation of the alternative distribution $Distrib_{Diff}$ similar to the magnitude of the two distributions it compares.
   The complete formula used to calculate the alternative distribution was:

$$Distrib_{Diff} = \frac{(Distrib_A - Distrib_B) + 2 * \frac{1}{nbins}}{2}$$

4- To avoid having false positives and greater effects due to the difference in two distributions, the resulting alternative distribution was normalized to a probabilistic distribution (sum = 1) by dividing each phase bin by the sum of all bins.
5- We calculated MOVI as the MVL of the resultant distribution $Distrib_{Diff}$ as follows:

$$MOVI = |\frac{\sum Amp_{bin} * e^{i\theta_{bin}}}{nbins}|$$

where Amp_{bin} is the amplitude of each phase bin and θ_{bin} is the angle of each phase bin and $nbins$ is the number of phase bins and MOVI was the calculated MVL of this distribution. The basic premise of MOVI is that if two distributions are opposite, the alternative distribution will be a resulting one with higher MVL than either of the original distributions. If two distributions are in the same direction, then the resultant distribution should be flat and MOVI would be low. And, if one distribution has very low PAC in the surrogate trials, MOVI would be similar to the one obtained from the experimental (real) PAC, avoiding, therefore, finding false positives due to a one directional PAC amplitude in the data.

For the statistical analysis of MOVI, we averaged the experimental MOVI value across patients and the surrogate distributions over patients and then compared the 1000 surrogate scores with the experimental value using a z transformation of the experimental value, which was computed as the experimental MOVI value minus the mean of the surrogate MOVI values, over the standard deviation of the surrogate MOVI distribution ([z = (MOVexp - mean(MOVIsurr)/std(MOVIsurr)]). We obtained a p-value associated to the z value by identifying the fraction of surrogate MOVI values below the experimental MOVI value. We considered significant an experimental MOVI value that was greater than 95% of surrogate MOVI values. Surrogates for MOVI were computed independently for each dataset A or B by shuffling trial labels 1000 times.

We used MOVI instead of more traditional methods for measuring distribution distance (Berens, 2009; Nielsen, 2019; VanRullen, 2016) because we wanted our measure to be dependent on the PAC strength between frequency pairs, and to be sensitive enough to pick on amplitude-driven opposition in angle preference. Other phase opposition indexes such as inter-trial coherence (ITC) or pairwise phase consistency (PPC) do not take into account PAC strength, as they rely on the unit normalization of vectors and might lead to phase opposition reports for frequency pairs where PAC is low or even absent, but with phase spuriously opposed. Furthermore, from a methodological point of view, methods such as ITC rely on the density of occurrences (VanRullen, 2016; Vinck et al., 2010) that does not consider coupling strength of angle preference and where each trial is summarized into a single unit-normalized vector that does not take into account the overall distribution of amplitude per phase but rather only detects the peak, which may compromise the results (i.e., inflating type I and type

II errors). Instead, MOVI is a measure that considers the average distribution across trials and that relies on common effects in terms of PAC and phase preference such as the Kullback-Leibler Distance (DKL) and the Jensen-Shannon Divergence (JSD), a symmetrical adaptation of the DKL (Nielsen, 2019), thereby improving the sensitivity to study theta-gamma phase opposition in task designs like ours. In fact, similar results were obtained using the DKL approach. DKL has been commonly used to compute the modulation index during PAC with an adaptation of the Shannon entropy formula, comparing an experimental distribution to a uniform distribution. However, DKL is used to assess the difference between two distributions A and B with the following formula:

$$DKL(A|B) = A * \log(\frac{A}{B})$$

To implement DKL in our data, we filtered and binned the data following the same procedure described in the MOVI subsection of the methods section of the main manuscript. However, we now directly compared the distributions without passing by an alternate distribution like in MOVI. The results using DKL replicated the ones described in the main paper using MOVI. More specifically, the use of DKL revealed significant gamma band activity coupling to opposed theta phase states during memory encoding and recall ($z = 3.48$, $p = 0.0005$) and that theta-gamma PAC opposition was statistically significant for remembered episodes ($z = 2.97$, $p = 0.003$) but not for forgotten episodes ($z = 0.51$, $p = 0.61$). These results provide converging evidence of theta-gamma phase opposition using two distinct analytical approaches in our data.

5.4.Supplemental Material

	Day 1		Day 2	
#Participant	**Remembered**	**Permuted**	**Remembered**	**Permuted**
S1	85	8.3	46.7	6.7
S2	76.7	10	55	10
S3	78.3	1.7	75	6.7
S4	36.7	6.7	40	8.3
S5	63.3	1.7	46.7	0
S6	76.7	10	71.7	6.7
S7	65	6.7	53.3	6.7
S8	63.6	11.7	43.6	6.7
S9	30	0	25	5
S10	73.3	3.3	75	1.7

Table 5-1. Individual behavioural data.

Percentage of picture series (i.e., episodes) that that included at least 2 pictures during the recall (i.e., remembered) during the test on Day 1 and on Day 2. "Permuted" refers to the proportion of recalled episodes that included the recall of the pictures in incorrect order.

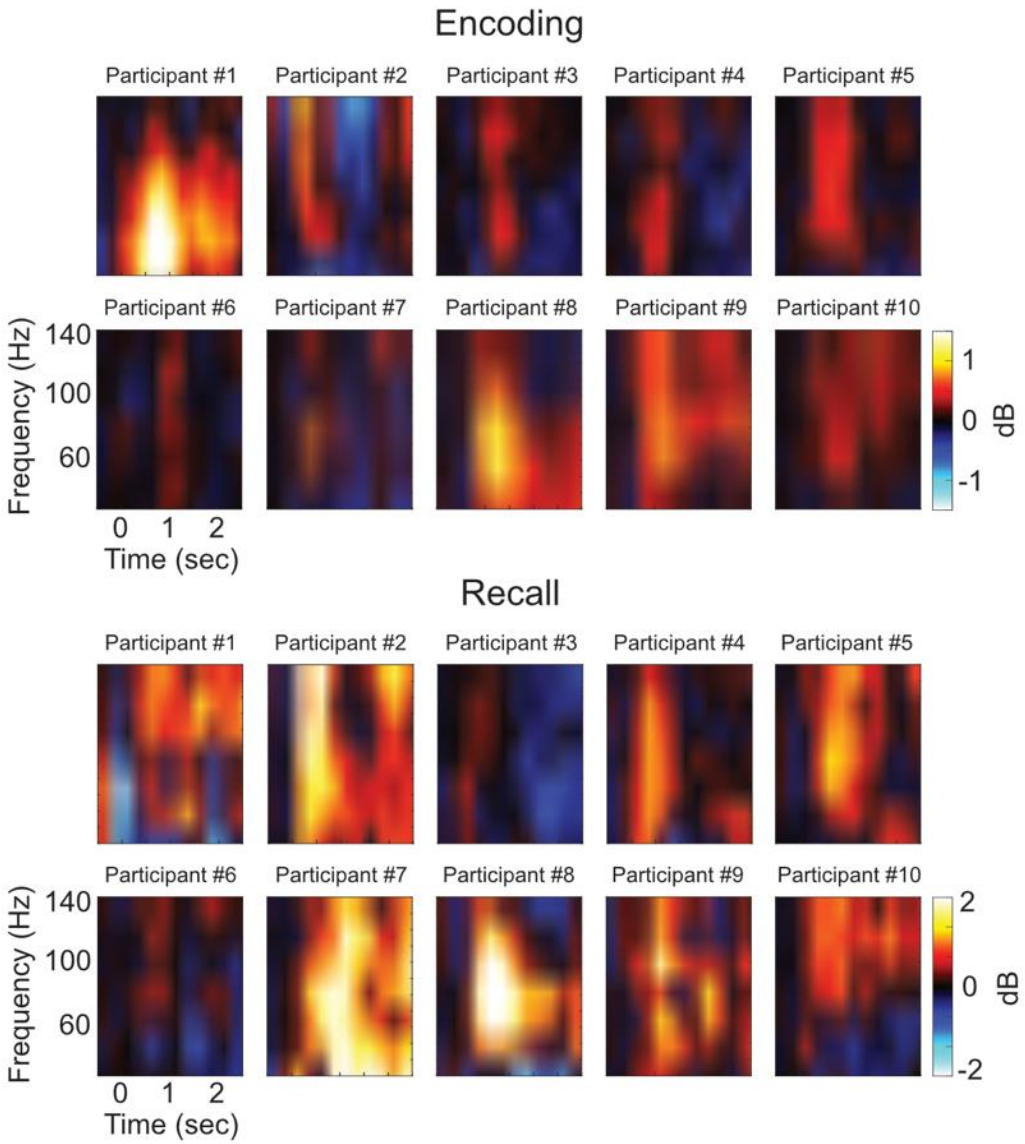

Figure 5-5: Individual hippocampal gamma power during memory encoding and recall.

Single-trial time-frequency analysis on hippocampal EEG data during the encoding of episodes and at their recall on day 2 for each participant of the sample. Spectral power images depict relative gamma power increases and decreases corrected with respect to a 0.5 s baseline window (see Methods).

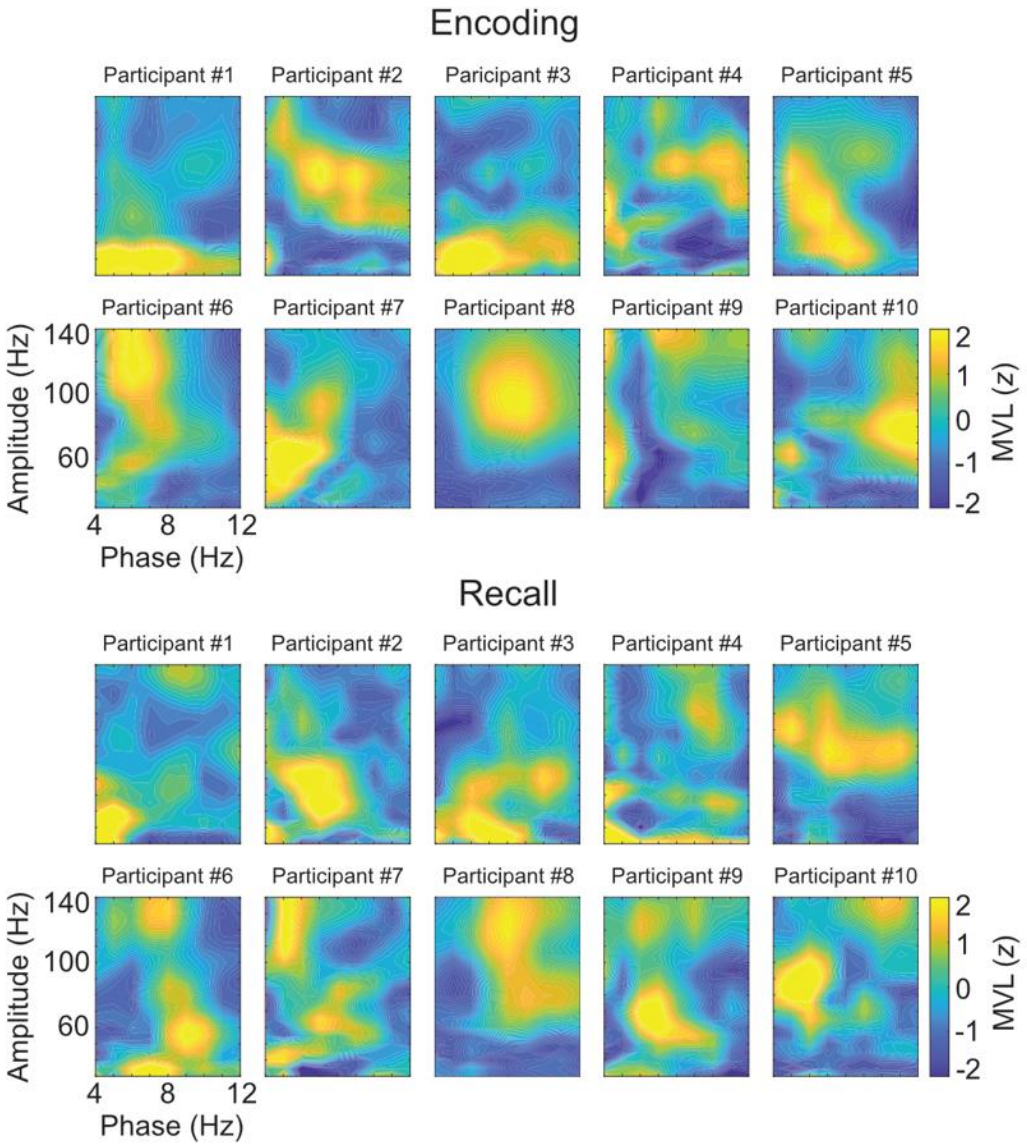

Figure 5-6: Individual theta-gamma phase-amplitude coupling (PAC) during memory encoding and recall.

We assessed the existence of theta-gamma PAC by using a comodulogram method as described in Tort et al, which allows PAC to be scanned from several narrow-filtered frequencies within the theta and gamma frequency bands and quantified the degree of PAC in each frequency pair by using the Mean Vector Length (MVL) method (see Methods). Each image depicts phase-amplitude comodulogram computed during memory encoding and recall on day 2 for each participant of the sample. X-axis indicates phases modulating the signal and the Y-axis represents the modulated amplitude.

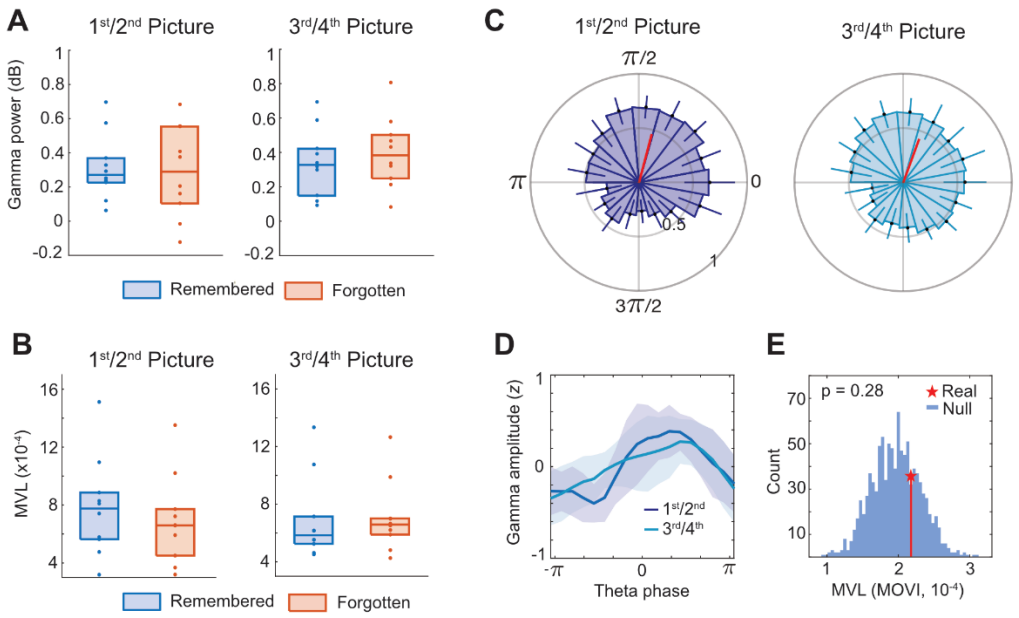

Figure 5-7: Gamma power, theta-gamma PAC and MOVI for 1st/2nd and 3rd/4th pictures from the episodic sequences at encoding.

We examined whether the results obtained when comparing remembered and forgotten episodes at encoding were consistent throughout the complete sequence of pictures. To address this issue, we calculated changes in gamma power, PAC and MOVI by grouping hippocampal iEEG signals elicited at the beginning (1st and 2nd picture) and at the end (3rd and 4th picture) of the episodic sequence and have compared the results within the significant clusters found with all trials (Figure 5-2B and E). (A) Hippocampal gamma power increase for the 1st/2nd and 3rd/4th pictures was similar in magnitude (repeated measures ANOVA, main effect of picture order: F(1,9) = 4.18, p = 0.07) and it did not differ for episodes that were later remembered or forgotten (main effect of memory: F(1,9) = 0.003, p = 0.96; interaction memory x stimulus: F(1,9) = 1.36, p = 0.27). (B) Theta-gamma MVL for the 1st/2nd and 3rd/4th pictures was similar in magnitude (repeated measures ANOVA, main effect of picture order: F(1,9) = 0.20, p = 0.66) and it did not differ for episodes that were later remembered or forgotten (main effect of memory: F(1,9) = 0.18, p = 0.69; interaction memory x stimulus: F(1,9) = 1.04, p = 0.33). For all box plots in (A) and (B), in the box plots the central mark is the median, and the edges of the box are the 25th and 75th percentiles.

Each dot on both plots represents the value for a participant in the corresponding condition. Each dashed line on the boxplot connects the value of a participant in two conditions. (C) Polar distribution of averaged gamma amplitude (z) across participants over theta phases for the 1st/2nd and 3rd/4th pictures. Error bars represent SEM across participants. Grand average across participants is depicted by the thick red line. (D) Average distribution of hippocampal gamma amplitude over theta phase for all participants for the 1st/2nd and 3rd/4th pictures. Shades represent standard error of the mean. (E) Experimental value of MOVI (red star) compared to surrogate value for all participants when comparing MOVI for 1st/2nd and 3rd/4th pictures (z = 0.61, p = 0.5). The results showed that gamma amplitude was coupled to similar theta phase states in the 1st/2nd and in the 3rd/4th pictures during encoding.

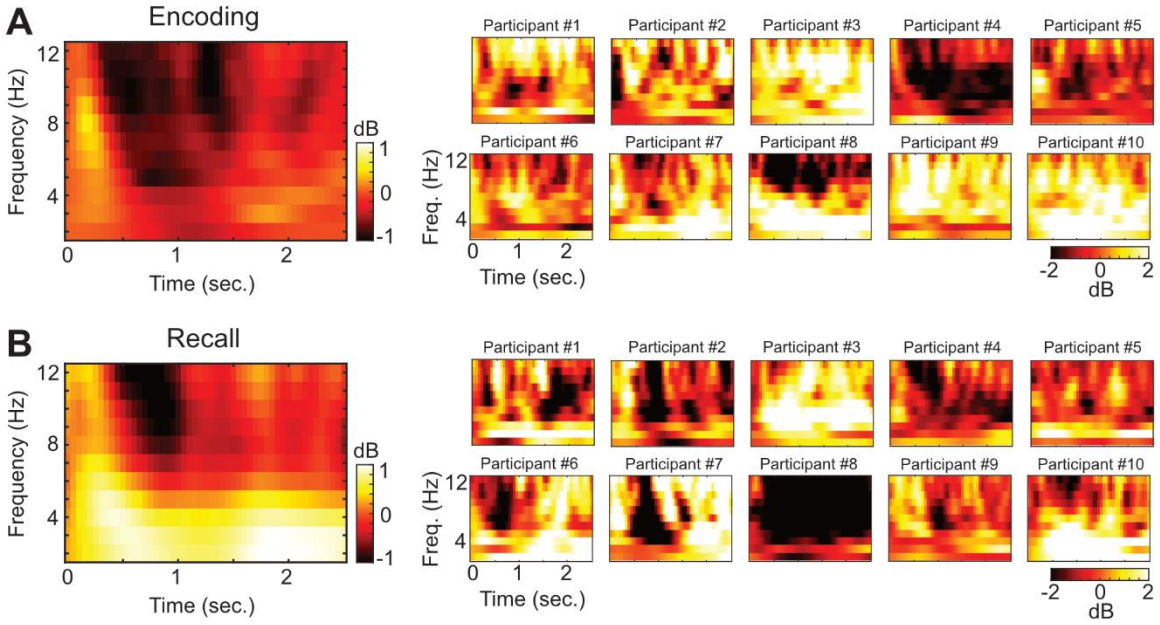

Figure 5-8: Hippocampal spectral power changes for 2 - 12 Hz during encoding and during recall.

Single-trial time-frequency analysis on hippocampal EEG data during the encoding of episodes and at their recall on day 2 for each participant of the sample. To compute the time-frequency decomposition of 2 - 12 Hz we used a hanning taper with a variable time window equal to 5 over each of the frequencies. The analysis was performed from 2 to 12 Hz with steps of 1 Hz and from -0.5 s to 2.5 s relative to stimulus onset with steps of 50 ms.

The spectral power data was then decibel baseline corrected with a baseline of -0.5 s to 0 s relative to picture onset for each patient separately.

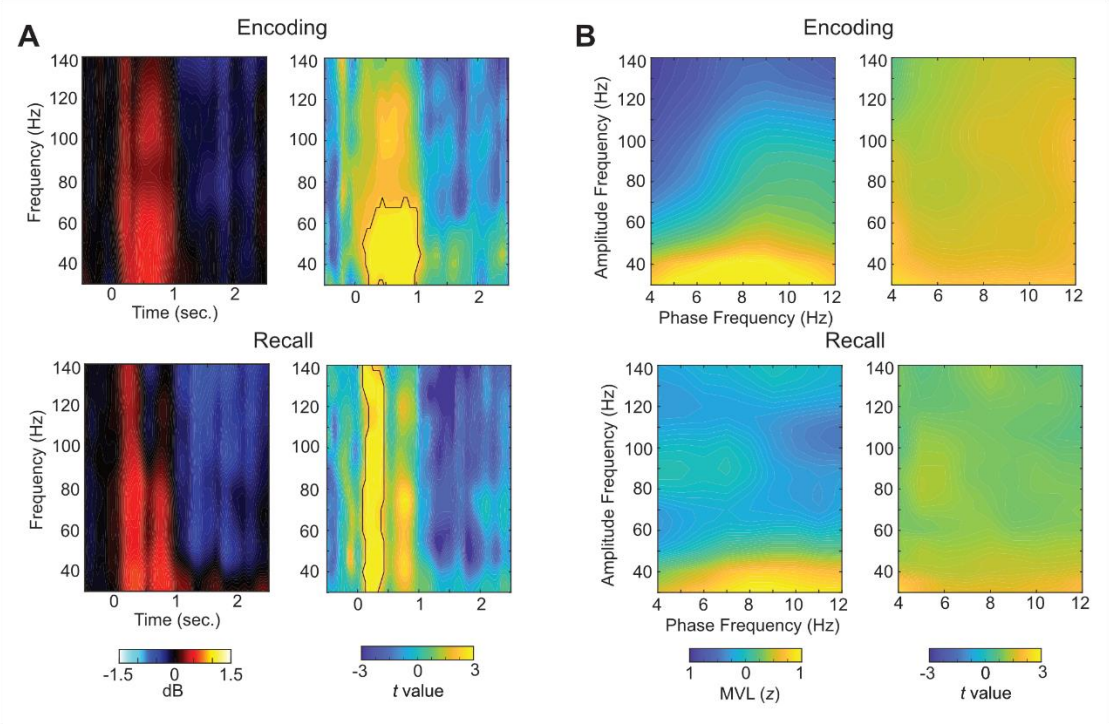

Figure 5-9: Gamma power and theta-gamma PAC in the Middle Temporal Gyrus.

(A) Gamma power modulation during memory encoding and recall from a participants' (N = 9) electrode located at the middle temporal gyrus and the corresponding time-frequency t-value map. A cluster-based permutation test identified a cluster of gamma power increase during encoding (t_{sum} = 434.1, t_{peak} = 5.29, p = 0.048) and during recall (t_{sum} = 408.05, t_{peak} = 4.44, p = 0.009). (B) Map of PAC at encoding and at recall from a participant's electrode located in the middle temporal gyrus and the corresponding phase-to-amplitude t-value map of MVL. A cluster-based permutation test for each of them revealed no statistically significant clusters (all, p > 0.05).

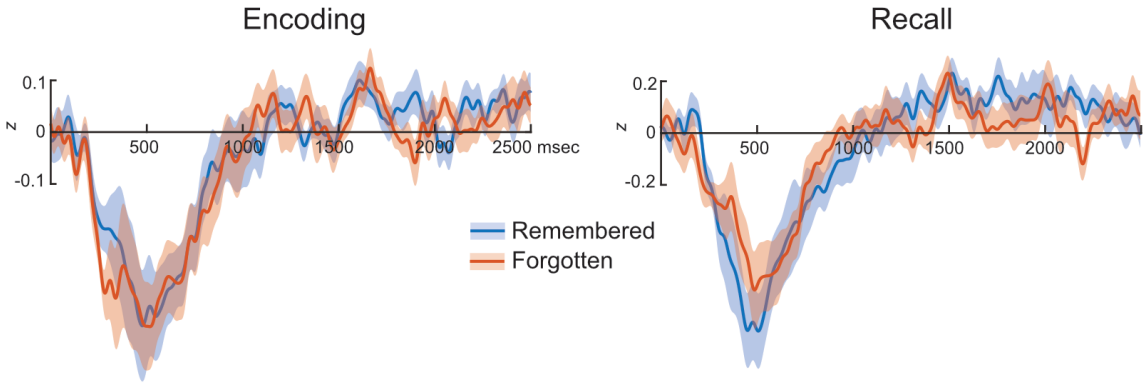

Figure 5-10: Hippocampal Event-Related Potentials (ERPs) during encoding and recall.

Participants' averaged ERPs from hippocampal electrodes for 'remembered' and 'forgotten' episodes during encoding and recall. The shaded area represents SEM across participants. A cluster-based permutation test revealed no statistical differences between ERPs of the two memory conditions, both during encoding and recall ($p > 0.05$).

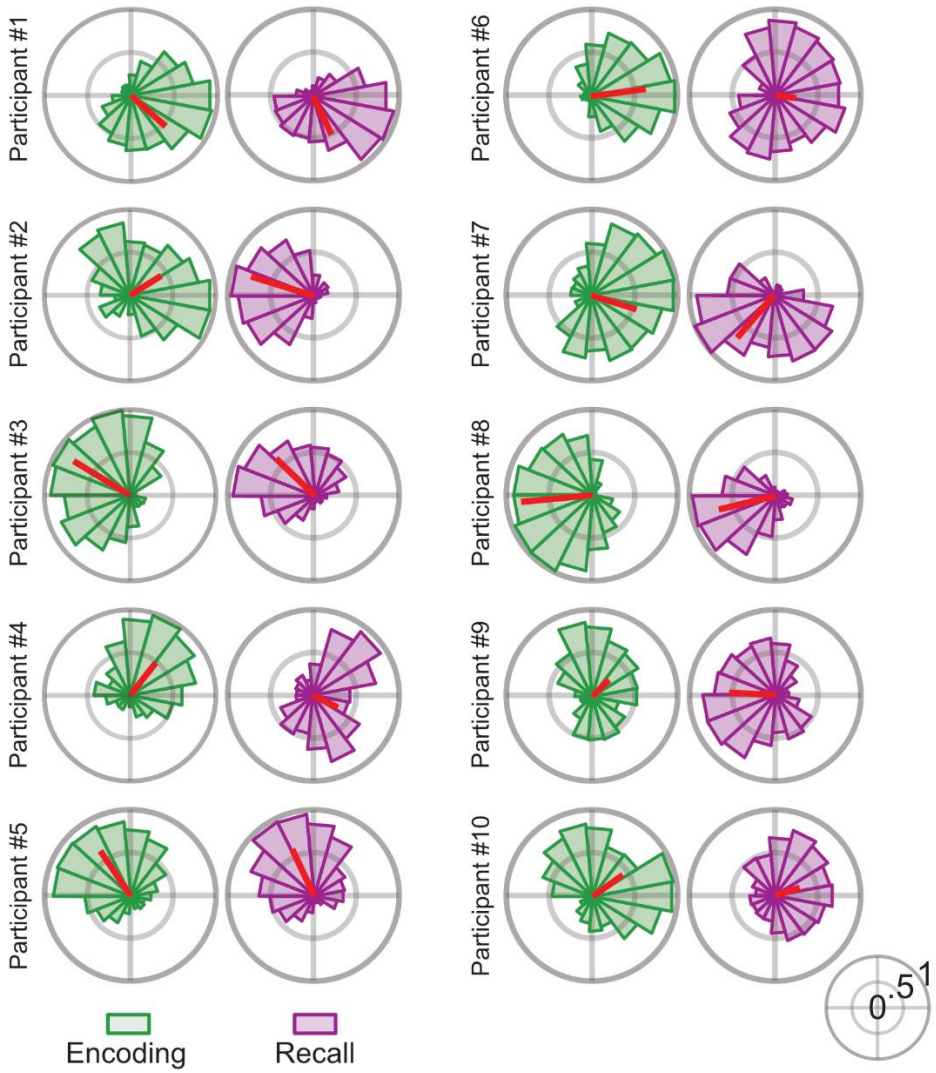

Figure 5-11: Individual distribution of gamma amplitude modulation over theta phases during encoding and during recall.

Polar distribution of averaged gamma amplitude (z) across trials over theta phases within the significant cluster of PAC found at encoding and at recall displayed in Figure 5-2 for each participant of the sample. Average across trials is depicted by the thick red line. Each of the participants showed consistent phase preference (Rayleigh's test, all $p < 0.05$) for all the theta-gamma PAC values within the statistically significant clusters depicted in Figure 5-2E).

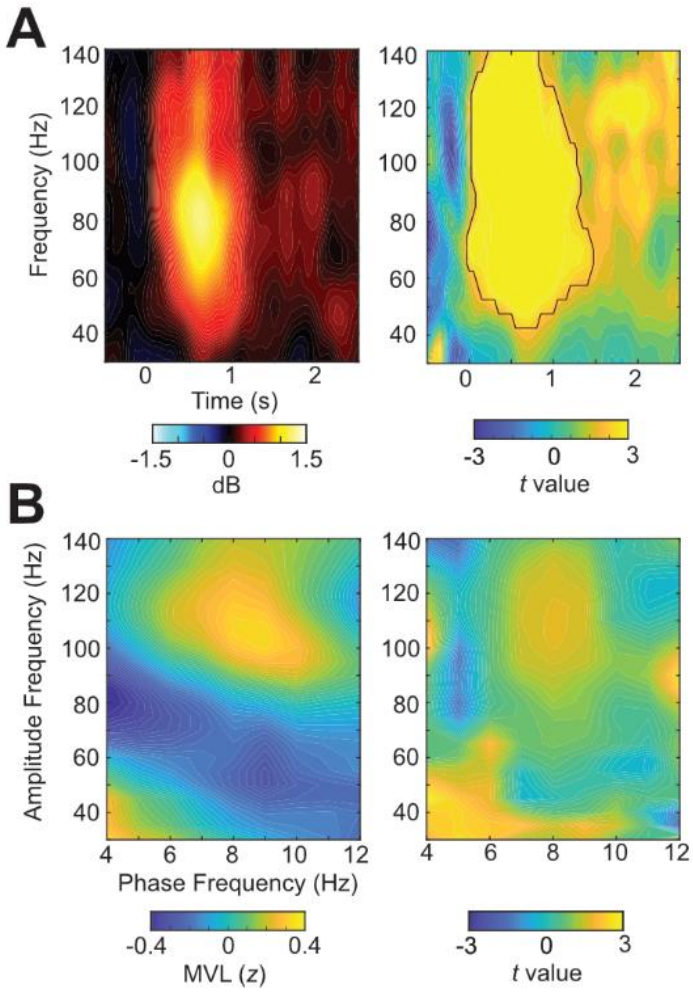

Figure 5-12: Hippocampal gamma power and theta-gamma PAC during recall on day 1.

(A) Averaged gamma power modulations during immediate recall across participants and the corresponding PAC t-value map. Thick black lines depict the cluster that reached statistical significance (cluster statistics: t_{sum} = 1862.8, t_{peak} = 8.61, p = 0.005). (B) Map of PAC at immediate recall across participants and the corresponding phase-to-amplitude t-value map of MVL. Our analysis found a cluster between 4 – 6 Hz for phase and 30 - 45Hz for amplitude but failed to survive the statistical comparison to surrogate cluster t-sums (t_{sum} = 19.7, t_{peak} = 2.99, p = 0.17).

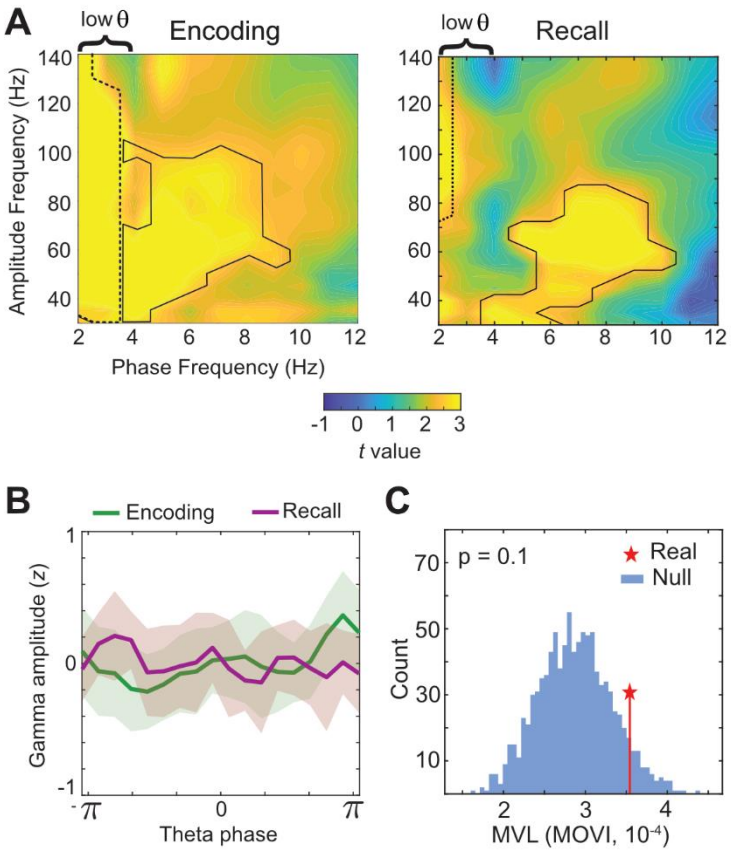

Figure 5-13: Low theta (2 – 3 Hz) - gamma phase-amplitude coupling during memory encoding and recall.

(A) Phase-to-amplitude t-value map during encoding and recall. Thick black solid lines depict the PAC cluster that reached statistical significance described in the main manuscript. Thick black dashed lines depict the gamma PAC to low theta (2 – 3 Hz) cluster identified during encoding ($p < 0.05$) and gamma PAC to low theta (2 Hz) identified during recall ($p = 0.02$). (B) Average distribution of hippocampal gamma amplitude over low theta phase from the two theta clusters identified during encoding (2 – 3 Hz) and recall (2 Hz) for all participants and for all trials. Shaded area represents the SEM across participants. (C) Experimental value of MOVI (red star) compared to surrogate value for all participants for low theta. We found that gamma band activity coupling to low theta phase states during memory encoding and recall were statistically opposed ($z = 1.42$, $p = 0.15$).

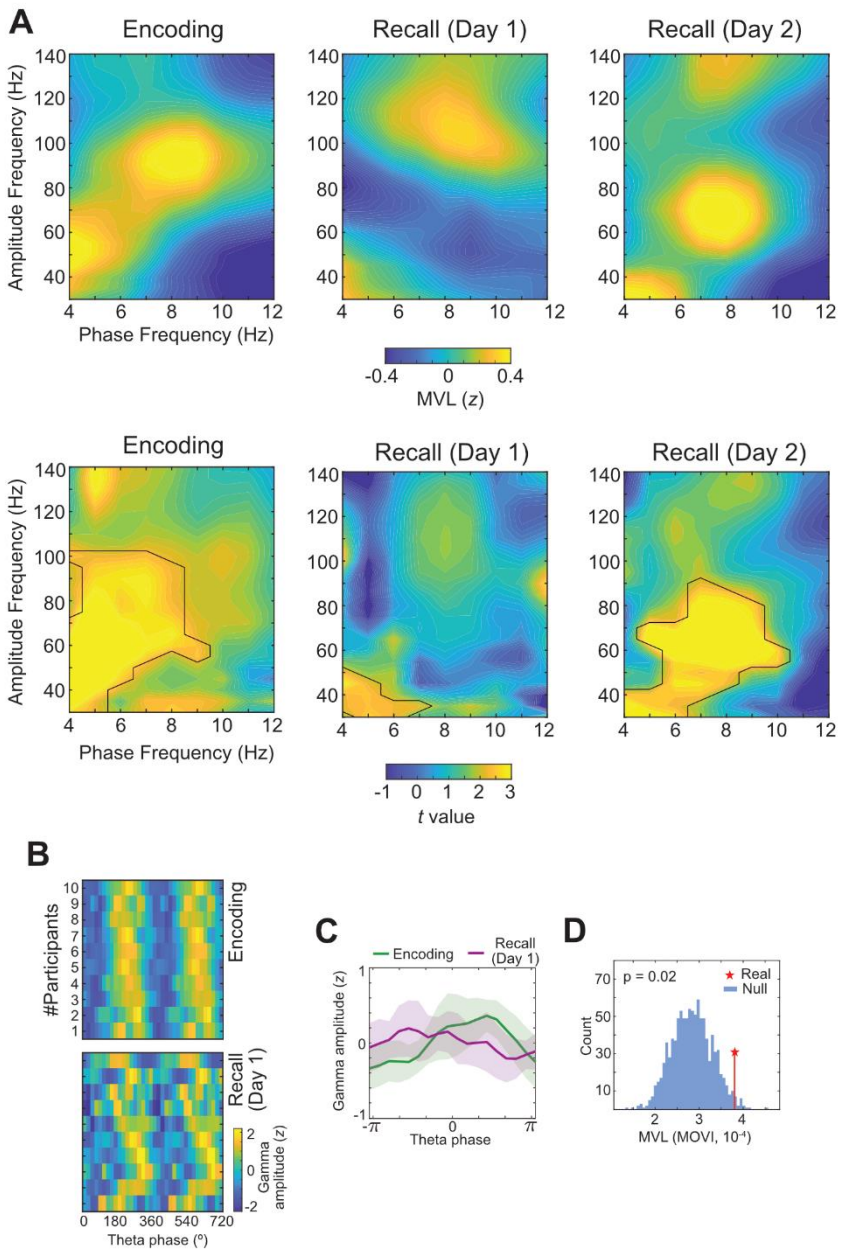

Figure 5-14: Hippocampal theta-gamma phase-amplitude coupling (PAC) during memory encoding and during recall using a time-shuffling approach to create null distributions.

We used a time-shuffling approach [56] to create surrogates to examine whether the PAC findings described in the manuscript, using a label shuffling approach, could be replicated with alternative methods described in the literature. To do so, for each trial of the amplitude data we cut the time-series pseudo randomly between the first 10% of timepoints and the last 10% of timepoints, and then inverted the first and second halves of the trial to have possible

coupling mechanisms inverted in the surrogate condition. Labels of trials were kept the same in this time-shuffling process. Time-shuffled trials were then binned and then the binned trials were averaged over trials as in the label-shuffling condition. We t-scored the experimental data across participants and then extracted clusters using a threshold of significance of 5%. We did the same with each of the 1000 surrogates and then compared the t-sums of the clusters found in the experimental data to the distribution of maximum t-sums found in surrogate iterations. We considered a cluster to be significant only if its experimental tsum exceeded 95% of surrogate tsums. (Top) Group-averaged of phase-amplitude comodulogram computed during memory encoding and recall on day 1 and day 2. (Bottom) Phase-to-amplitude t-value map during encoding and recall. Thick black lines depict the cluster that resulted statistically significant during encoding and recall ($p < 0.05$). Cluster-based statistics confirmed a statistically significant theta-gamma PAC cluster, comprising amplitude modulations in the ~ 40 – 110 Hz frequency range that were coupled to ~ 4 – 9 Hz phases during encoding (cluster statistics: $t_{sum} = 181.7$, $t_{peak} = 5.47$, $p < 0.001$) and amplitude modulations at ~ 50 – 90 Hz frequency range that were coupled to the ongoing theta phases within the ~ 5 – 10 Hz frequency range during recall on day 2 (cluster statistics: $t_{sum} = 144.7$, $t_{peak} = 5.55$, $p < 0.001$). For recall day 1, the cluster that failed to be significant with label shuffling was found significant with the time-shuffling approach ($t_{sum} = 26.8$, $t_{peak} = 3.02$, $p = 0.005$). (B) Distribution of hippocampal gamma amplitude over a cycle of theta at encoding and recall from day 1 for all trials for each participant. Participants' distributions have been realigned to the mean angle direction of encoding and the recall distributions have been realigned relative to each participant's encoding distribution for this figure only. (C) Average distribution of hippocampal gamma amplitude over theta phase for all patients for all trials. Shaded area represents the SEM across participants. (D) Experimental value of MOVI (red star) compared to surrogate value for all participants for all trials ($z = 2.09$, $p = 0.036$).

6. Chapter 6: General Discussion

6.1.Summary of the results

The main objective of the two studies included in this thesis is to explore the neural mechanisms that supported memory encoding and retrieval in humans, and the methods of analysis that allow the quantification those mechanisms in electrophysiological signals. The results of the two studies helped advance the understanding of the neural signatures of memory formation and recall. In the following, the result of each study will be briefly outlined.

6.1.1. Study 1: Measuring phase-amplitude coupling opposition in neurophysiological signals with the Mean Opposition Vector Index (MOVI)

Given that phase amplitude coupling and phase preference processes appear to underlie mnemonic processes, adequate techniques of analysis to distinguish these unique features in neurophysiological data are needed. Current accepted techniques tend to summarise data into unit-normalized vectors, which informs on angle preference of trials or epochs, but removes the coupling strength aspect of the data. Because of this, in Study 1, we aimed to find a way to measure phase-preference differences between neurophysiological datasets by taking into account phase-amplitude coupling strength. We developed a new method, which we termed the Mean Opposition Vector Index (MOVI), to analyze phase-opposition and compared it to an existing more established method (the Jansen-Shannon Divergence (JSD)). We compared both indexes on synthetic data where the parameters of the datasets – such as PAC strength, angle of preference, noise – were known previous to the analysis. We showed that MOVI had a superior sensitivity distinguishing phase-preference differences and adds a coupling-strength dimension that is missing in most traditional analyses studying phase-preference difference or opposition. Additionally, we showed that MOVI was more adapted to the study of neurophysiological data as it was more resistant to noise than JSD, and that it encompassed several settings making it adapted for exploratory studies or analyses.

6.1.2. Study 2: Gamma amplitude is coupled to opposed theta phases during encoding and recall in the human hippocampus.

In Study 2, we aimed to explore theta-gamma interactions in the hippocampus and sought to examine their interaction in the context of encoding and retrieval memory processes. In this study, participants encoded sequences of pictures depicting meaningful episodic-like events. We applied phase-amplitude coupling analysis and phase-opposition analysis on intracortical electroencephalography recordings and the encoding and the recall stage and found evidence that gamma activity was coupled to opposed theta phase states during encoding and recall. Additionally, we found that this opposition was associated with successful memory encoding and recall. Finally, we found that both delayed and immediate recall had shown significant opposition in phase-preference with encoding.

Taken together, these results showcase that encoding and recall rest on distinct theta-gamma interactions. This is akin to results found in rodents, and compatible with mechanistic models of encoding and recall based on rodent literature. Therefore, our studies bridge the gap between rodent and human literature.

6.2. The Importance of theta-gamma interactions for memory processes

Having shown the relationship between PAC and memory formation and retrieval in Study 2, a remaining question is whether phase-amplitude interactions in the human hippocampus are similar to those observed in rodents, and whether they can account for a wide range of memory processes.

The study of theta-gamma interactions encompasses two main mechanisms: Phase-amplitude coupling and phase-preference directionality. PAC analyses how high-frequency activity is nested within a preferential phase but does not inform on phase preference. Phase-preference directionality informs on the consistency of phase preference of a nested high-frequency oscillation but does not inform on the strength of coupling. In order to observe if phase-amplitude interactions in the human hippocampus are similar to those observed in rodents, we needed to look into analysis methods that encompassed both main mechanisms: PAC and phase-preference directionality.

To this end, in Study 1 we looked more closely at the methods and techniques that allow us to detect coupling directionality and that helped us understand these underlying mechanisms. This study was necessary because we wanted to have a comprehensive overview of the phase-coupling mechanisms to be explored in Study 2. Other techniques of detection of phase-preference were useful or informative only once other parameters were controlled for, and we wanted to find a method to analyze phase-preference mechanisms that encompassed several settings such as stability across trials, phase-coupling strength, and that still could differentiate between different conditions.

Additionally, we aimed to use a method of analysis of phase-preference differences that encompassed phase coupling strength, and could observe differences driven by consistent preferences and coupling across trials. To this end, when we developed our method, we transformed trials into binned distributions, similar to what is done with DKL. By binning each trial, it allowed us to average the distributions over trials and obtain an average binned

distribution that encompassed the average phase-preference of all trials, and their average phase preference. In that sense, if each trial was significantly coupled but each to a different angle, the average distribution would have resulted flat. By averaging trials this way, we focused on the observation of common preferences across trials. These binned distributions were then vectorized, similarly to the pre-processing of data for the PACOI technique used in (Costa et al., 2022). Together, these modifications made for an analysis method that encompassed phase-coupling strength with a summarization across trials within two distinct datasets. Our index therefore studies the opposition of phase preference between datasets that are specific to significantly coupled frequencies.

In Study 1 we explored the validity of this method comparing it with a similar more established one on synthetic data. It allowed us to test the limitations and advantages of our method compared to others, and to better understand the results we found in Study 2 when using this index.

In Study 2, similarly to previous studies on PAC and memory, we found phase-coupling mechanisms that were hippocampus specific and that reacted to our encoding and recall task (both immediate and delayed). First, we observed a strong coupling between theta and gamma during encoding and recall. Both frequency bands exhibited an increase in power as shown in the Time-Frequency Analysis (TFA). Neither power nor PAC strength predicted successful memory formation or retrieval, measured by accuracy during the recall task. This could be due to several factors: Study 2 was a free recall task, and most studies that found correlations between PAC strength and memory performance used recognition tasks. In the case of recognition tasks, memory is either present, or it is not. Participants usually need to discriminate between images or words they already have seen, and new ones. Success in distinguishing old from new items measures memory performance. Recognition of old items elicits neural responses in the human hippocampus, where gamma power increases during successful recognition, as well as PAC strength (Axmacher et al., 2010; Staresina et al., 2016). On the other hand, our task was a free recall task of a sequence of pictures. If patients recognized the cue as an image they had already seen but were unable to cite the sequence of images linked to it, we could still observe neural signatures specific to recognition, but not

to recall of linked items, which could explain why we observed increases in gamma power and PAC strength that did not significantly differ between remembered and forgotten sequences.

We therefore reasoned that perhaps it was not the strength of coupling that was important, but rather the direction, and the phase preference of PAC. In line with this hypothesis, we found that gamma power was coupled to opposed phases of theta during encoding and recall. These results are coherent with the model of (Hasselmo et al., 2002) based on rodent literature. The finding speaks not only on a similarity between rodents and humans, but also on underlying mechanisms that are specific to item-context associations and of sequential information being stored, much like real-life episodic events.

We found in Study 2 that Encoding and Recall mechanisms rest on different phase-amplitude phase preferences. Additionally, this phase-amplitude interaction is not only predictive of memory processes (encoding or recall) but also of their success (memory performance). We also found that during encoding, all pictures exhibited a consistent phase preference regardless of image order. Similarly, we found that both recall tasks exhibited a similar phase preference, opposed to encoding. These results suggest that gamma activity is consistently nested into opposed phases of theta during encoding and recall processes, regardless of consolidation (immediate or delayed recall), or position of the item within the sequence. Therefore this phase-preference opposition speaks to cohesive mechanisms that are predictive of memory processes.

Altogether, we conclude that hippocampal theta-gamma phase-amplitude coupling is an underlying neural mechanism supporting memory formation and retrieval, and that the theta rhythm might act as a dynamic switch between those two mechanisms. Although previous studies showed that theta-gamma interactions are correlated to specific item encoding within a context (Heusser et al., 2016), we do not preclude that our findings speak to a larger framework where the study of phase preference in theta-gamma interactions may be the reunion of three models of encoding and recall: First the idea that theta oscillations mediate communication between the hippocampus and the cortex (Hasselmo et al., 2002) and the communication within hippocampal subfields. Secondly, the idea that encoding and recall

avoid interfering with each other not solely by relying on different gamma bands (Colgin, 2015a), but also by nesting gamma within different phases of theta, which ensures a dynamic switch between mnemonic modalities to avoid overlap, but still ensure communication. Finally, the idea that phase-preference of nested gamma speaks about network communication at large, and that PAC preference may inform on the direction of this communication (Bonnefond et al., 2017).

6.3. Do hippocampal phase-amplitude coupling findings speak about a network interaction?

Our studies show a local synchronization of oscillations between low and high frequencies. As our recordings were limited to the hippocampus, we cannot directly ascertain the extent to which this effect is influenced by network activity. However, by drawing upon previous studies, we can make inferences regarding the implications of our findings.

Previous studies on humans (Costa et al., 2022; Griffiths et al., 2019) showed that the synchronization of high-frequency activity between the hippocampus and other areas is relevant to memory formation. For example, successful aversive memory formation was found to be directly linked to amygdala-hippocampal communication. Specifically, the phase of amygdalar theta at which hippocampal neurons preferentially fired was predictive of encoding success (Costa et al., 2022). The conclusion of the study was that amygdala theta phase coordinated amygdala-hippocampal communication that facilitated emotional memory formation.

Another study (Griffiths et al., 2019) found that decreases in neocortical alpha/beta power (8Hz-20hz) preceded hippocampal gamma activity during encoding. Conversely, during recall, hippocampal slow-gamma preceded neocortical beta decreases. The study suggested that this coupling with opposed directionality during encoding and recall reflected the flow of information from the cortex to the hippocampus during encoding, and from the hippocampus to the cortex during retrieval.

Recent studies using close-loop stimulation (Ezzyat et al., 2017; Ezzyat et al., 2018) found that electric stimulations delivered in the lateral temporal lobe were predictive of subsequent memory performance when delivered at times where a decoding approach identified high encoding states characterized by an interaction between low and high-frequency bands. The high encoding are consistent with patterns of power modulations identified in the human hippocampus by (Staresina et al., 2016) that were associated with successful memory retrieval. Another study (Titiz et al., 2017) found that theta-burst microstimulation in the entorhinal cortex increased the ability of the participants to recognize better images and faces in an old/new memory recognition paradigm. In this study, experimenters delivered microstimulation in a theta-burst pattern in the entorhinal cortex of 13 neurosurgical patients while they performed a recognition task with an old / new paradigm. During the stimulation, patients recognized with higher accuracy old images over new ones. Overall, these previous findings speak to the fact that hippocampal activity is influenced by its communication with other brain areas, mediated by low-frequency oscillations.

Since hippocampal activity and memory processes are mediated by communication with other brain areas, processes like encoding and recall may depend on distinct phase state preferences. In humans, directionality of communication between the cortex and the hippocampus identified by (Griffiths et al., 2019) was predictive of memory processes, where cortical activity preceded hippocampal activity during encoding, and the other way around during recall. These findings are consistent with previous rodent literature (Pernia-Andrade & Jonas, 2014) that links entorhinal-hippocampal communication with local hippocampal LFP changes. Locally, this could be reflected by encoding or recall taking place preferentially during certain phases of theta. The study of oscillations of (Kerren et al., 2018) found that oscillatory patterns of theta oscillations were opposed during encoding and recall states. Given that cortical oscillations influence hippocampal activity, the phase preference of memory mechanisms could also be reflected in how the activity of the medial temporal lobe reacts to theta oscillations. The findings of (Pacheco Estefan et al., 2021), where representational signals were clustered to opposed theta cycles during encoding and retrieval speak to this idea. Representational signals were extracted with Representational Similarity Analysis that extracted patterns of activity during encoding and recall and focused on how

much these signals were correlated. In this study, the correlation between high-frequency activity patterns was locked to opposed phases of theta during encoding and recall.

In Study 2, we found that hippocampal high-frequency activity was coupled to opposed phases of theta during encoding and recall. These findings are consistent with previous studies showing that theta oscillations influence local hippocampal LFP. Nested high-frequency oscillations into distinct theta phase-states may reflect a direction of communication between the hippocampus and cortical areas, contributing preferentially to either encoding or recall processes.

6.4. Do our studies bridge the gap with rodent studies?

In Study 2, we found that theta-gamma interactions in the hippocampus supported successful encoding and recall of episodic memory. Although these results are coherent with what was found in previous rodent studies (Manns et al., 2007; Trimper, Galloway, Jones, Mandi, & Manns, 2017) there are still important gaps that exist between humans and rodents.

The main issue revolves around the variation in surgical precision observed during intracranial recordings. When working with rodents, an exceptionally precise anatomical localization at the micrometer level when implanting electrodes can be achieved. This level of precision is unattainable in human studies due to medical considerations. Epileptic patients, for medical reasons, undergo electrode implantations, but the placement and path of these electrodes are determined by the surgical and medical team based on the patient's medical requirements. Consequently, patients are not always implanted in the specific regions of interest (ROI) that we are interested in studying. This, combined with the low data acquisition rate from epileptic patients (approximately 1 per month per hospital, and not necessarily in the ROI), and the potential for surgical inaccuracies (resulting in electrodes not reaching the target area), makes it exceedingly challenging to accumulate sufficient data for a comprehensive analysis of a single precise region, let alone the interaction between multiple regions. Achieving such an analysis would necessitate several patients with electrodes implanted in similar combinations of areas, further complicating the research process.

Our study uncovered theta-gamma interactions that are consistent with rodent studies (Manns et al., 2007) but lacks the spatial precision that would allow for the study of the role of hippocampal subfields, or their relationship. Because of this main difference, it is difficult to compare studies on rodents where precise analysis of the region of interest is possible and studies in humans that have to work around the "randomness" of electrode placement. In Study 2, we included data from hippocampal recordings from 10 patients, but not all in the same hippocampus region: 5 of them were implanted in the anterior hippocampus, 4 of them in the medial, and 1 of them in the posterior, 5 of them in the left hippocampus and 5 in the right.

The second main difference is in the model themselves (rodent and human), in the sense that tasks and experimental protocols need to be adapted to the cognitive capabilities of the model, and to the responses they can provide. For example, humans can provide verbal responses to stimuli, and can give precise feedback. On the other hand, the study of rodents relies on the observation of external cues, such as freezing during a fear response, or path analysis in maze experiments. Similarly, tasks done on mice are difficult to do on humans because of methodological limitations. In rodents, it is possible to obtain recordings from deep brain areas with invasive methods that for ethical reasons cannot be done on humans. Most human neuroimaging techniques (e.g., fMRI, sEEG, MEG) require people to remain seated and often as still as possible. This limits studies on tasks that require movement or navigation. Although recent advances have been made, and it is possible to study how navigational skills evolve in virtual environments (Howard et al., 2014), spatial studies on humans still cannot compare to studies done on rodents. Additionally, studies on rodents often explore spatial navigation (N. Burgess, Maguire, & O'Keefe, 2002; O'Keefe & Burgess, 1996), fear conditioning (Kitamura et al., 2017) or associative memory (Yamaguchi, Aota, Sato, Wagatsuma, & Wu, 2004), while studies on humans also explore episodic memory (Piolino, Desgranges, & Eustache, 2009; Silva, Baldassano, & Fuentemilla, 2019; Svoboda, McKinnon, & Levine, 2006) or sequential episodes (Heusser et al., 2016). Although these types of memories may rely on similar mechanisms, we know that episodic memory differs from fear conditioning or spatial navigation. In that sense it is difficult to generalize findings of

spatial navigation and fear conditioning in rodents to how episodic memory is formed and retrieved in humans. Thus, experiments on humans are essential to better understand human cognition, as inference from animal models is limited. Studies with deep electrodes provide a unique opportunity to study high-level cognitive mechanisms that provide a meaningful insight into memory formation and retrieval. Additionally, studies on humans have the advantage that they can be directed. For example, it is easy to instruct humans to purely do a recall or encoding exercise (Colgin, 2015a) whereas this distinction in rodents may prove more challenging (Igarashi et al., 2014). Nevertheless, several features of neurophysiological activity in rodents have been also observed in humans and provide meaningful insight into mechanisms of memory formation and retrieval.

The first feature observed in the rodent hippocampus was that of theta dependent memory formation and retrieval. The theta rhythm represents the “online” state of the hippocampus and is underlying all mnemonic processes (Buzsaki, 2002). Studies on spatial navigation (O'Keefe & Dostrovsky, 1971; O'Keefe & Recce, 1993; Wills, Cacucci, Burgess, & O'Keefe, 2010) underlie the importance of this rhythm in hippocampal dependent mnemonic processes. Studies on humans (Cornwell, Johnson, Holroyd, Carver, & Grillon, 2008; Kerren et al., 2018) confirmed the important role of hippocampal theta in the encoding and recall of memories. Our findings support this idea by showing the presence of theta activity in the hippocampus during the encoding and retrieval in our task. Our study, taken together with previous literature, underlies the importance of hippocampal theta rhythm in the formation and retrieval of memory traces.

The second feature observed in rodents is the role of high-frequency gamma power in the encoding of memories. Studies on rodents (Bragin et al., 1995; Buzsaki & Wang, 2012) show that increases in gamma power are linked to successful memory formation. These findings were replicated in humans (Lam et al., 2016; Lin et al., 2019; Staresina et al., 2016) where increases in gamma activity are linked to successful encoding or recall of memories. In our study we also observed an increase in gamma power during encoding and recall, however, we did not observe significant differences between successful and unsuccessful processes, which may be linked to the sequential nature of our study, and to the fact that our retrieval

task was a free recall exercise and not a recognition one. In fact, patients in Study 2 said they often recognized the cue, even when they did not recall the associated images of the sequence. This means that during our recall task, when patients looked at the cue, it could have evoked a recognition response, thus increasing gamma activity even for non-remembered sequences. We can speculate based on our results that an increase in gamma activity may therefore inform on the recognition of a cue, rather than the recall of associated items.

A third feature identified in rodents when it comes to hippocampal activity and memory, is the interaction between theta and gamma oscillations mediating the communication between hippocampal subfields (Hyman et al., 2003) and between the hippocampus and cortical areas (Pernia-Andrade & Jonas, 2014). For example, a study showed that certain phases of theta, which they called “high phases”, corresponded to a higher signal input from the entorhinal cortex, while the “low phase” corresponded to a high signal input from hippocampal CA3, and high signal output towards the subiculum from hippocampal CA1 and CA3 (Hyman et al., 2003). Another study found that during a spatial memory task there was a coupling of theta-gamma oscillations in pyramidal cells of the CA1 that corresponded to entorhinal gamma activity during high theta and that coincided with CA3 gamma activity during descending and low phases of theta (Schomburg et al., 2014). Finally, another study (Bragin et al., 1995) showed that entorhinal lesions reduced theta-gamma coding and reduced memory performance, especially in the dentate gyrus of the hippocampus. Together this literature shows that the memory performance related to theta-gamma oscillations reflects the communication between hippocampal subfields and cortical areas.

In our study 2, we were only able to observe the hippocampus as a whole, which limits the interpretation and adaptability to models developed around rodent literature (Hasselmo et al., 2002). However, we found similar results than in the study conducted by Manns and colleagues (Manns et al., 2007) where spiking in the CA1 of the rodent hippocampus was coupled to opposed phases of hippocampal theta during encoding and retrieval. Comparatively, we managed to show that phase-preference of high-frequency activity was not exclusive to spatial navigation processes, but was also present in episodic memory

encoding and recall. Additionally, our findings provide evidence that the computational model based on rodents of (Hasselmo et al., 2002) proposing that theta phases separate encoding and retrieval processes extends to humans as well. It also speaks to the fact that the theta rhythm might be coordinating a dynamic communication between the hippocampus and other brain areas (Ezzyat et al., 2017; Ezzyat et al., 2018; Griffiths et al., 2019; Manns et al., 2007) where coupling directionality locally is representative of communication between different areas necessary for memory storage.

The last feature studied in rodents is how theta-gamma interactions underlie plasticity mechanisms necessary to memory formation and retrieval. In the case of our study, we could not directly observe LTP and LTD, however, by studying memory performance on the same day and on the following, we could infer on how well a sequence was encoded. In rodents, theta-gamma interactions were shown to increase plasticity in the hippocampus where gamma activity during a phase of theta promoted LTP, and promoted LTD during the opposed phase of theta (Hyman et al., 2003). This increase in LTP reflected an increase in memory performance, thus suggesting that theta-gamma interactions drive hippocampal plasticity mechanisms essential to memory formation. In Study 2, we found that when encoding and recall were significantly opposed, patients had a higher memory performance, suggesting that theta-gamma phase preference plays a role not only in distinguishing mnemonic mechanisms (encoding and recall) but also influences the stability of memory traces, and thus memory performance.

Although our findings cannot speak of the network interactions between the hippocampus and the cortex, our findings provide the missing element to a comprehensive overview of the role of theta-gamma interactions in memory processes in humans. Our results show that theta-gamma interactions in the hippocampus predict memory processes (encoding, recall) and their success based on subsequent memory performance. These findings are similar to neural properties found in rodents, and coherent with the model based on rodents proposed by (Hasselmo et al., 2002). Our study thus bridges neural theta-gamma interaction findings between the two species.

6.5.Limitations and other considerations

6.5.1. Epilepsy and hospital limitations

Because our study was conducted on epileptic patients, we had to adapt our design to hospital procedures, and to the fact that epileptic patients get tired faster than healthy participants. Because of this, we had to significantly shorten our protocol by reducing baseline and stimuli times, and by reducing the number of pictures per series from an original 6 pictures to 4. These limitations reduced the power of our analyses, especially after artifact rejection and separation by accuracy.

Additionally, recruitment of epileptic patients is a slow process. We managed to obtain recordings in our target area from 10 patients, but analyzed the structural data of 20, where we had to discard patients because they were not implanted in temporal areas, or because although it was planned for patients to have hippocampal recordings, the electrode never made it to the ROI during surgery. Because of this, the number of patients included in the final sample of the study reduced the statistical power of our second-level analyses. Normally, in the time allocated for the thesis, we could have obtained a larger number of recordings, however, the COVID-19 pandemic made it impossible to have access to epileptic patients between 2020 and 2022. This significantly reduced the number of patients we otherwise could have recorded.

Another limitation previously mentioned by working with epileptic patients is the fact that each implantation is different. Therefore, it is difficult to perform network connectivity analyses and statistical assessments at the second level.

Finally, working with epileptic patients raises the question of whether epileptic activity disrupts in some way memory formation, and if what we observe as gamma activity is not epileptic activity. In one way we control for both of these by removing trials that exhibit disruptive epileptic activity, it is however possible that non-disruptive epileptic activity is not identified and still makes it in the data. To some extent, epilepsy does influence memory

formation (Miller, Mothakunnel, Flanagan, Nikpour, & Thayer, 2017) as patients with focal epilepsy exhibit a higher forgetting rate for long-term memory. This could have been problematic for our study as our experiment lasted 2 days. However, recall performance was similar across patients on day 2, although they all had a different locus of epilepsy, suggesting that the epileptic locus did not play a role in disrupting memory processes. Additionally, we took precautions such as selecting electrodes far from the epileptic locus, and selecting trials strictly to ensure there was no disruptive epileptic activity. By doing so we limited the impact that epileptic activity could have had on our design, and ensured that our results are reliable and inferential to processes happening in healthy people.

6.5.2. Particularity of our experimental task: picture sequence, free recall, 2-day format

Our experimental task was different from the ones we usually see in intracranial EEG studies that tend to use recognition memory (Staresina et al., 2016), context-item associations (Tort et al., 2009) or associative memory (Pacheco Estefan et al., 2021). On the other hand, our task involved the encoding of sequential and congruent images and two distinct recall tasks with the same cues. These differences in the protocol raise three main concerns:

First, the series in our tasks were episodes. They were composed of several items that were congruently encompassed in a similar context. Therefore during encoding patients could encode three different aspects of the sequences: First, the contextual aspect, that spoke to the overall message of the images, for example a birthday party when the images were a balloon, a cake, a piñata, and a game. Second, the items, where each image had to be recalled separately, and may have elicited a different response than a context (Silva et al., 2019). Third, the temporal aspect, where the temporal sequence of the image had to be recalled in order, which could have elicited different neurophysiological mechanisms than associative pairing (Heusser et al., 2016).

Additionally, our task included two recall tasks: one right after encoding and one a day after. It is unusual to see in intracranial studies 2-day task design due to the difficulty of acquisition

of such data, hospital regulations, and possible disruptions caused by epileptic seizures. Hence there are several limitations that may arise from this particular protocol.

First, is the testing effect, where repetitions of a stimulus enhance retrieval likelihood (Polack & Miller, 2022) and can also modify memory traces (Diekelmann, Buchel, Born, & Rasch, 2011). Although recall on day 2 was less precise than on day 1, memory traces seemed to be stable according to the verbal recollection given by patients. Despite this, memories on day 2 may have been affected by the recall task on day 1.

Secondly, on day 2, patients recalled memories that had been consolidated. In other experiments (Axmacher et al., 2010; Heusser et al., 2016; Staresina et al., 2016), recall takes place shortly after encoding, but in our case 24 hours passed between the first recall task and the second. Because of this time-lapse, we observed not only early memory traces but also consolidated memory traces, that may rely on slightly different processes. Our analyses, however, show that phase-preference opposition between encoding and recall remains stable for both recall tasks.

Finally, our task was a verbal cued and free recall, where patients had to recall a whole sequence only based on the first image of each. In that sense, one limitation is that we worked under the assumption that seeing the cue was sufficient to elicit a memory response of the whole sequence. In the case of Study 2, we found that this assumption did not change the interpretation of our results, as we were focusing on common phase-coupling mechanisms during encoding and recall. Additionally, phase-preference did not change as a function of picture order, which further consolidates the idea that picture order did not influence the results. However, it would be interesting in the future to specifically look at the amount of reinstatement of non-cue images in recall events in order to back up this assumption. One way of doing it would be with Representational-Similarity Analysis (RSA) (Pacheco Estefan et al., 2021; Silva et al., 2019; Staresina et al., 2016; Wu, Vinals, Ben-Yakov, Staresina, & Fuentemilla, 2022) in order to evaluate the similarity of neural signatures between encoding and recall of non-cue items.

Another limitation comes from the fact that patients did a verbal recall and answers were recorded through an external recorder, which means that it would be difficult to examine the precise timing associations between neural signals and memory retrieval of the picture sequence. In the same way, we measured neural responses during cue presentation during recall, which means that there could have been many factors interacting at that moment given the nature of the task and the recall. There is still much to explore in that sense in order to disentangle recognition of a context from the association to other items.

6.5.3. Data Simulation compared to real electrophysiological data

In Study 1, we simulated data only for a pair of coupled frequencies (5Hz for low frequency and 80Hz for high frequencies). Several studies have simulated data using sine functions (Cohen, 2008; Tort et al., 2010) using several settings, but the one that seems more elusive is the simulation of neurophysiological noise. On one hand, we consider that there is random noise, which explains our use of pink noise (Cohen, 2017), on the other hand, the interconnected nature of the human brain makes it that several mechanisms happening in other regions of the brain will inevitably influence ongoing local oscillations in ways that we cannot yet predict. For this reason, we also added a noise function that generates random coupling between low and high frequencies. Finally, there are other oscillations happening in the studied range that may or may not explain the observed mechanisms, but disentangling the exact function of these frequencies and these oscillations is still challenging. For this reason, simulated neurophysiological data has still different properties than real electrophysiological data, and although we are getting closer to simulating more accurately LFP signals, we have to take into consideration that when testing a new analysis or technique on neurophysiological data, we are testing them on data that is much “cleaner” than the one we can observe in real-life situations, and does not include the several interactions that we know happen in brains. This can be specifically seen in the memory network, where for example the CA1 subfield of the hippocampus receives projections from several cortical areas, from within other hippocampal subfields, and from reward / novelty loops at the same time. In this case, even though we can analyze LFP in concomitance with a behavioral output, disentangling the different mechanisms and accurately representing them in a simulation is still challenging.

7. Chapter 7: Conclusions

- Hippocampal activity elicited during encoding and cue presentation is stable and drives an increase in high-frequency power and a decrease in low-frequency power, similar to previous studies on the matter. Such activation did not quantify memory success, but was specific to the hippocampus and time-locked to memory functions.
- Hippocampal phase-amplitude coupling is associated with memory functions and seems to be essential to memory formation, but not necessarily to the retrieval of sequences. It is elicited specifically in the hippocampus and in a stable manner across all items within a sequence, and during cue presentation during recall.
- Phase-preference of coupled gamma power to theta phase appears to be essential to memory encoding and recall, and direction of phase preference seems to be predictive not only of memory function but also of the presence of memory traces for sequential episodic information. This phase preference appears to be an underlying mechanism that speaks to the interconnected nature of the memory system and to how different areas involved in mnemonic processes interact and communicate.
- Phase preference between recall processes seems to be stable between day 1 and day 2, and phase preference across item-encoding also appears to be stable, suggesting that this phase preference during coupling is not due only to item-specific neural signatures but to general mechanisms happening during these two memory functions.
- Techniques and analyses used to study phase-coupling and phase-preference mechanisms are varied, and a specific interest should be given to the choice of these analyses in order to accurately answer a question and solve a problem, as all analyses, although similar, give slightly different insights into underlying coupling mechanisms essential to memory processes and functions.
- Simulation of electrophysiological data can be used to test and compare different analysis techniques, but confirmation of these comparisons on real data is needed

because of the intrinsic differences still existing between simulations and real neurophysiological data.

8. References

Aggleton, J. P., & Brown, M. W. (1999). Episodic memory, amnesia, and the hippocampal-anterior thalamic axis. *Behav Brain Sci, 22*(3), 425-444; discussion 444-489.

Akhter, S., Aziz, R. K., Kashef, M. T., Ibrahim, E. S., Bailey, B., & Edwards, R. A. (2017). Kullback Leibler divergence in complete bacterial and phage genomes. *PeerJ, 5*, e4026. doi:10.7717/peerj.4026

Amengual, J. L., Vernet, M., Adam, C., & Valero-Cabre, A. (2017). Local entrainment of oscillatory activity induced by direct brain stimulation in humans. *Sci Rep, 7*, 41908. doi:10.1038/srep41908

Aru, J., Aru, J., Priesemann, V., Wibral, M., Lana, L., Pipa, G., . . . Vicente, R. (2015). Untangling cross-frequency coupling in neuroscience. *Curr Opin Neurobiol, 31*, 51-61. doi:10.1016/j.conb.2014.08.002

Axmacher, N., Henseler, M. M., Jensen, O., Weinreich, I., Elger, C. E., & Fell, J. (2010). Cross-frequency coupling supports multi-item working memory in the human hippocampus. *Proc Natl Acad Sci U S A, 107*(7), 3228-3233. doi:10.1073/pnas.0911531107

Bahramisharif, A., Jensen, O., Jacobs, J., & Lisman, J. (2018). Serial representation of items during working memory maintenance at letter-selective cortical sites. *PLoS Biol, 16*(8), e2003805. doi:10.1371/journal.pbio.2003805

Berens, P. (2009). CircStat: A MATLAB Toolbox for Circular Statistics. *Journal of Statistical Software, 31*(10), 1 - 21. doi:10.18637/jss.v031.i10

Bieri, K. W., Bobbitt, K. N., & Colgin, L. L. (2014). Slow and fast gamma rhythms coordinate different spatial coding modes in hippocampal place cells. *Neuron, 82*(3), 670-681. doi:10.1016/j.neuron.2014.03.013

Bliss, T. V., & Collingridge, G. L. (1993). A synaptic model of memory: long-term potentiation in the hippocampus. *Nature, 361*(6407), 31-39. doi:10.1038/361031a0

Bonnefond, M., Kastner, S., & Jensen, O. (2017). Communication between Brain Areas Based on Nested Oscillations. *eNeuro, 4*(2). doi:10.1523/ENEURO.0153-16.2017

Bontempi, B., Laurent-Demir, C., Destrade, C., & Jaffard, R. (1999). Time-dependent reorganization of brain circuitry underlying long-term memory storage. *Nature, 400*(6745), 671-675. doi:10.1038/23270

Bragin, A., Jando, G., Nadasdy, Z., Hetke, J., Wise, K., & Buzsaki, G. (1995). Gamma (40-100 Hz) oscillation in the hippocampus of the behaving rat. *J Neurosci, 15*(1 Pt 1), 47-60.

Brainard, D. H. (1997). The Psychophysics Toolbox. *Spat Vis, 10*(4), 433-436.

Burgess, A. P., & Gruzelier, J. H. (1997). Short duration synchronization of human theta rhythm during recognition memory. *Neuroreport, 8*(4), 1039-1042. doi:10.1097/00001756-199703030-00044

Burgess, N., Maguire, E. A., & O'Keefe, J. (2002). The human hippocampus and spatial and episodic memory. *Neuron, 35*(4), 625-641.

Burke, J. F., Long, N. M., Zaghloul, K. A., Sharan, A. D., Sperling, M. R., & Kahana, M. J. (2014). Human intracranial high-frequency activity maps episodic memory formation in space and time. *Neuroimage, 85 Pt 2*, 834-843. doi:10.1016/j.neuroimage.2013.06.067

Burke, J. F., Sharan, A. D., Sperling, M. R., Ramayya, A. G., Evans, J. J., Healey, M. K., . . . Kahana, M. J. (2014). Theta and high-frequency activity mark spontaneous recall of episodic memories. *J Neurosci, 34*(34), 11355-11365. doi:10.1523/JNEUROSCI.2654-13.2014

Buzsaki, G. (1989). Two-stage model of memory trace formation: a role for "noisy" brain states. *Neuroscience, 31*(3), 551-570. doi:10.1016/0306-4522(89)90423-5

Buzsaki, G. (2002). Theta oscillations in the hippocampus. *Neuron, 33*(3), 325-340.

Buzsaki, G., Anastassiou, C. A., & Koch, C. (2012). The origin of extracellular fields and currents--EEG, ECoG, LFP and spikes. *Nat Rev Neurosci, 13*(6), 407-420. doi:10.1038/nrn3241

Buzsaki, G., & Wang, X. J. (2012). Mechanisms of gamma oscillations. *Annu Rev Neurosci, 35*, 203-225. doi:10.1146/annurev-neuro-062111-150444

Canolty, R. T., Edwards, E., Dalal, S. S., Soltani, M., Nagarajan, S. S., Kirsch, H. E., . . . Knight, R. T. (2006). High gamma power is phase-locked to theta oscillations in human neocortex. *Science, 313*(5793), 1626-1628. doi:10.1126/science.1128115

Chicco, D., Totsch, N., & Jurman, G. (2021). The Matthews correlation coefficient (MCC) is more reliable than balanced accuracy, bookmaker informedness, and markedness in two-class confusion matrix evaluation. *BioData Min, 14*(1), 13. doi:10.1186/s13040-021-00244-z

Cirelli, C., & Tononi, G. (2017). The Sleeping Brain. *Cerebrum, 2017*.

Cohen, M. X. (2008). Assessing transient cross-frequency coupling in EEG data. *J Neurosci Methods, 168*(2), 494-499. doi:10.1016/j.jneumeth.2007.10.012

Cohen, M. X. (2017). Multivariate cross-frequency coupling via generalized eigendecomposition. *Elife, 6*. doi:10.7554/eLife.21792

Colgin, L. L. (2015a). Do slow and fast gamma rhythms correspond to distinct functional states in the hippocampal network? *Brain Res, 1621*, 309-315. doi:10.1016/j.brainres.2015.01.005

Colgin, L. L. (2015b). Theta-gamma coupling in the entorhinal-hippocampal system. *Curr Opin Neurobiol, 31*, 45-50. doi:10.1016/j.conb.2014.08.001

Colgin, L. L., Denninger, T., Fyhn, M., Hafting, T., Bonnevie, T., Jensen, O., . . . Moser, E. I. (2009). Frequency of gamma oscillations routes flow of information in the hippocampus. *Nature, 462*(7271), 353-357. doi:10.1038/nature08573

Contreras, D., & Steriade, M. (1995). Cellular basis of EEG slow rhythms: a study of dynamic corticothalamic relationships. *J Neurosci, 15*(1 Pt 2), 604-622. doi:10.1523/JNEUROSCI.15-01-00604.1995

Cornwell, B. R., Johnson, L. L., Holroyd, T., Carver, F. W., & Grillon, C. (2008). Human hippocampal and parahippocampal theta during goal-directed spatial navigation predicts performance on a virtual Morris water maze. *J Neurosci, 28*(23), 5983-5990. doi:10.1523/JNEUROSCI.5001-07.2008

Costa, M., Lozano-Soldevilla, D., Gil-Nagel, A., Toledano, R., Oehrn, C. R., Kunz, L., . . . Strange, B. A. (2022). Aversive memory formation in humans involves an amygdala-hippocampus phase code. *Nat Commun, 13*(1), 6403. doi:10.1038/s41467-022-33828-2

Csorba, B. A., Krause, M. R., Zanos, T. P., & Pack, C. C. (2022). Long-range cortical synchronization supports abrupt visual learning. *Curr Biol, 32*(11), 2467-2479 e2464. doi:10.1016/j.cub.2022.04.029

Delorme, A., & Makeig, S. (2004). EEGLAB: an open source toolbox for analysis of single-trial EEG dynamics including independent component analysis. *J Neurosci Methods, 134*(1), 9-21. doi:10.1016/j.jneumeth.2003.10.009

Diekelmann, S., Buchel, C., Born, J., & Rasch, B. (2011). Labile or stable: opposing consequences for memory when reactivated during waking and sleep. *Nat Neurosci, 14*(3), 381-386. doi:10.1038/nn.2744

Douchamps, V., Jeewajee, A., Blundell, P., Burgess, N., & Lever, C. (2013). Evidence for encoding versus retrieval scheduling in the hippocampus by theta phase and acetylcholine. *J Neurosci, 33*(20), 8689-8704. doi:10.1523/JNEUROSCI.4483-12.2013

Eichenbaum, H. (1992). The hippocampal system and declarative memory in animals. *J Cogn Neurosci, 4*(3), 217-231. doi:10.1162/jocn.1992.4.3.217

Eichenbaum, H., Sauvage, M., Fortin, N., Komorowski, R., & Lipton, P. (2012). Towards a functional organization of episodic memory in the medial temporal lobe. *Neurosci Biobehav Rev, 36*(7), 1597-1608. doi:10.1016/j.neubiorev.2011.07.006

Ezzyat, Y., Kragel, J. E., Burke, J. F., Levy, D. F., Lyalenko, A., Wanda, P., . . . Kahana, M. J. (2017). Direct Brain Stimulation Modulates Encoding States and Memory Performance in Humans. *Curr Biol, 27*(9), 1251-1258. doi:10.1016/j.cub.2017.03.028

Ezzyat, Y., Wanda, P. A., Levy, D. F., Kadel, A., Aka, A., Pedisich, I., . . . Kahana, M. J. (2018). Closed-loop stimulation of temporal cortex rescues functional networks and improves memory. *Nat Commun, 9*(1), 365. doi:10.1038/s41467-017-02753-0

Fell, J., Fernandez, G., Klaver, P., Axmacher, N., Mormann, F., Haupt, S., & Elger, C. E. (2006). Rhinal-hippocampal coupling during declarative memory formation: dependence on item characteristics. *Neurosci Lett, 407*(1), 37-41. doi:10.1016/j.neulet.2006.07.074

Fernandez-Ruiz, A., Oliva, A., Nagy, G. A., Maurer, A. P., Berenyi, A., & Buzsaki, G. (2017). Entorhinal-CA3 Dual-Input Control of Spike Timing in the Hippocampus by Theta-Gamma Coupling. *Neuron, 93*(5), 1213-1226 e1215. doi:10.1016/j.neuron.2017.02.017

Fischl, B. (2012). FreeSurfer. *Neuroimage, 62*(2), 774-781. doi:10.1016/j.neuroimage.2012.01.021

Fischl, B., Sereno, M. I., & Dale, A. M. (1999). Cortical surface-based analysis. II: Inflation, flattening, and a surface-based coordinate system. *Neuroimage, 9*(2), 195-207. doi:10.1006/nimg.1998.0396

Forrester, N. (2021). Mental health of graduate students sorely overlooked. *Nature, 595*(7865), 135-137. doi:10.1038/d41586-021-01751-z

Fossati, P. (2013). Imaging autobiographical memory. *Dialogues Clin Neurosci, 15*(4), 487-490.

Fries, P. (2005). A mechanism for cognitive dynamics: neuronal communication through neuronal coherence. *Trends Cogn Sci, 9*(10), 474-480. doi:10.1016/j.tics.2005.08.011

Fuentemilla, L., Penny, W. D., Cashdollar, N., Bunzeck, N., & Duzel, E. (2010). Theta-coupled periodic replay in working memory. *Curr Biol, 20*(7), 606-612. doi:10.1016/j.cub.2010.01.057

Gabrieli, J. D., Cohen, N. J., & Corkin, S. (1988). The impaired learning of semantic knowledge following bilateral medial temporal-lobe resection. *Brain Cogn, 7*(2), 157-177. doi:10.1016/0278-2626(88)90027-9

Genzel, L., Kroes, M. C., Dresler, M., & Battaglia, F. P. (2014). Light sleep versus slow wave sleep in memory consolidation: a question of global versus local processes? *Trends Neurosci, 37*(1), 10-19. doi:10.1016/j.tins.2013.10.002

Genzel, L., Spoormaker, V. I., Konrad, B. N., & Dresler, M. (2015). The role of rapid eye movement sleep for amygdala-related memory processing. *Neurobiol Learn Mem, 122*, 110-121. doi:10.1016/j.nlm.2015.01.008

Gerber, E. M. (2023). permutest (https://www.mathworks.com/matlabcentral/fileexchange/71737-permutest), MATLAB Central File Exchange. Retrieved November 15, 2023.

Giraud, A. L., & Poeppel, D. (2012). Cortical oscillations and speech processing: emerging computational principles and operations. *Nat Neurosci, 15*(4), 511-517. doi:10.1038/nn.3063

Goyal, A., Miller, J., Qasim, S. E., Watrous, A. J., Zhang, H., Stein, J. M., . . . Jacobs, J. (2020). Functionally distinct high and low theta oscillations in the human hippocampus. *Nat Commun, 11*(1), 2469. doi:10.1038/s41467-020-15670-6

Griffiths, B. J., Parish, G., Roux, F., Michelmann, S., van der Plas, M., Kolibius, L. D., . . . Hanslmayr, S. (2019). Directional coupling of slow and fast hippocampal gamma with neocortical alpha/beta oscillations in human episodic memory. *Proc Natl Acad Sci U S A, 116*(43), 21834-21842. doi:10.1073/pnas.1914180116

Hainmueller, T., & Bartos, M. (2018). Parallel emergence of stable and dynamic memory engrams in the hippocampus. *Nature*. doi:10.1038/s41586-018-0191-2

Hamalainen, M. S. (1991). Basic principles of magnetoencephalography. *Acta Radiol Suppl, 377*, 58-62.

Hasselmo, M. E., Bodelon, C., & Wyble, B. P. (2002). A proposed function for hippocampal theta rhythm: separate phases of encoding and retrieval enhance reversal of prior learning. *Neural Comput, 14*(4), 793-817. doi:10.1162/089976602317318965

Hasselmo, M. E., & Stern, C. E. (2014). Theta rhythm and the encoding and retrieval of space and time. *Neuroimage, 85 Pt 2*, 656-666. doi:10.1016/j.neuroimage.2013.06.022

Headley, D. B., & Weinberger, N. M. (2011). Gamma-band activation predicts both associative memory and cortical plasticity. *J Neurosci, 31*(36), 12748-12758. doi:10.1523/JNEUROSCI.2528-11.2011

Hebb, D. O. (1955). Drives and the C.N.S. (conceptual nervous system). *Psychol Rev, 62*(4), 243-254. doi:10.1037/h0041823

Heusser, A. C., Poeppel, D., Ezzyat, Y., & Davachi, L. (2016). Episodic sequence memory is supported by a theta-gamma phase code. *Nat Neurosci, 19*(10), 1374-1380. doi:10.1038/nn.4374

Hirabayashi, T., Tamura, K., Takeuchi, D., Takeda, M., Koyano, K. W., & Miyashita, Y. (2014). Distinct neuronal interactions in anterior inferotemporal areas of macaque monkeys during retrieval of object association memory. *J Neurosci, 34*(28), 9377-9388. doi:10.1523/JNEUROSCI.0600-14.2014

Howard, L. R., Javadi, A. H., Yu, Y., Mill, R. D., Morrison, L. C., Knight, R., . . . Spiers, H. J. (2014). The hippocampus and entorhinal cortex encode the path and Euclidean distances to goals during navigation. *Curr Biol, 24*(12), 1331-1340. doi:10.1016/j.cub.2014.05.001

Huxter, J. R., Senior, T. J., Allen, K., & Csicsvari, J. (2008). Theta phase-specific codes for two-dimensional position, trajectory and heading in the hippocampus. *Nat Neurosci, 11*(5), 587-594. doi:10.1038/nn.2106

Hyafil, A., Giraud, A. L., Fontolan, L., & Gutkin, B. (2015). Neural Cross-Frequency Coupling: Connecting Architectures, Mechanisms, and Functions. *Trends Neurosci, 38*(11), 725-740. doi:10.1016/j.tins.2015.09.001

Hyman, J. M., Wyble, B. P., Goyal, V., Rossi, C. A., & Hasselmo, M. E. (2003). Stimulation in hippocampal region CA1 in behaving rats yields long-term potentiation when delivered to the peak of theta and long-term depression when delivered to the trough. *J Neurosci, 23*(37), 11725-11731.

Igarashi, K. M., Lu, L., Colgin, L. L., Moser, M. B., & Moser, E. I. (2014). Coordination of entorhinal-hippocampal ensemble activity during associative learning. *Nature, 510*(7503), 143-147. doi:10.1038/nature13162

Ito, H. T., & Schuman, E. M. (2007). Frequency-dependent gating of synaptic transmission and plasticity by dopamine. *Front Neural Circuits, 1*, 1. doi:10.3389/neuro.04.001.2007

Ito, H. T., & Schuman, E. M. (2008). Frequency-dependent signal transmission and modulation by neuromodulators. *Front Neurosci, 2*(2), 138-144. doi:10.3389/neuro.01.027.2008

Jacobs, J., Kahana, M. J., Ekstrom, A. D., & Fried, I. (2007). Brain oscillations control timing of single-neuron activity in humans. *J Neurosci, 27*(14), 3839-3844. doi:10.1523/JNEUROSCI.4636-06.2007

Jensen, O., & Colgin, L. L. (2007). Cross-frequency coupling between neuronal oscillations. *Trends Cogn Sci, 11*(7), 267-269. doi:10.1016/j.tics.2007.05.003

Jensen, O., & Lisman, J. E. (1996). Hippocampal CA3 region predicts memory sequences: accounting for the phase precession of place cells. *Learn Mem, 3*(2-3), 279-287. doi:10.1101/lm.3.2-3.279

Jezek, K., Henriksen, E. J., Treves, A., Moser, E. I., & Moser, M. B. (2011). Theta-paced flickering between place-cell maps in the hippocampus. *Nature, 478*(7368), 246-249. doi:10.1038/nature10439

Ji, S., Zhang, Z., Ying, S., Wang, L., Zhao, X., & Gao, Y. (2022). Kullback-Leibler Divergence Metric Learning. *IEEE Trans Cybern, 52*(4), 2047-2058. doi:10.1109/TCYB.2020.3008248

Jobst, B. C., Bartolomei, F., Diehl, B., Frauscher, B., Kahane, P., Minotti, L., . . . Gotman, J. (2020). Intracranial EEG in the 21st Century. *Epilepsy Curr, 20*(4), 180-188. doi:10.1177/1535759720934852

Jones, M. W., & Wilson, M. A. (2005). Theta rhythms coordinate hippocampal-prefrontal interactions in a spatial memory task. *PLoS Biol, 3*(12), e402. doi:10.1371/journal.pbio.0030402

Kensinger, E. A., & Schacter, D. L. (2007). Remembering the specific visual details of presented objects: neuroimaging evidence for effects of emotion. *Neuropsychologia, 45*(13), 2951-2962. doi:10.1016/j.neuropsychologia.2007.05.024

Kerren, C., Linde-Domingo, J., Hanslmayr, S., & Wimber, M. (2018). An Optimal Oscillatory Phase for Pattern Reactivation during Memory Retrieval. *Curr Biol, 28*(21), 3383-3392 e3386. doi:10.1016/j.cub.2018.08.065

Kitamura, T., Ogawa, S. K., Roy, D. S., Okuyama, T., Morrissey, M. D., Smith, L. M., . . . Tonegawa, S. (2017). Engrams and circuits crucial for systems consolidation of a memory. *Science, 356*(6333), 73-78. doi:10.1126/science.aam6808

Kitamura, T., Sun, C., Martin, J., Kitch, L. J., Schnitzer, M. J., & Tonegawa, S. (2015). Entorhinal Cortical Ocean Cells Encode Specific Contexts and Drive Context-Specific Fear Memory. *Neuron, 87*(6), 1317-1331. doi:10.1016/j.neuron.2015.08.036

Kunec, S., Hasselmo, M. E., & Kopell, N. (2005). Encoding and retrieval in the CA3 region of the hippocampus: a model of theta-phase separation. *J Neurophysiol, 94*(1), 70-82. doi:10.1152/jn.00731.2004

Kunz, L., Wang, L., Lachner-Piza, D., Zhang, H., Brandt, A., Dumpelmann, M., . . . Axmacher, N. (2019). Hippocampal theta phases organize the reactivation of large-scale electrophysiological representations during goal-directed navigation. *Sci Adv, 5*(7), eaav8192. doi:10.1126/sciadv.aav8192

Lam, N. H. L., Schoffelen, J. M., Udden, J., Hulten, A., & Hagoort, P. (2016). Neural activity during sentence processing as reflected in theta, alpha, beta, and gamma oscillations. *Neuroimage, 142*, 43-54. doi:10.1016/j.neuroimage.2016.03.007

Landfield, P. W., McGaugh, J. L., & Tusa, R. J. (1972). Theta rhythm: a temporal correlate of memory storage processes in the rat. *Science, 175*(4017), 87-89. doi:10.1126/science.175.4017.87

Lega, B., Burke, J., Jacobs, J., & Kahana, M. J. (2016). Slow-Theta-to-Gamma Phase-Amplitude Coupling in Human Hippocampus Supports the Formation of New Episodic Memories. *Cereb Cortex, 26*(1), 268-278. doi:10.1093/cercor/bhu232

Lever, C., Burton, S., Jeewajee, A., Wills, T. J., Cacucci, F., Burgess, N., & O'Keefe, J. (2010). Environmental novelty elicits a later theta phase of firing in CA1 but not subiculum. *Hippocampus, 20*(2), 229-234. doi:10.1002/hipo.20671

Li, K. T., Liang, J., & Zhou, C. (2021). Gamma Oscillations Facilitate Effective Learning in Excitatory-Inhibitory Balanced Neural Circuits. *Neural Plast, 2021*, 6668175. doi:10.1155/2021/6668175

Lin, J. J., Umbach, G., Rugg, M. D., & Lega, B. (2019). Gamma oscillations during episodic memory processing provide evidence for functional specialization in the longitudinal axis of the human hippocampus. *Hippocampus, 29*(2), 68-72. doi:10.1002/hipo.23016

Lisman, J. (2005). The theta/gamma discrete phase code occuring during the hippocampal phase precession may be a more general brain coding scheme. *Hippocampus, 15*(7), 913-922. doi:10.1002/hipo.20121

Lisman, J. E., & Grace, A. A. (2005). The hippocampal-VTA loop: controlling the entry of information into long-term memory. *Neuron, 46*(5), 703-713. doi:10.1016/j.neuron.2005.05.002

Lisman, J. E., & Idiart, M. A. (1995). Storage of 7 +/- 2 short-term memories in oscillatory subcycles. *Science, 267*(5203), 1512-1515. doi:10.1126/science.7878473

Lisman, J. E., & Jensen, O. (2013). The theta-gamma neural code. *Neuron, 77*(6), 1002-1016. doi:10.1016/j.neuron.2013.03.007

Lohnas, L. J., Duncan, K., Doyle, W. K., Thesen, T., Devinsky, O., & Davachi, L. (2018). Time-resolved neural reinstatement and pattern separation during memory decisions in human hippocampus. *Proc Natl Acad Sci U S A, 115*(31), E7418-E7427. doi:10.1073/pnas.1717088115

Long, N. M., & Kuhl, B. A. (2021). Cortical Representations of Visual Stimuli Shift Locations with Changes in Memory States. *Curr Biol, 31*(5), 1119-1126 e1115. doi:10.1016/j.cub.2021.01.004

Madronal, N., Delgado-Garcia, J. M., Fernandez-Guizan, A., Chatterjee, J., Kohn, M., Mattucci, C., . . . Gruart, A. (2016). Rapid erasure of hippocampal memory following inhibition of dentate gyrus granule cells. *Nat Commun, 7*, 10923. doi:10.1038/ncomms10923

Manning, J. R., Polyn, S. M., Baltuch, G. H., Litt, B., & Kahana, M. J. (2011). Oscillatory patterns in temporal lobe reveal context reinstatement during memory search. *Proc Natl Acad Sci U S A, 108*(31), 12893-12897. doi:10.1073/pnas.1015174108

Manns, J. R., Zilli, E. A., Ong, K. C., Hasselmo, M. E., & Eichenbaum, H. (2007). Hippocampal CA1 spiking during encoding and retrieval: relation to theta phase. *Neurobiol Learn Mem, 87*(1), 9-20. doi:10.1016/j.nlm.2006.05.007

Maris, E., & Oostenveld, R. (2007). Nonparametric statistical testing of EEG- and MEG-data. *J Neurosci Methods, 164*(1), 177-190. doi:10.1016/j.jneumeth.2007.03.024

Martinelli, P., Sperduti, M., & Piolino, P. (2013). Neural substrates of the self-memory system: new insights from a meta-analysis. *Hum Brain Mapp, 34*(7), 1515-1529. doi:10.1002/hbm.22008

Michelmann, S., Treder, M. S., Griffiths, B., Kerren, C., Roux, F., Wimber, M., . . . Hanslmayr, S. (2018). Data-driven re-referencing of intracranial EEG based on independent component analysis (ICA). *J Neurosci Methods, 307*, 125-137. doi:10.1016/j.jneumeth.2018.06.021

Miller, L. A., Mothakunnel, A., Flanagan, E., Nikpour, A., & Thayer, Z. (2017). Accelerated Long Term Forgetting in patients with focal seizures: Incidence rate and contributing factors. *Epilepsy Behav, 72*, 108-113. doi:10.1016/j.yebeh.2017.04.039

Milner, B., & Klein, D. (2016). Loss of recent memory after bilateral hippocampal lesions: memory and memories-looking back and looking forward. *J Neurol Neurosurg Psychiatry, 87*(3), 230. doi:10.1136/jnnp-2015-311092

Mori, M., Abegg, M. H., Gahwiler, B. H., & Gerber, U. (2004). A frequency-dependent switch from inhibition to excitation in a hippocampal unitary circuit. *Nature, 431*(7007), 453-456. doi:10.1038/nature02854

Morris, R. G. (2001). Episodic-like memory in animals: psychological criteria, neural mechanisms and the value of episodic-like tasks to investigate animal models of neurodegenerative disease. *Philos Trans R Soc Lond B Biol Sci, 356*(1413), 1453-1465. doi:10.1098/rstb.2001.0945

Moscovitch, M., Nadel, L., Winocur, G., Gilboa, A., & Rosenbaum, R. S. (2006). The cognitive neuroscience of remote episodic, semantic and spatial memory. *Curr Opin Neurobiol, 16*(2), 179-190. doi:10.1016/j.conb.2006.03.013

Moscovitch, M., Rosenbaum, R. S., Gilboa, A., Addis, D. R., Westmacott, R., Grady, C., . . . Nadel, L. (2005). Functional neuroanatomy of remote episodic, semantic and spatial memory: a unified account based on multiple trace theory. *J Anat, 207*(1), 35-66. doi:10.1111/j.1469-7580.2005.00421.x

Mumby, D. G., Astur, R. S., Weisend, M. P., & Sutherland, R. J. (1999). Retrograde amnesia and selective damage to the hippocampal formation: memory for places and object discriminations. *Behav Brain Res, 106*(1-2), 97-107. doi:10.1016/s0166-4328(99)00097-2

Muschalla, B., & Schonborn, F. (2021). Induction of false beliefs and false memories in laboratory studies-A systematic review. *Clin Psychol Psychother, 28*(5), 1194-1209. doi:10.1002/cpp.2567

Nakamura, N. H., Flasbeck, V., Maingret, N., Kitsukawa, T., & Sauvage, M. M. (2013). Proximodistal segregation of nonspatial information in CA3: preferential recruitment of a proximal CA3-distal CA1 network in nonspatial recognition memory. *J Neurosci, 33*(28), 11506-11514. doi:10.1523/JNEUROSCI.4480-12.2013

Nakashiba, T., Buhl, D. L., McHugh, T. J., & Tonegawa, S. (2009). Hippocampal CA3 output is crucial for ripple-associated reactivation and consolidation of memory. *Neuron, 62*(6), 781-787. doi:10.1016/j.neuron.2009.05.013

Nielsen, F. (2019). On the Jensen-Shannon Symmetrization of Distances Relying on Abstract Means. *Entropy (Basel), 21*(5). doi:10.3390/e21050485

Norman, Y., Yeagle, E. M., Khuvis, S., Harel, M., Mehta, A. D., & Malach, R. (2019). Hippocampal sharp-wave ripples linked to visual episodic recollection in humans. *Science, 365*(6454). doi:10.1126/science.aax1030

O'Keefe, J. (1993). Hippocampus, theta, and spatial memory. *Curr Opin Neurobiol, 3*(6), 917-924. doi:10.1016/0959-4388(93)90163-s

O'Keefe, J., & Burgess, N. (1996). Geometric determinants of the place fields of hippocampal neurons. *Nature, 381*(6581), 425-428. doi:10.1038/381425a0

O'Keefe, J., & Burgess, N. (2005). Dual phase and rate coding in hippocampal place cells: theoretical significance and relationship to entorhinal grid cells. *Hippocampus, 15*(7), 853-866. doi:10.1002/hipo.20115

O'Keefe, J., & Conway, D. H. (1978). Hippocampal place units in the freely moving rat: why they fire where they fire. *Exp Brain Res, 31*(4), 573-590.

O'Keefe, J., & Dostrovsky, J. (1971). The hippocampus as a spatial map. Preliminary evidence from unit activity in the freely-moving rat. *Brain Res, 34*(1), 171-175.

O'Keefe, J., & Recce, M. L. (1993). Phase relationship between hippocampal place units and the EEG theta rhythm. *Hippocampus, 3*(3), 317-330. doi:10.1002/hipo.450030307

Ogawa, S., Lee, T. M., Kay, A. R., & Tank, D. W. (1990). Brain magnetic resonance imaging with contrast dependent on blood oxygenation. *Proc Natl Acad Sci U S A, 87*(24), 9868-9872.

Ogawa, S., Tank, D. W., Menon, R., Ellermann, J. M., Kim, S. G., Merkle, H., & Ugurbil, K. (1992). Intrinsic signal changes accompanying sensory stimulation: functional brain mapping with magnetic resonance imaging. *Proc Natl Acad Sci U S A, 89*(13), 5951-5955.

Oliva, A., Fernandez-Ruiz, A., Buzsaki, G., & Berenyi, A. (2016). Spatial coding and physiological properties of hippocampal neurons in the Cornu Ammonis subregions. *Hippocampus, 26*(12), 1593-1607. doi:10.1002/hipo.22659

Oostenveld, R., Fries, P., Maris, E., & Schoffelen, J. M. (2011). FieldTrip: Open source software for advanced analysis of MEG, EEG, and invasive electrophysiological data. *Comput Intell Neurosci, 2011*, 156869. doi:10.1155/2011/156869

Pacheco Estefan, D., Zucca, R., Arsiwalla, X., Principe, A., Zhang, H., Rocamora, R., . . . Verschure, P. (2021). Volitional learning promotes theta phase coding in the human hippocampus. *Proc Natl Acad Sci U S A, 118*(10). doi:10.1073/pnas.2021238118

Paller, K. A., & Wagner, A. D. (2002). Observing the transformation of experience into memory. *Trends Cogn Sci, 6*(2), 93-102.

Park, J. M., Jung, S. C., & Eun, S. Y. (2014). Long-term Synaptic Plasticity: Circuit Perturbation and Stabilization. *Korean J Physiol Pharmacol, 18*(6), 457-460. doi:10.4196/kjpp.2014.18.6.457

Pavlides, C., Greenstein, Y. J., Grudman, M., & Winson, J. (1988). Long-term potentiation in the dentate gyrus is induced preferentially on the positive phase of theta-rhythm. *Brain Res, 439*(1-2), 383-387. doi:10.1016/0006-8993(88)91499-0

Pernia-Andrade, A. J., & Jonas, P. (2014). Theta-gamma-modulated synaptic currents in hippocampal granule cells in vivo define a mechanism for network oscillations. *Neuron, 81*(1), 140-152. doi:10.1016/j.neuron.2013.09.046

Piolino, P., Desgranges, B., & Eustache, F. (2009). Episodic autobiographical memories over the course of time: cognitive, neuropsychological and neuroimaging findings. *Neuropsychologia, 47*(11), 2314-2329. doi:10.1016/j.neuropsychologia.2009.01.020

Polack, C. W., & Miller, R. R. (2022). Testing improves performance as well as assesses learning: A review of the testing effect with implications for models of learning. *J Exp Psychol Anim Learn Cogn, 48*(3), 222-241. doi:10.1037/xan0000323

Poulter, S., Lee, S. A., Dachtler, J., Wills, T. J., & Lever, C. (2021). Vector trace cells in the subiculum of the hippocampal formation. *Nat Neurosci, 24*(2), 266-275. doi:10.1038/s41593-020-00761-w

Proekt, A. (2018). Brief Introduction to Electroencephalography. *Methods Enzymol, 603*, 257-277. doi:10.1016/bs.mie.2018.02.009

Ray, S., & Maunsell, J. H. (2015). Do gamma oscillations play a role in cerebral cortex? *Trends Cogn Sci, 19*(2), 78-85. doi:10.1016/j.tics.2014.12.002

Reddy, L., Self, M. W., Zoefel, B., Poncet, M., Possel, J. K., Peters, J. C., . . . Roelfsema, P. R. (2021). Theta-phase dependent neuronal coding during sequence learning in human single neurons. *Nat Commun, 12*(1), 4839. doi:10.1038/s41467-021-25150-0

Rizzuto, D. S., Madsen, J. R., Bromfield, E. B., Schulze-Bonhage, A., & Kahana, M. J. (2006). Human neocortical oscillations exhibit theta phase differences between encoding and retrieval. *Neuroimage, 31*(3), 1352-1358. doi:10.1016/j.neuroimage.2006.01.009

Robinson, N. T. M., Priestley, J. B., Rueckemann, J. W., Garcia, A. D., Smeglin, V. A., Marino, F. A., & Eichenbaum, H. (2017). Medial Entorhinal Cortex Selectively Supports Temporal Coding by Hippocampal Neurons. *Neuron, 94*(3), 677-688 e676. doi:10.1016/j.neuron.2017.04.003

Rosen, Z. B., Cheung, S., & Siegelbaum, S. A. (2015). Midbrain dopamine neurons bidirectionally regulate CA3-CA1 synaptic drive. *Nat Neurosci, 18*(12), 1763-1771. doi:10.1038/nn.4152

Rosenbaum, R. S., Priselac, S., Kohler, S., Black, S. E., Gao, F., Nadel, L., & Moscovitch, M. (2000). Remote spatial memory in an amnesic person with extensive bilateral hippocampal lesions. *Nat Neurosci, 3*(10), 1044-1048. doi:10.1038/79867

Roux, F., Parish, G., Chelvarajah, R., Rollings, D. T., Sawlani, V., Hamer, H., . . . Hanslmayr, S. (2022). Oscillations support short latency co-firing of neurons during human episodic memory formation. *Elife, 11*. doi:10.7554/eLife.78109

Roy, D. S., Arons, A., Mitchell, T. I., Pignatelli, M., Ryan, T. J., & Tonegawa, S. (2016). Memory retrieval by activating engram cells in mouse models of early Alzheimer's disease. *Nature, 531*(7595), 508-512. doi:10.1038/nature17172

Rutishauser, U. (2019). Testing Models of Human Declarative Memory at the Single-Neuron Level. *Trends Cogn Sci, 23*(6), 510-524. doi:10.1016/j.tics.2019.03.006

Rutishauser, U., Ross, I. B., Mamelak, A. N., & Schuman, E. M. (2010). Human memory strength is predicted by theta-frequency phase-locking of single neurons. *Nature, 464*(7290), 903-907. doi:10.1038/nature08860

Saint Amour di Chanaz, L., Perez-Bellido, A., Wu, X., Lozano-Soldevilla, D., Pacheco-Estefan, D., Lehongre, K., . . . Fuentemilla, L. (2023). Gamma amplitude is coupled to opposed hippocampal theta-phase states during the encoding and retrieval of episodic memories in humans. *Curr Biol*. doi:10.1016/j.cub.2023.03.073

Schacter, D. L., Addis, D. R., & Buckner, R. L. (2007). Remembering the past to imagine the future: the prospective brain. *Nat Rev Neurosci, 8*(9), 657-661. doi:10.1038/nrn2213

Schaul, N. (1998). The fundamental neural mechanisms of electroencephalography. *Electroencephalogr Clin Neurophysiol, 106*(2), 101-107. doi:10.1016/s0013-4694(97)00111-9

Schomburg, E. W., Fernandez-Ruiz, A., Mizuseki, K., Berenyi, A., Anastassiou, C. A., Koch, C., & Buzsaki, G. (2014). Theta phase segregation of input-specific gamma patterns in entorhinal-hippocampal networks. *Neuron, 84*(2), 470-485. doi:10.1016/j.neuron.2014.08.051

Scoville, W. B., & Milner, B. (1957). Loss of recent memory after bilateral hippocampal lesions. *J Neurol Neurosurg Psychiatry, 20*(1), 11-21. doi:10.1136/jnnp.20.1.11

Scoville, W. B., & Milner, B. (2000). Loss of recent memory after bilateral hippocampal lesions. 1957. *J Neuropsychiatry Clin Neurosci, 12*(1), 103-113. doi:10.1176/jnp.12.1.103

Sederberg, P. B., Schulze-Bonhage, A., Madsen, J. R., Bromfield, E. B., Litt, B., Brandt, A., & Kahana, M. J. (2007). Gamma oscillations distinguish true from false memories. *Psychol Sci, 18*(11), 927-932. doi:10.1111/j.1467-9280.2007.02003.x

Seung, H. S. (2000). Half a century of Hebb. *Nat Neurosci, 3 Suppl*, 1166. doi:10.1038/81430

Siegle, J. H., & Wilson, M. A. (2014). Enhancement of encoding and retrieval functions through theta phase-specific manipulation of hippocampus. *Elife, 3*, e03061. doi:10.7554/eLife.03061

Silva, M., Baldassano, C., & Fuentemilla, L. (2019). Rapid Memory Reactivation at Movie Event Boundaries Promotes Episodic Encoding. *J Neurosci, 39*(43), 8538-8548. doi:10.1523/JNEUROSCI.0360-19.2019

Sinnamon, H. M., Freniere, S., & Kootz, J. (1978). Rat hippocampus and memory for places of changing significance. *J Comp Physiol Psychol, 92*(1), 142-155. doi:10.1037/h0077446

Sjostrom, P. J., Turrigiano, G. G., & Nelson, S. B. (2001). Rate, timing, and cooperativity jointly determine cortical synaptic plasticity. *Neuron, 32*(6), 1149-1164. doi:10.1016/s0896-6273(01)00542-6

Solomon, E. A., Kragel, J. E., Sperling, M. R., Sharan, A., Worrell, G., Kucewicz, M., . . . Kahana, M. J. (2017). Widespread theta synchrony and high-frequency desynchronization underlies enhanced cognition. *Nat Commun, 8*(1), 1704. doi:10.1038/s41467-017-01763-2

Solomon, E. A., Lega, B. C., Sperling, M. R., & Kahana, M. J. (2019). Hippocampal theta codes for distances in semantic and temporal spaces. *Proc Natl Acad Sci U S A, 116*(48), 24343-24352. doi:10.1073/pnas.1906729116

Squire, L. R., & Zola, S. M. (1996). Structure and function of declarative and nondeclarative memory systems. *Proc Natl Acad Sci U S A, 93*(24), 13515-13522. doi:10.1073/pnas.93.24.13515

Staresina, B. P., Bergmann, T. O., Bonnefond, M., van der Meij, R., Jensen, O., Deuker, L., . . . Fell, J. (2015). Hierarchical nesting of slow oscillations, spindles and ripples in the human hippocampus during sleep. *Nat Neurosci, 18*(11), 1679-1686. doi:10.1038/nn.4119

Staresina, B. P., Michelmann, S., Bonnefond, M., Jensen, O., Axmacher, N., & Fell, J. (2016). Hippocampal pattern completion is linked to gamma power increases and alpha power decreases during recollection. *Elife, 5*. doi:10.7554/eLife.17397

Staubli, U., & Lynch, G. (1987). Stable hippocampal long-term potentiation elicited by 'theta' pattern stimulation. *Brain Res, 435*(1-2), 227-234. doi:10.1016/0006-8993(87)91605-2

Stone, S. S., Teixeira, C. M., Devito, L. M., Zaslavsky, K., Josselyn, S. A., Lozano, A. M., & Frankland, P. W. (2011). Stimulation of entorhinal cortex promotes adult neurogenesis and facilitates spatial memory. *J Neurosci, 31*(38), 13469-13484. doi:10.1523/JNEUROSCI.3100-11.2011

Svoboda, E., McKinnon, M. C., & Levine, B. (2006). The functional neuroanatomy of autobiographical memory: a meta-analysis. *Neuropsychologia, 44*(12), 2189-2208. doi:10.1016/j.neuropsychologia.2006.05.023

Takashima, A., Jensen, O., Oostenveld, R., Maris, E., van de Coevering, M., & Fernandez, G. (2006). Successful declarative memory formation is associated with ongoing activity during encoding in a distributed neocortical network related to working memory: a magnetoencephalography study. *Neuroscience, 139*(1), 291-297. doi:10.1016/j.neuroscience.2005.05.067

Takashima, A., Petersson, K. M., Rutters, F., Tendolkar, I., Jensen, O., Zwarts, M. J., . . . Fernandez, G. (2006). Declarative memory consolidation in humans: a prospective functional magnetic resonance imaging study. *Proc Natl Acad Sci U S A, 103*(3), 756-761. doi:10.1073/pnas.0507774103

Ter Wal, M., Linde-Domingo, J., Lifanov, J., Roux, F., Kolibius, L. D., Gollwitzer, S., . . . Wimber, M. (2021). Theta rhythmicity governs human behavior and hippocampal signals during memory-dependent tasks. *Nat Commun, 12*(1), 7048. doi:10.1038/s41467-021-27323-3

Tesche, C. D., & Karhu, J. (2000). Theta oscillations index human hippocampal activation during a working memory task. *Proc Natl Acad Sci U S A, 97*(2), 919-924. doi:10.1073/pnas.97.2.919

Titiz, A. S., Hill, M. R. H., Mankin, E. A., Z, M. A., Eliashiv, D., Tchemodanov, N., . . . Fried, I. (2017). Theta-burst microstimulation in the human entorhinal area improves memory specificity. *Elife, 6*. doi:10.7554/eLife.29515

Tonegawa, S., Morrissey, M. D., & Kitamura, T. (2018). The role of engram cells in the systems consolidation of memory. *Nature Reviews Neuroscience*. doi:10.1038/s41583-018-0031-2

Tonegawa, S., Pignatelli, M., Roy, D. S., & Ryan, T. J. (2015). Memory engram storage and retrieval. *Curr Opin Neurobiol, 35*, 101-109. doi:10.1016/j.conb.2015.07.009

Tononi, G., & Cirelli, C. (2006). Sleep function and synaptic homeostasis. *Sleep Med Rev, 10*(1), 49-62. doi:10.1016/j.smrv.2005.05.002

Tort, A. B., Komorowski, R., Eichenbaum, H., & Kopell, N. (2010). Measuring phase-amplitude coupling between neuronal oscillations of different frequencies. *J Neurophysiol, 104*(2), 1195-1210. doi:10.1152/jn.00106.2010

Tort, A. B., Komorowski, R. W., Manns, J. R., Kopell, N. J., & Eichenbaum, H. (2009). Theta-gamma coupling increases during the learning of item-context associations. *Proc Natl Acad Sci U S A, 106*(49), 20942-20947. doi:10.1073/pnas.0911331106

Tort, A. B., Kramer, M. A., Thorn, C., Gibson, D. J., Kubota, Y., Graybiel, A. M., & Kopell, N. J. (2008). Dynamic cross-frequency couplings of local field potential oscillations in rat striatum and hippocampus during performance of a T-maze task. *Proc Natl Acad Sci U S A, 105*(51), 20517-20522. doi:10.1073/pnas.0810524105

Trevethan, R. (2017). Sensitivity, Specificity, and Predictive Values: Foundations, Pliabilities, and Pitfalls in Research and Practice. *Front Public Health, 5*, 307. doi:10.3389/fpubh.2017.00307

Trimper, J. B., Galloway, C. R., Jones, A. C., Mandi, K., & Manns, J. R. (2017). Gamma Oscillations in Rat Hippocampal Subregions Dentate Gyrus, CA3, CA1, and Subiculum Underlie Associative Memory Encoding. *Cell Rep, 21*(9), 2419-2432. doi:10.1016/j.celrep.2017.10.123

Tsodyks, M. V., Skaggs, W. E., Sejnowski, T. J., & McNaughton, B. L. (1996). Population dynamics and theta rhythm phase precession of hippocampal place cell firing: a spiking neuron model. *Hippocampus, 6*(3), 271-280. doi:10.1002/(SICI)1098-1063(1996)6:3<271::AID-HIPO5>3.0.CO;2-Q

Tulving, E. (2002). Episodic memory: from mind to brain. *Annu Rev Psychol, 53*, 1-25. doi:10.1146/annurev.psych.53.100901.135114

Tulving, E., & Markowitsch, H. J. (1998). Episodic and declarative memory: role of the hippocampus. *Hippocampus, 8*(3), 198-204. doi:10.1002/(SICI)1098-1063(1998)8:3<198::AID-HIPO2>3.0.CO;2-G

Tulving, E., Schacter, D. L., McLachlan, D. R., & Moscovitch, M. (1988). Priming of semantic autobiographical knowledge: a case study of retrograde amnesia. *Brain Cogn, 8*(1), 3-20. doi:10.1016/0278-2626(88)90035-8

van Driel, J., Cox, R., & Cohen, M. X. (2015). Phase-clustering bias in phase-amplitude cross-frequency coupling and its removal. *J Neurosci Methods, 254*, 60-72. doi:10.1016/j.jneumeth.2015.07.014

VanRullen, R. (2016). How to Evaluate Phase Differences between Trial Groups in Ongoing Electrophysiological Signals. *Front Neurosci, 10*, 426. doi:10.3389/fnins.2016.00426

Varela, F., Lachaux, J. P., Rodriguez, E., & Martinerie, J. (2001). The brainweb: phase synchronization and large-scale integration. *Nat Rev Neurosci, 2*(4), 229-239. doi:10.1038/35067550

Vinck, M., van Wingerden, M., Womelsdorf, T., Fries, P., & Pennartz, C. M. (2010). The pairwise phase consistency: a bias-free measure of rhythmic neuronal synchronization. *Neuroimage, 51*(1), 112-122. doi:10.1016/j.neuroimage.2010.01.073

Vivekananda, U., Bush, D., Bisby, J. A., Baxendale, S., Rodionov, R., Diehl, B., . . . Burgess, N. (2021). Theta power and theta-gamma coupling support long-term spatial memory retrieval. *Hippocampus, 31*(2), 213-220. doi:10.1002/hipo.23284

Wang, D. X., Schmitt, K., Seger, S., Davila, C. E., & Lega, B. C. (2021). Cross-regional phase amplitude coupling supports the encoding of episodic memories. *Hippocampus, 31*(5), 481-492. doi:10.1002/hipo.23309

Westner, B. U., Dalal, S. S., Gramfort, A., Litvak, V., Mosher, J. C., Oostenveld, R., & Schoffelen, J. M. (2022). A unified view on beamformers for M/EEG source reconstruction. *Neuroimage, 246*, 118789. doi:10.1016/j.neuroimage.2021.118789

Wills, T. J., Cacucci, F., Burgess, N., & O'Keefe, J. (2010). Development of the hippocampal cognitive map in preweanling rats. *Science, 328*(5985), 1573-1576. doi:10.1126/science.1188224

Winson, J. (1978). Loss of hippocampal theta rhythm results in spatial memory deficit in the rat. *Science, 201*(4351), 160-163. doi:10.1126/science.663646

Woolston, C. (2021). Depression and anxiety 'the norm' for UK PhD students. *Nature*. doi:10.1038/d41586-021-03761-3

Wu, X., Vinals, X., Ben-Yakov, A., Staresina, B. P., & Fuentemilla, L. (2022). Post-encoding Reactivation Is Related to Learning of Episodes in Humans. *J Cogn Neurosci, 35*(1), 74-89. doi:10.1162/jocn_a_01934

Yamaguchi, Y., Aota, Y., Sato, N., Wagatsuma, H., & Wu, Z. (2004). Synchronization of neural oscillations as a possible mechanism underlying episodic memory: a study of theta rhythm in the hippocampus. *J Integr Neurosci, 3*(2), 143-157.

Zheng, C., Bieri, K. W., Hsiao, Y. T., & Colgin, L. L. (2016). Spatial Sequence Coding Differs during Slow and Fast Gamma Rhythms in the Hippocampus. *Neuron, 89*(2), 398-408. doi:10.1016/j.neuron.2015.12.005

Zhou, Y., Sheremet, A., Qin, Y., Kennedy, J. P., DiCola, N. M., Burke, S. N., & Maurer, A. P. (2019). Methodological Considerations on the Use of Different Spectral Decomposition Algorithms to Study Hippocampal Rhythms. *eNeuro, 6*(4). doi:10.1523/ENEURO.0142-19.2019